



---

# A Search for Astrophysical Tau Neutrinos with IceCube using an Advanced Statistical Approach

---

*Author:*  
**Simon DE KOCKERE**

*Promotor:*  
**Prof. Dr. Dirk RYCKBOSCH**

*A thesis submitted in fulfillment of the requirements  
for the degree of Master of Science in Physics and Astronomy  
in the*



Department of Physics and Astronomy

June 15, 2018



# *Abstract*

## **A Search for Astrophysical Tau Neutrinos with IceCube using an Advanced Statistical Approach**

by Simon DE KOCKERE

At the time of writing no analysis so far has been able to disclose any possible tau neutrino event candidates from the IceCube Neutrino Observatory data. In particular its so-called Double Bang signature has however very appealing characteristics, generally yielding both a good energy as well as angular resolution. In contrast to the two other types of neutrino flavors tau neutrino events are believed to be purely astrophysical, making them particularly interesting astronomical messengers. Moreover measuring the corresponding event rate could yield consequential limits on the flavor ratio of the astrophysical neutrinos reaching Earth. This thesis reports the results of an attempt to improve the Double Bang tau neutrino event search by Matthias Vraeghe. To that end a more advanced statistical approach has been included which tries to separate the signals of interest from the background using a test statistic based on different likelihood distributions of variables introduced in the original analysis. The performance of the modified data reduction scheme is compared with that of the original analysis by applying both to the same simulated data sets. It is found that replacing the more straightforward approach of simply placing limits on the variables by the more advanced method does not improve the final results. Combining the two approaches however seems to increase the final signal-to-background ratio of the tau neutrino events and the Double Bang events in particular without without significantly reducing their number of expected remaining events.



## *Acknowledgements*

Many thanks goes to the promotor of this master's thesis, Prof. Dr. Dirk Ryckbosch, whose open door and encouraging comments guided me through this project. I would like to thank Ward Van Driessche, for his helpful tutorials and instructions, Matthias Vraeghe, who in busy times still found moments to spare to help me get acquainted with his work and answer many questions, and Mathieu Labare, for getting me started and sharing with me his insights and never-ending enthusiasm. Special thanks goes to my fellow thesis students here at the campus and all my other friends, for the pleasant working atmosphere, enjoyable breaks or both. And last but not least I would also like to thank my parents, as without their support none of this would ever have been possible.



# Contents

<b>Abstract</b>	<b>iii</b>
<b>Acknowledgements</b>	<b>v</b>
<b>Contents</b>	<b>vii</b>
<b>List of Figures</b>	<b>ix</b>
<b>List of Tables</b>	<b>xi</b>
<b>Nederlandse Samenvatting</b>	<b>xiii</b>
<b>Introduction</b>	<b>xv</b>
<b>1 The Neutrino</b>	<b>1</b>
1.1 The Standard Model . . . . .	1
1.2 Discovery of the Neutrino . . . . .	3
1.3 Neutrino Interactions . . . . .	6
1.4 Neutrino Flavour Oscillations . . . . .	7
<b>2 Astroparticles</b>	<b>9</b>
2.1 Cosmic Rays . . . . .	9
2.1.1 Discovery . . . . .	9
2.1.2 Primary and Secondary Cosmic Rays . . . . .	9
2.1.3 Energy Spectrum . . . . .	11
2.1.4 Galactic Cosmic Rays . . . . .	14
2.1.5 Extragalactic Cosmic Rays . . . . .	16
2.2 Astrophysical Neutrinos . . . . .	18
2.2.1 Predictions . . . . .	18
2.2.2 Observation . . . . .	19
<b>3 The IceCube Neutrino Observatory</b>	<b>23</b>
3.1 General Detector Layout . . . . .	23
3.1.1 IceCube In-Ice Array . . . . .	24
3.1.2 DeepCore . . . . .	25
3.1.3 IceTop . . . . .	25
3.1.4 IceCube Laboratory . . . . .	25
3.2 Digital Optical Module . . . . .	25
3.2.1 Photomultiplier Tube . . . . .	26
3.2.2 Main Board . . . . .	27
3.2.3 Flasher Board . . . . .	27
3.3 Data Acquisition System . . . . .	27
3.4 Signal Topologies . . . . .	28
3.4.1 Cascade . . . . .	28

3.4.2	Track . . . . .	29
3.4.3	Double Bang . . . . .	29
3.5	Simulation and Software . . . . .	31
3.6	Experimental Capabilities . . . . .	32
<b>4</b>	<b>Tau Neutrino Search</b>	<b>35</b>
4.1	Double Bang Search by Matthias Vraeghe . . . . .	35
4.1.1	Definition of Double Bang Event . . . . .	36
4.1.2	Level 3 and 4 . . . . .	36
4.1.3	Level 5 . . . . .	36
4.1.4	Level 6 . . . . .	36
4.1.5	Level 7 . . . . .	37
4.1.6	Results . . . . .	38
4.2	An Advanced Statistical Approach . . . . .	38
4.2.1	Likelihood Distributions . . . . .	39
4.2.2	TS distributions . . . . .	40
4.3	Results . . . . .	44
4.3.1	Modified Level 6 . . . . .	44
4.3.2	Level 7 via Modified Level 6 . . . . .	49
4.3.3	Level 7+ . . . . .	53
<b>5</b>	<b>Conclusions and Outlook</b>	<b>59</b>
<b>A</b>	<b>Likelihood Distributions</b>	<b>63</b>
A.1	Astro Tau Neutrino . . . . .	63
A.2	Corsika . . . . .	64
A.3	Astro Electron Neutrino . . . . .	65
A.4	Astro Muon Neutrino . . . . .	66
A.5	Atmos Electron Neutrino . . . . .	67
A.6	Atmos Muon Neutrino . . . . .	68
<b>B</b>	<b>TS Distributions</b>	<b>69</b>
<b>C</b>	<b>Communication to the General Public</b>	<b>75</b>

# List of Figures

1.1	The fraction of electrons emitted during the beta decay of a $^{14}\text{C}$ nucleus in function of the energy. . . . .	4
1.2	The two possible types of neutrino interactions. . . . .	6
1.3	Example of a neutrino deep scattering process. . . . .	7
2.1	The increase of ionizing radiation with altitude. . . . .	10
2.2	Illustration of a small air shower. . . . .	11
2.3	Fluxes of nuclei of the primary cosmic radiation. . . . .	12
2.4	The energy spectrum of primary cosmic rays. . . . .	13
2.5	Abundances of elements observed in the cosmic rays and elements in the proto-sun. . . . .	15
2.6	The Crab Nebula . . . . .	16
2.7	An illustration of an AGN. . . . .	17
2.8	High-energy events detected in four years of IceCube data as a function of deposited energy. . . . .	20
2.9	Best fit for the astrophysical neutrino spectrum following the results of the IceCube experiment. . . . .	20
2.10	The profile likelihood scan of the neutrino flavor ratio as measured on Earth. . . . .	21
3.1	The IceCube Neutrino Observatory. . . . .	24
3.2	The digital optical module (DOM). . . . .	26
3.3	Example of a cascade-like signal following a NC or CC electron neutrino interaction. . . . .	29
3.4	Example of a track-like signal created by a muon. . . . .	30
3.5	Example of a Double Bang signal following a tau neutrino interaction. . . . .	31
4.1	The number of expected remaining events per 1251 days of IceCube data as a function of the cut levels of the astrophysical tau neutrino search by Matthias Vraeghe. . . . .	38
4.2	The likelihood distributions for the Double Bang signal. . . . .	41
4.3	The normalized TS distributions of the optimal TS parameter. . . . .	43
4.4	The expected results after processing to the modified Level 6 using the cut $\text{TS} < 0.682$ . . . . .	47
4.5	The expected results after processing to the modified Level 6 using the cut $\text{TS} < 0.561$ . . . . .	48
4.6	The expected results after processing to the modified Level 6 using the cut $\text{TS} < 0.995$ . . . . .	48
4.7	The expected results after processing to the modified Level 6 using the cut $\text{TS} < 0.600$ . . . . .	49
4.8	The expected results after processing to the modified Level 6 and Level 7 using the cut $\text{TS} < 0.682$ . . . . .	51

4.9	The expected results after processing to the modified Level 6 and Level 7 using the cut $TS < 0.561$ . . . . .	52
4.10	The expected results after processing to the modified Level 6 and Level 7 using the cut $TS < 0.995$ . . . . .	52
4.11	The expected results after processing to the modified Level 6 and Level 7 using the cut $TS < 0.600$ . . . . .	53
4.12	The expected results after processing to Level 7+ using the cut $TS < 0.682$ . . . . .	56
4.13	The expected results after processing to Level 7+ using the cut $TS < 0.561$ . . . . .	57
4.14	The expected results after processing to Level 7+ using the cut $TS < 0.995$ . . . . .	57
4.15	The expected results after processing to Level 7+ using the cut $TS < 0.600$ . . . . .	58
4.16	The expected results after processing to Level 7+ using the cut $TS < 0.839$ . . . . .	58
A.1	The likelihood distributions for the Astro Tau Neutrino signal. . . . .	63
A.2	The likelihood distributions for the Corsika signal. . . . .	64
A.3	The likelihood distributions for the Astro Electron Neutrino signal. . . . .	65
A.4	The likelihood distributions for the Astro Muon Neutrino signal. . . . .	66
A.5	The likelihood distributions for the Atmos Electron Neutrino signal. . . . .	67
A.6	The likelihood distributions for the Atmos Muon Neutrino signal. . . . .	68
B.1	The normalized TS distributions for an example TS parameter (1). . . . .	69
B.2	The normalized TS distributions for an example TS parameter (2). . . . .	70
B.3	The normalized TS distributions for an example TS parameter (3). . . . .	70
B.4	The normalized TS distributions for an example TS parameter (4). . . . .	71
B.5	The normalized TS distributions for an example TS parameter (5). . . . .	71
B.6	The normalized TS distributions for an example TS parameter (6). . . . .	72
B.7	The normalized TS distributions for an example TS parameter (7). . . . .	72
B.8	The normalized TS distributions for an example TS parameter (8). . . . .	73
B.9	The normalized TS distributions for an example TS parameter (9). . . . .	73

# List of Tables

1.1	The bosons of the Standard Model. . . . .	2
1.2	The fermions of the Standard Model. . . . .	2
4.1	The types of signals considered in the advanced statistical approach. . .	39
4.2	The expected results after processing to the modified Level 6 using different cut values. . . . .	45
4.3	The expected results after processing to the modified Level 6 and Level 7 using different cut values. . . . .	50
4.4	The expected results after processing to Level 7+ using different cut values. . . . .	54



# Nederlandse Samenvatting

Begin vorige eeuw kwam men tot de ontdekking dat de Aarde voortdurend wordt gebombardeerd door geladen deeltjes die van buiten het Zonnestelsel komen, doorgaans de kosmische straling genoemd. Merkwaaardig genoeg kunnen deze deeltjes tot wel meer dan tien miljoen keer zo veel energie hebben als wat we momenteel met de meest energetische deeltjesversnellers hier op aarde kunnen bereiken. Wetenschappers zijn zich dan ook beginnen afvragen van waar die deeltjes, die voornamelijk protonen bleken te zijn, nu precies vandaan komen en welke fascinerende mechanismen in de ruimte in staat zijn om ze zo veel energie te geven.

Al gauw botsten ze echter op een fundamenteel probleem. Doordat de deeltjes waaruit de kosmische straling bestaat een lading dragen zijn ze onderhevig aan allerlei interacties tijdens hun reis naar de Aarde. Zo worden ze bijvoorbeeld afgebogen door magnetische velden, waaronder dat van de Aarde zelf, of worden ze verstrooid door wolken van gas en stof. Dit betekent dat het detecteren van de kosmische straling hier op Aarde of met behulp van satellieten in de nabije ruimte niet kan uitwijzen waar de deeltjes precies vandaan komen en dus ook niet welke processen er nu juist voor zorgen dat sommigen zo veel energie hebben.

Gelukkig kan een zeer bijzonder elementair deeltje, het neutrino, ons uit deze benarde situatie redden. In tegenstelling tot de kosmische straling draagt het neutrino geen elektrische lading en kan het enkel zwak interageren, wat betekent dat het ongestoord doorheen de ruimte kan propageren. Er wordt verwacht dat daar waar de geladen kosmische deeltjes tot waanzinnige energieën worden versneld de interacties van deze deeltjes met materie in de omgeving leiden tot de productie van neutrino's. Die astrofysische neutrino's bereiken net als de kosmische straling zelf ook de Aarde, met het grote verschil dat zij wel wijzen daar hun bron. Detectie van neutrino's zou ons dus op een zeer elegante manier kunnen vertellen waar de kosmische straling vandaan komt en vooral welke versnellingsmechanismen hen tot zo'n hoge energieën kunnen brengen.

Met dit in het achterhoofd heeft men een gigantische detector gebouwd op de Zuidpool, uiteindelijk tot het IceCube Neutrino Observatory gedoopt en actief sinds 2013. Opgebouwd uit 5160 optische modules verspreid over een kubieke kilometer Antarctisch ijs is het met zijn enorm volume in staat zo'n zelden interagerend neutrino toch af en toe eens op te vangen. Neutrino's die in het ijs interageren geven aanleiding tot de ontwikkeling van lichtsignalen die gedetecteerd worden door de modules. Op basis hiervan worden dan de verschillende eigenschappen van het interagerende deeltje door wetenschappers gereconstrueerd om zo op een vernieuwende manier ons Universum te bestuderen. Het observatorium heeft echter te kampen met zeer veel andere signalen die die van de astrofysische neutrino's overschaduwen, voornamelijk afkomstig van neutrino's en andere deeltjes gecreëerd tijdens botsingen van de kosmische straling met moleculen in de atmosfeer van de Aarde. De voornaamste uitdaging van de meeste IceCube analyses is dan ook de interessante signalen uit de berg van data proberen te halen.

Dit werk tracht de zoektocht naar astrofysische tau neutrino signalen met het Double Bang signatuur in IceCube van Matthias Vraeghe te verbeteren door het toevoegen van een meer geavanceerde statistische methode in zijn data analyse. Het tau neutrino is één van de drie gekende soorten neutrino's met als groot voordeel dat we verwachten dat ze enkel astrofysisch van oorsprong kunnen zijn. Verder levert het Double Bang signatuur, een specifiek tau neutrino signaal, een goede resolutie op bij zowel de bepaling van de energie van het neutrino als richting waaruit het gekomen is. Het bepalen van de hoeveelheid tau neutrino's die de Aarde bereiken per tijdseenheid zou ook interessante informatie kunnen opleveren over de interacties van kosmische straling in de omgeving van hun versnellers. Tot nu toe heeft nog geen enkele IceCube analyse tau neutrino signalen aan het licht kunnen brengen, dit omdat ze niet eenvoudig te onderscheiden zijn van de andere signalen.

De meer geavanceerde statistische methode tracht Double Bang signalen verder te scheiden van de rest aan de hand van een variabele gebaseerd op verschillende likelihooddistributies van parameters geïntroduceerd door Matthias Vraeghe. Op basis van een studie van de methode met gesimuleerde data verwachten we dat de toevoeging ervan aan de analyse de signaal-achtergrond verhoudingen verder verhoogt zonder het aantal overblijvende tau neutrino signalen en meer specifiek het aantal overblijvende Double Bang signalen significant te verlagen.

# Introduction

At the beginning of the 20th century it was discovered that the Earth is constantly bombarded by charged particles coming from outer space, usually referred to as cosmic radiation. To everyone's surprise some of these particles were found to have energies ten million times higher than can be achieved in our most modern particle accelerators. This made scientists wonder where exactly these charged particles, which turned out to be mostly protons, come from and what kind of mechanisms lead to such incredible accelerations.

They soon realized however that merely detecting the cosmic radiation itself would not provide sufficient information to solve both questions. As they are electromagnetically charged these cosmic particles undergo many interactions during their propagation through space, e.g. deflection in magnetic fields or scattering by clouds of gas and dust, meaning that a cosmic radiation particle arriving at Earth does not point towards its origin. This loss of directional information forms a major problem in the search for the origin of cosmic radiations and the study of their acceleration mechanisms.

Fortunately a very peculiar elementary particle, the neutrino, can possibly save us from this seemingly hopeless situation. In contrast to the cosmic radiation particles neutrinos carry no electrical charge and can only interact weakly, meaning they can propagate freely through outer space. We can expect the cosmic radiation to collide with nearby matter right after being accelerated, hereby creating high-energetic neutrinos. Some of these neutrinos will, just like the cosmic ray particles do, reach Earth, with however the main difference that they do point towards their sources. Detection of these astrophysical neutrinos could thus very elegantly show us where the cosmic radiation comes from and reveal the location of the phenomena capable of accelerating charged particles to such high energies.

The property of neutrinos making them ideal astronomical messengers however also makes them very hard to study. Only with gigantic detectors it is possible to detect from time to time one of these highly energetic neutrinos. With this in mind an enormous observatory has been constructed at the South Pole, named the IceCube Neutrino Observatory and taking data since 2013. Consisting of 5160 optical modules spread over a cubic kilometer of Antarctic ice, it can detect astrophysical neutrinos at a modest but feasible rate. Neutrinos interacting with the ice will leave a signal of light which is subsequently observed by the modules, enabling scientists to reconstruct their properties and so study the Universe through a new type of window. Analyses at the observatory however have to deal with a lot of other types of signals overshadowing those of the astrophysical neutrinos, mainly coming from neutrinos and other particles created during the energetic collisions of the cosmic rays with molecules in the atmosphere of the Earth. The main challenge of many IceCube analyses is therefore efficiently distinguishing the signals of interest from a huge amount of other signals.

This work aims to improve the search for astrophysical tau neutrino signals with a Double Bang signature in IceCube by Matthias Vraeghe by including a more advanced statistical approach. The tau neutrino is only one of the three known types of

neutrinos which are believed to be purely astrophysical. Moreover the Double Bang signature, a specific signal that can only be created by tau neutrino interactions, generally yields a good resolution for both the reconstruction of the neutrino energy as well as the direction it came from. Determination of the rate of tau neutrinos arriving at Earth could also tell us something more about the interactions of cosmic radiation at their acceleration sites. So far no IceCube analysis has been able to disclose any tau neutrino events, mainly because they are hard to distinguish from other types of events.

In Chapter 1 an introduction to the standard model used in particle physics is given, mainly focusing on neutrinos. Chapter 2 presents an overview of the study of astrophysical particles, hereby outlining the initial motive for constructing the IceCube Neutrino Observatory. The IceCube experiment is described in more detail in Chapter 3. In Chapter 4 Matthias' analysis as well as the more advanced approach and its performance are discussed, with the conclusions and outlooks given in Chapter 5.

## Chapter 1

# The Neutrino

For quite some time now humanity has been trying to solve one of the most fundamental questions one can ask: What is the Universe made of? The search for satisfying answers has led us to the formulation of all sorts of theories, leading up to the creation of the nowadays well known periodic table and culminating in the so-called Standard Model of particle physics [1, 2]. This model describes our current understandings of matter and their interactions, excluding gravitation, agreeing with all experimental results obtained so far. The recent observation of a new particle compatible with the predicted Brout-Englert-Higgs boson provided the final piece of the puzzle, validating once again the principles and assumptions of the Standard Model [3, 4]. After an overview of the general features of the Standard Model this chapter will focus on the discovery and properties of a specific kind of its postulated particles, the neutrino.

### 1.1 The Standard Model

In order to describe matter and their interactions the Standard Model postulates the existence of so-called elementary particles, particles believed to be point-like and hence not composed of other particles. These elementary particles are then divided into two groups based on their spin value, a property which represents their intrinsic angular momentum. Using units of the reduced Planck constant  $\hbar$  we have particles with an integer spin value, the bosons, and particles with a half-integer spin value, the fermions.

The bosons are listed in Table 1.1, with  $c$  de speed of light in vacuum. Each boson, with the exception of the Brout-Englert-Higgs boson, corresponds to a fundamental interaction. The Standard Model assumes that every possible interaction of particles except for gravitation<sup>1</sup> can be explained with the existence of three fundamental interactions, and that these fundamental interactions take place through the exchange of their corresponding boson. The photon is responsible for the electromagnetic interactions. Coupling to the photon requires an electromagnetic charge, which means particles with no electromagnetic charge cannot undergo electromagnetic interactions. The gluon corresponds to the strong interaction. Only particles with a color charge couple to the gluons. The  $W^\pm$  and  $Z$  bosons correspond to the weak interaction. All elementary particles except for the photon and the gluon can interact weakly. As indicated by its name the weak interaction has by far the smallest coupling constant, implying a very small interaction probability compared to the other two interactions. Of the three interactions only the electromagnetic interaction has

---

<sup>1</sup>Inclusion of gravity is currently one of the main problems of the Standard Model [6]. Given the masses of the subatomic particles, gravitational interaction between these particles can however be completely neglected.

Name	Symbol	Mass (MeV/ $c^2$ )	Electric Charge	Color Charge	Interaction
photon	$\gamma$	0	0	No	Electromagnetic
gluon	$g$	0	0	Yes	Strong
Z boson	$Z$	$91.2 \times 10^3$	0	No	Weak
W boson	$W^\pm$	$80.4 \times 10^3$	$\pm 1$	No	
Brout-Englert-Higgs boson	$H$	$125 \times 10^3$	0	No	

TABLE 1.1: The bosons of the Standard Model together with the corresponding interactions. With spin given in units of  $\hbar$  they have integer spin values. The unit of electric charge is chosen such that the charge of the electron is  $-1$ . The  $W^+$  and  $W^-$  are each others antiparticles. The other bosons form their own antiparticle. The masses of the photon and the gluon given here are the theoretical values. More detailed information can be found in reference [5].

	Name	Symbol	Mass (MeV/ $c^2$ )	Electric Charge	Color Charge
Leptons	electron	$e^-$	0.51	$-1$	No
	electron neutrino	$\nu_e$	$< 2 \times 10^{-6}$	0	
	muon	$\mu^-$	106	$-1$	
	muon neutrino	$\nu_\mu$	$< 2 \times 10^{-6}$	0	
	tau	$\tau^-$	$1.78 \times 10^3$	$-1$	
	tau neutrino	$\nu_\tau$	$< 2 \times 10^{-6}$	0	
Quarks	up quark	$u$	2.2	$2/3$	Yes
	down quark	$d$	4.7	$-1/3$	
	charm quark	$c$	$1.28 \times 10^3$	$2/3$	
	strange quark	$s$	96	$-1/3$	
	top quark	$t$	$173 \times 10^3$	$2/3$	
	bottom quark	$b$	$4.18 \times 10^3$	$-1/3$	

TABLE 1.2: The fermions of the Standard Model divided into leptons and quarks. With spin given in units of  $\hbar$  they have half-integer spin values. The unit of electric charge is chosen such that the charge of the electron is  $-1$ . The dashed lines indicate the further subdivision of the leptons and quarks in generations. The corresponding antiparticles are omitted. More detailed information can be found in reference [5].

an infinite range [2]. The Brout-Englert-Higgs boson is linked to the Brout-Englert-Higgs mechanism which generates the masses of the elementary fermions<sup>2</sup> as well as the massive bosons [7, 8].

As shown in Table 1.2, the fermions are further divided into leptons and quarks. The most widely known lepton is the electron, as it is present in large numbers in matter here on earth. Since it has an electric charge it can interact electromagnetically. Muons and taus have the same properties as the electrons with exception of their higher mass values, implying these leptons are not stable and will eventually decay. All three above-mentioned leptons have a corresponding neutrino. Only a small upper limit on the masses of the neutrinos exist so far. The assumption that they even have non-zero mass values is supported by the observation of neutrino oscillations (see Section 1.4). Of all the elementary fermions only the neutrinos do not carry an electromagnetic or color charge, which means they can only interact weakly. The quarks have besides an electric charge also a color charge, implying the quarks can interact strongly as well. Quarks can change their type through the weak interaction, preferring transition within the same generation. They are by definition the primary constituents of all the hadrons, which includes the baryons and the mesons. Baryons are particles composed of three quarks, like the proton and the neutron, while mesons consist of a quark and an antiquark, e.g. the pion and the kaon.

The Standard Model also includes the concept of antiparticles. Every particle has its corresponding antiparticle<sup>3</sup>, which has the same mass but carries opposite charges. For electric charges this translates to a change of sign, while opposite color charges are represented by anticolors. Besides charges other so-called quantum numbers of particles and their corresponding antiparticles have opposite values as well. These are numbers related to conservation laws postulated by the Standard Model. Next to the conservation of energy, which leads to for example the constraint of particle decays to lower mass particles only, and the conservation of charge, also laws like the conservation of lepton numbers and the conservation of baryon number pose restrictions on the possible reactions. Every lepton generation has its own lepton number with a value of 1 for the two particles belonging to that generation, a value of  $-1$  for their corresponding antileptons and a value of 0 for all other particles. The quarks have a baryon number value of  $1/3$ , while the antiquarks have a baryon number value of  $-1/3$ . All other elementary particles have a baryon number value of 0.

## 1.2 Discovery of the Neutrino

As mentioned in the previous section the neutrinos are the only elementary fermions that do not carry an electromagnetic or color charge, which leads to the conclusion that neutrinos only participate in weak interactions. Consequently a neutrino will rarely interact, providing the main reason why its discovery is a rather unique story [9, 10].

The existence of the neutrino was postulated to solve the problem concerning beta decays, a decay in which a radioactive nucleus emits an electron. Treating this decay as a two-body problem, the first body being the nucleus and the second one

---

<sup>2</sup>It is actually not yet clear if this holds true for the neutrinos, as their remarkably low mass values may suggest another mass-generating mechanism. A plausible candidate here is the so-called seesaw mechanism.

<sup>3</sup>A particle can also be its own antiparticle, as is the case with the neutral bosons.

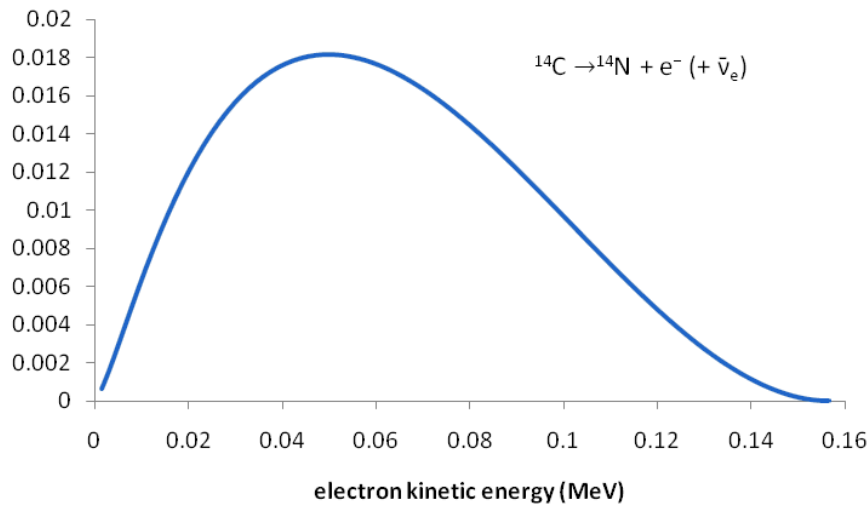


FIGURE 1.1: The fraction of electrons emitted during the beta decay of a  $^{14}\text{C}$  nucleus in function of the energy [11]. The blue curve clearly shows a continuous spectrum, in contrast to the prediction of a two-body model of the decay.

the electron, and using the principle of conservation of energy and momentum it can be shown that the energy of the emitted electron should be the same for every decay. However, as illustrated in Figure 1.1, the energy spectrum of the emitted electrons forms a broad peak, contradicting this prediction.

As the conservation of energy and momentum is a well-established and fundamental law of physics, many scientists felt simply dismissing it did not provide an acceptable solution. Therefore Wolfgang Pauli suggested in 1930 that the beta decay actually consists of a three-body system made up of the nucleus, the electron and a yet unseen third particle. Including this third particle the prediction of the fixed electron energy no longer holds, indeed solving the beta decay problem. In order to preserve the conservation of charge and explain why it was never seen before, the new particle had to be neutral. In the following year the neutron was discovered which, as the beta decay energy spectrum required a neutral particle with much lower mass value, inspired Enrico Fermi to name Pauli's new particle the neutrino<sup>4</sup>.

Fermi further developed a theory of beta decay including the neutrino, leading him to the first formulation of the weak interaction [12]. In the following years a lot of experiments were carried out with the aim to study beta decays of other nuclei and although all results agreed beautifully with Fermi's theory the demand of the detection of the neutrino as final proof remained. In 1954, 24 years after its postulation, such proof was presented by Fred Reines and Clyde Cowan. The Standard Model, as did Fermi, describes the beta decay of a nucleus as the decay of a neutron inside the nucleus to a proton, hereby emitting an electron and an electron antineutrino<sup>5</sup>:

$$n \rightarrow p + e + \bar{\nu}_e .$$

As can be understood from Section 1.1, the creation of the electron antineutrino ensures the conservation of lepton numbers. If an abundant source of protons would

<sup>4</sup>In the Italian language the prefix '-ino' can be used to make a diminutive of a word.

<sup>5</sup>The existence of the different generations of leptons was not yet exposed at the time Fermi formulated his theory, leading him to refer to the electron antineutrinos as just antineutrinos.

be placed close by an intense flux of electron antineutrinos, the reaction

$$p + \bar{\nu}_e \rightarrow n + e^+$$

is expected to take place. Hereby  $e^+$  is the antielectron, more commonly referred to as the positron, with the symbol denoting its positive charge. This is exactly what Cowan and Reines relied upon. By placing giant tanks filled with water as proton sources close by a nuclear reactor at the Savannah River Plant in South Carolina, the two scientists were able to observe the created neutrons and positrons through their characteristic emission of gamma rays [13].

Around the same time of the postulation of the neutrino and the development of Fermi's theory the existence of the muon was discovered [14, 15]. About a decade before the Reines-Cowan experiment it was found to decay to a single electron, which again hinted to the existence of yet undetected neutral particles. As the spectrum of the electron energy once more demanded a three-body system, it was assumed that now not one but two such particles accompanied the electron. Most physicist felt these two particles should be different, something that could only be demonstrated in 1962 by Leon Lederman, Melvin Schwartz and Jack Steinberger [16, 17]. They established the existence of two different kinds of neutrinos by showing that in the reactions of the form

$$\nu + n \rightarrow p + l^-,$$

with  $l^-$  a negatively charged lepton, the assumed second type of neutrinos only yields protons accompanied with muons. Keeping in mind the principle of conservation of lepton numbers, the Standard Model indeed only allows the reactions

$$\begin{aligned} \nu_e + n &\rightarrow p + e \\ \nu_\mu + n &\rightarrow p + \mu, \end{aligned}$$

while ruling out the reactions

$$\begin{aligned} \nu_e + n &\rightarrow p + \mu \\ \nu_\mu + n &\rightarrow p + e. \end{aligned}$$

The result of the experiment of Lederman, Schwartz and Steinberger's demanded a distinction in lepton numbers, dividing the four leptons into an electron generation and a muon generation and thus demonstrating the existence of different types of neutrinos. For the decay of the muon we then find

$$\mu \rightarrow e + \nu_\mu + \bar{\nu}_e,$$

once again in agreement with the principle of conservation of lepton numbers.

The discovery of the tau lepton in 1975 by Martin Perl and collaborators led to the assumption of the existence of a third kind of neutrino, forming together with the newly discovered particle a third generation of leptons [18]. Its detection could however only be established 25 years later by the DONUT (Direct Observation of the NU Tau) Collaboration at Fermilab [19]. It was predicted that the production of  $D_S^+$  mesons, particles made from a charm quark and a strange antiquark, would through leptonic decays yield antitau leptons accompanied by tau neutrinos. In the same way  $D_S^-$  mesons, particles made from a charm antiquark and a strange quark, can lead to the creation of tau leptons accompanied by tau antineutrinos. The two

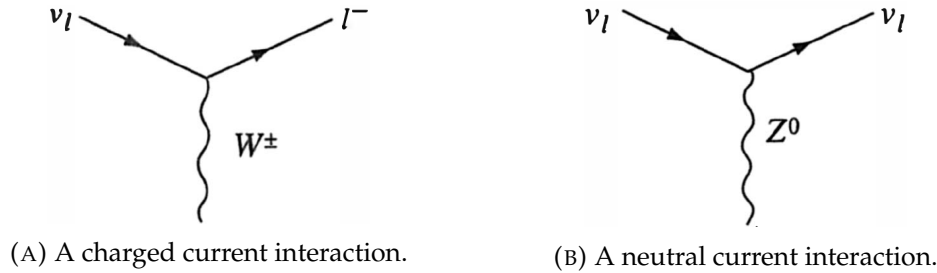


FIGURE 1.2: The two possible types of neutrino interactions [7].

reactions are simply given by

$$\begin{aligned} D_S^+ &\rightarrow \tau^+ + \nu_\tau \\ D_S^- &\rightarrow \tau^- + \bar{\nu}_\tau . \end{aligned}$$

Letting these neutrinos interact with steel plates through the same reaction used by Schwartz and Steinberger to demonstrate the existence of a second type of neutrinos now resulted in the creation of tau leptons, confirming the existence of the expected third type of neutrinos. As shown in Table 1.2, the existence of the three types of neutrinos, often referred to as the three different neutrino flavors, is currently still a feature of the Standard Model of particle physics.

### 1.3 Neutrino Interactions

As mentioned before the neutrino can only interact weakly, implying it couples to the  $W^\pm$  and  $Z$  bosons only. A neutrino interacting through the exchange of a  $W^\pm$  boson is referred to as a charged current (CC) interaction, while an interaction through the exchange of a  $Z$  boson is called a neutral current (NC) interaction. The corresponding diagrams are shown in Figure 1.2. Both of these diagrams respect indeed the principles of conservation of charge and lepton numbers. During a charged current interaction the neutrino is transformed into its corresponding lepton. Depending on whether it is incoming or outgoing the charge of the  $W$  boson will be respectively negative or positive, while the charge of the lepton will always be negative. In case of an antineutrino the signs of all the charges are reversed. Only in the neutral current interaction the outgoing particle is again a neutrino.

Interactions can occur both elastic or inelastic. In an elastic interaction the resulting particles are the same as the initial ones, while in an inelastic interaction they can be different. The neutrino interactions of most importance later on in this work are deep inelastic scattering processes with nucleons, i.e. a proton or a neutron [20]. During such process an incoming neutrino interacts with a constituent quark of the nucleon, hence the term deep, through a CC or NC interaction, transferring a substantial amount of energy and momentum to the quark and so leading to its emission out of the nucleon. As the quarks mainly interact through the strong interaction the emission of the quark leads to hadronization, i.e. the creation of additional quarks forming new hadrons. This way the nucleon shatters into lots of new particles after the interaction, as shown in Figure 1.3.

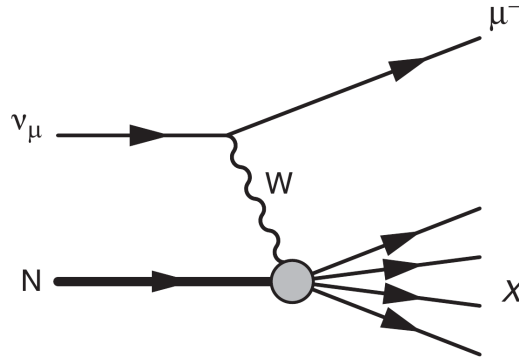
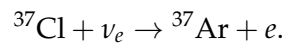


FIGURE 1.3: Example of a neutrino deep scattering process [8].

## 1.4 Neutrino Flavour Oscillations

The neutrinos have been assumed massless for a long time. It was only due to the discovery of a peculiar property of the neutrinos that the current Standard Model now incorporates non-zero neutrino mass values: neutrino oscillations.

The nuclear fusion processes in the Sun produce next to our daily dose of sunlight also a large flux of electron neutrinos, more commonly referred to as solar neutrinos. In the sixties physicists like John Bahcall and Ray Davis devoted time and effort in calculating the expected solar neutrino flux at the surface of the Earth and designing an experimental setup able to compare it with measurements [21]. These attempts led to the construction of the famous Homestake Solar Neutrino Experiment, announcing its first results in 1968 and earning Davis the Nobel Prize in physics in 2002 [8, 22]. Using a tank filled with 380 000 liters of perchloroethylene ( $C_2Cl_4$ ) located in the Homestake Gold Mine to shield it from background effects, Davis was able to detect solar neutrinos based on the inverse  $\beta$ -decay process



By extracting the newly formed radioactive  ${}^{37}\text{Ar}$  atoms from the tank and subsequently counting them through their radioactive decays, a rate of approximately one neutrino every two days was observed. The expected rate of neutrino detections however was about three times higher, around 1.7 neutrino interactions a day. This remarkable disagreement between theory and experiment became known as the solar neutrino problem and in the following decades several other neutrino experiments based on different detection methods confirmed the deficit of electron neutrinos coming from the Sun [23, 24, 25].

The most obvious explanation solving the mystery would simply be incorrect calculations of the expected solar neutrino flux. However, throughout the remainder of the 20th century these calculations were revised and refined many times by different researchers without any progress towards a solution [26]. To top it off the theoretical model of the sun agreed well with all other observations, making it seem even more unlikely the disagreement between theory and experiment was due to a misunderstanding in the solar processes. Therefore a more exciting and intriguing explanation was needed. Already in 1969 Bruno Pontecorvo and Vladimir Gribov had come up with an idea that eventually would solve the solar neutrino problem, suggesting neutrinos propagate differently than initially thought. If the neutrinos do have a non-zero mass value, however small it may be, the Standard Model can allow them to undergo flavor oscillations. A neutrino that initially started out as one

type of neutrino can switch into the other types back and forth during travel of large distances, in this way oscillating between the different neutrino flavors.

At first few physicists took their idea seriously, but as more and more observations were made the idea of neutrino flavor oscillations started to gain in popularity. The decisive evidence was delivered by the Sudbury Neutrino Observatory (SNO), designed to measure both the electron neutrino flux as well as the total neutrino flux coming from the Sun [8, 26, 27]. Using 1000 tons of heavy water, consisting of  $D_2O$  molecules with D the bound state of a proton and a neutron usually referred to as the deuteron, the SNO collaboration was able to observe three different types of neutrino interactions. The CC interaction

$$\nu_e + D \rightarrow e + p + p$$

creates an electron and is sensitive to the electron neutrino flux only. A detectable neutron is created in the NC interactions

$$\nu_l + D \rightarrow \nu_l + n + p,$$

in which all neutrino flavors can participate. Finally elastic scattering processes with the atomic electrons,

$$\nu_l + e \rightarrow \nu_l + e,$$

provide an additional way of detecting again all neutrino flavors. The combined measurements of these three different interactions indeed yields sufficient information to determine both the the electron neutrino flux and the total neutrino flux, even presenting constraints on the  $\nu_\mu + \nu_\tau$  flux as well. As no muon or tau neutrinos are created by the sun, the total observed  $\nu_e + \nu_\tau$  flux should be consistent with zero if neutrinos do not undergo flavor oscillations. However the SNO experiment did observe a substantial  $\nu_e + \nu_\tau$  flux, about twice the value of the solar electron neutrino flux, for the first time ever giving clear evidence for neutrino flavor oscillations. To everyone's great relief the total solar neutrino flux measured by the SNO experiment was also consistent with the predicted electron neutrino flux generated by the Sun, which means that the concept of neutrino flavor oscillations indeed clears up the otherwise hard to solve solar neutrino problem.

The extend to which neutrinos undergo these flavor oscillations depends on their masses. No neutrino masses would mean no oscillations. The fact that we do observe neutrino flavor oscillations thus assures us that neutrinos have non-zero masses. No experiment to date has however been able to determine their exact values. At the moment the most accurate constraint is obtained from cosmology [8]. As they contribute to the total mass density of the Universe, the mass values of the neutrinos have an impact on its evolution following the Big Bang. Cosmological measurements therefor seem to indicate that the sum of the neutrino masses should at most be something of the order of  $1 \text{ eV}/c^2$ :

$$\sum_{i=1}^3 m_i \lesssim 1 \text{ eV}/c^2.$$

The neutrinos are thus by far the lightest fermions currently included in the Standard Model. Together with their other peculiar properties it should not be surprising a lot of efforts are still made in the study of neutrinos, originally introduced to account for an anomaly in the beta decays of radioactive nuclei, in the hope they will once again cause commotion and excitement in the world of subatomic physics.

## Chapter 2

# Astroparticles

With its approximately 27 km circumference and collision energy of about 13 TeV, the LHC at CERN is currently the largest and most energetic particle accelerator on Earth. This technical feat enabled the discovery of the Brout-Englert-Higgs boson and is to date still used intensively in a variety of studies. However astonishing our man-made accelerators may be, they are by far surpassed by accelerating mechanisms taking place throughout the cosmos. Cosmic rays, charged particles mainly originating from outside the Solar System of which some have incredible amounts of energy, are bombarding Earth's atmosphere at a constant rate, leaving scientists to wonder what kind of processes can lead to such accelerations. This chapter will give a brief overview of the study of astrophysical particles, in which a distinction can be made between photons in the form of high-energy gamma-rays, the charged particles making up the cosmic rays and finally astrophysical neutrinos. As they are not relevant for this work, the high-energy gamma-rays and low-energy astrophysical neutrinos, like solar neutrinos, will not be discussed.

## 2.1 Cosmic Rays

### 2.1.1 Discovery

The existence of cosmic rays was first established by Victor Hess in 1912 [28]. He did so by measuring the ionization of air during a balloon flight. Assuming the Earth is the only source of ionizing radiation, one would expect the ionization of air to drop as the balloon climbs in altitude. During the rise of the first few 100 meters this is indeed what Hess observed. Starting around an altitude of about 1 km he noticed however that the ionization of the air began to increase again, as shown by Figure 2.1 a trend that continued to last as he rose higher and higher. These results can easily be explained by considering the possibility of the existence of ionizing radiation penetrating the atmosphere from above. As this radiation needs to travel further through the atmosphere in order to get closer to Earth's surface we can indeed expect its ionization capabilities to increase with altitude. As there was no change in ionization during the night or solar eclipse, the Sun could readily be excluded as a possible source.

### 2.1.2 Primary and Secondary Cosmic Rays

Cosmic rays can be subdivided into two groups based on their origin. The charged particles originating from astrophysical sources form the primary cosmic rays. Upon impact with Earth's atmosphere these primary cosmic rays, as well as incoming gamma-rays and astrophysical neutrinos, can create showers of particles which will

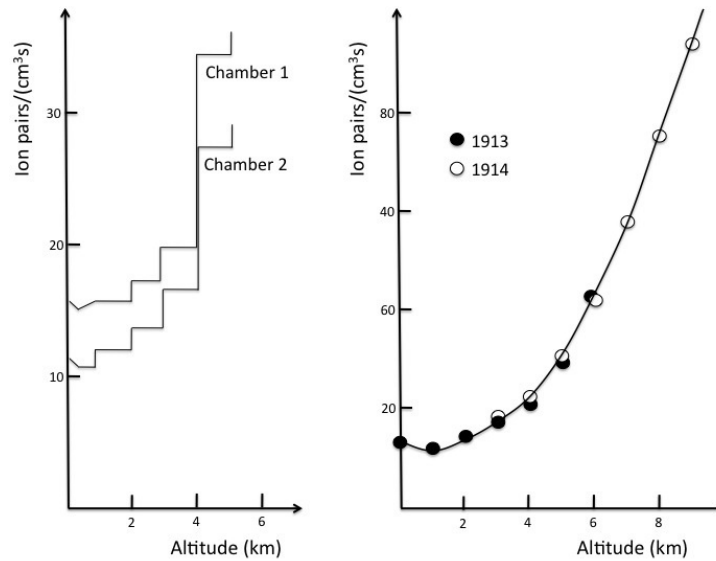


FIGURE 2.1: The increase of ionizing radiation with altitude [29].  
 Left: The results of Victor Hess. Right: The results of a reproduction of the experiment by Kolhörster.

then travel further towards the surface, of which the charged components are called secondary cosmic rays.

In 1929 Walter Bothe and Werner Kolhörster were able to show using a Geiger-Müller counter that the tracks of cosmic rays observed on ground level are curved by magnetic fields [30], indicating the charged nature of the secondary cosmic rays. Nowadays dedicated observatories like the Pierre Auger Observatory in Argentina are being used to study the air showers created in the atmosphere in more detail. Most of the showers are initiated by the primary cosmic ray nuclei entering the atmosphere [31]. The secondaries created in the initial interaction will in their turn start additional cascades of interactions, contributing to the air shower. The majority of collision processes in the atmosphere involve hadrons leading to the creation of both neutral as well as charged mesons, mainly pions and kaons. Muons and neutrinos join the shower through the decay of the newly created charged mesons. The neutral mesons together with a fraction of the muons start off electromagnetic cascades, including electrons, positrons and photons. As the shower advances towards the surface it also spreads out laterally, this way reaching a radius of several meters up to a few kilometers depending on the type of primary particle. An example of a small air shower is shown in Figure 2.2.

During the years following the discovery of the cosmic rays a heated debate arose concerning the nature of the primary particles. The renowned physicist Robert Millikan favored a theory of primary gamma rays, introducing the name cosmic rays, while the equally well-known physicist Arthur Compton supported the possibility of charged particles as primaries [33, 34]. Even though we still use the term used by Millikan several observations started to make clear the primary particles reaching the atmosphere of the Earth carry a positive electrical charge, ending the discussion in Compton's favor. The discovery of the latitude effect by Jacob Clay, a term given to the observation that the measured cosmic ray intensity depends on the latitudinal position on Earth, could be ascribed to the geomagnetic field by Bothe and Kolhörster given the primary cosmic rays are made up of charged particles. This idea was supported by evidence showing that more cosmic rays are coming from the west

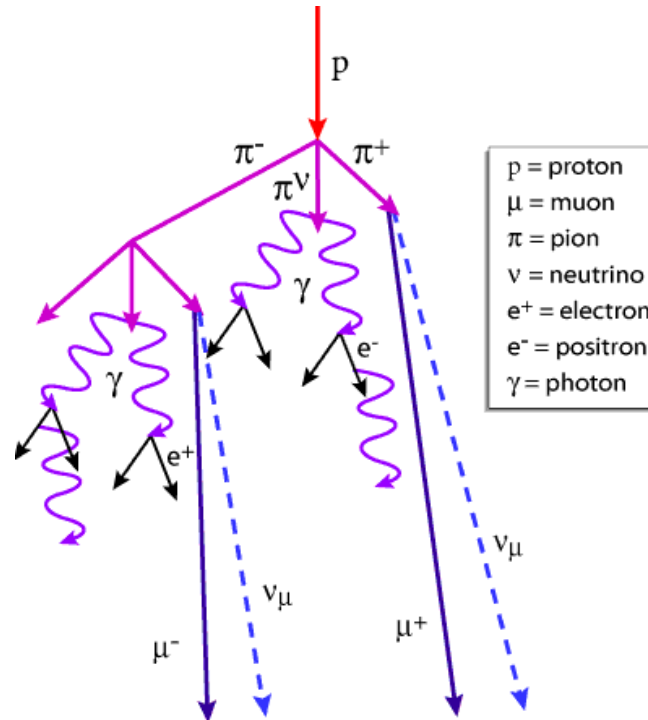


FIGURE 2.2: Illustration of a small air shower created in the atmosphere by an incident proton [32].

than from the east. The determination of the sign of this so-called east-west asymmetry in 1934 showed that the primaries are positively charged particles. The following decades have led to experiments using more advanced balloon-borne or even space-based equipment, demonstrating that the primary cosmic rays are mainly composed of protons. Figure 2.3 shows a combination of the results of several experiments studying the composition of primary cosmic rays in different energy ranges, with the proton indicated as a hydrogen nucleus.

### 2.1.3 Energy Spectrum

Perhaps the most fascinating property of the cosmic rays is the energy spectrum of the primaries, showing how much particles with a given energy reach Earth's atmosphere. Keeping in mind that currently the most powerful accelerator on Earth can reach collision energies of about  $13 \times 10^{12}$  eV, Figure 2.4 clearly shows that somehow in outer space particles can be accelerated up to energies more than  $10^7$  times larger than we have ever been able to. Apart from its incredible energy range the spectrum exhibits some other interesting features [5, 35]. We see that in general

$$F(E) \propto E^{-\gamma}, \quad (2.1)$$

which clearly has the form of a power law, with  $F(E)$  the flux of incoming primary cosmic rays and  $\gamma$  the spectral index. Starting at energies of the order  $10^{10}$  eV the energy spectrum falls with a spectral index of -2.7. Arriving at energies of about  $10^{15} - 10^{16}$  eV the spectrum suddenly steepens towards a spectral index of -3.1. This sudden steepening is commonly referred to as the knee of the energy spectrum. Approaching the energy range of  $10^{18.5}$  eV the spectrum becomes less steep again, forming what is called its ankle. These sudden changes in the spectral index seem to indicate that there are different sources and acceleration mechanisms at work.

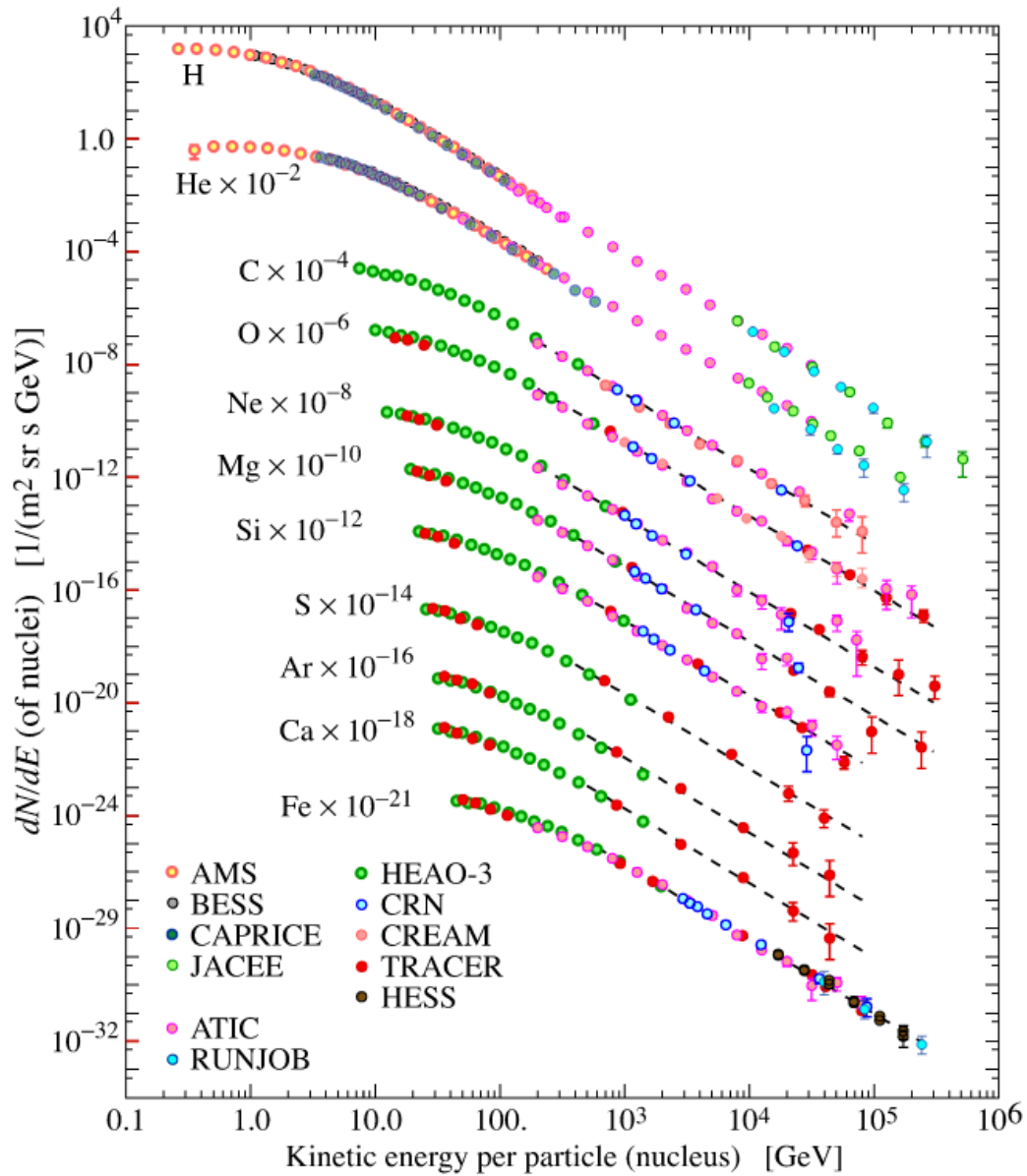


FIGURE 2.3: Fluxes of nuclei of the primary cosmic radiation in particles per energy-per-nucleus in function of energy-per-nucleus [5].

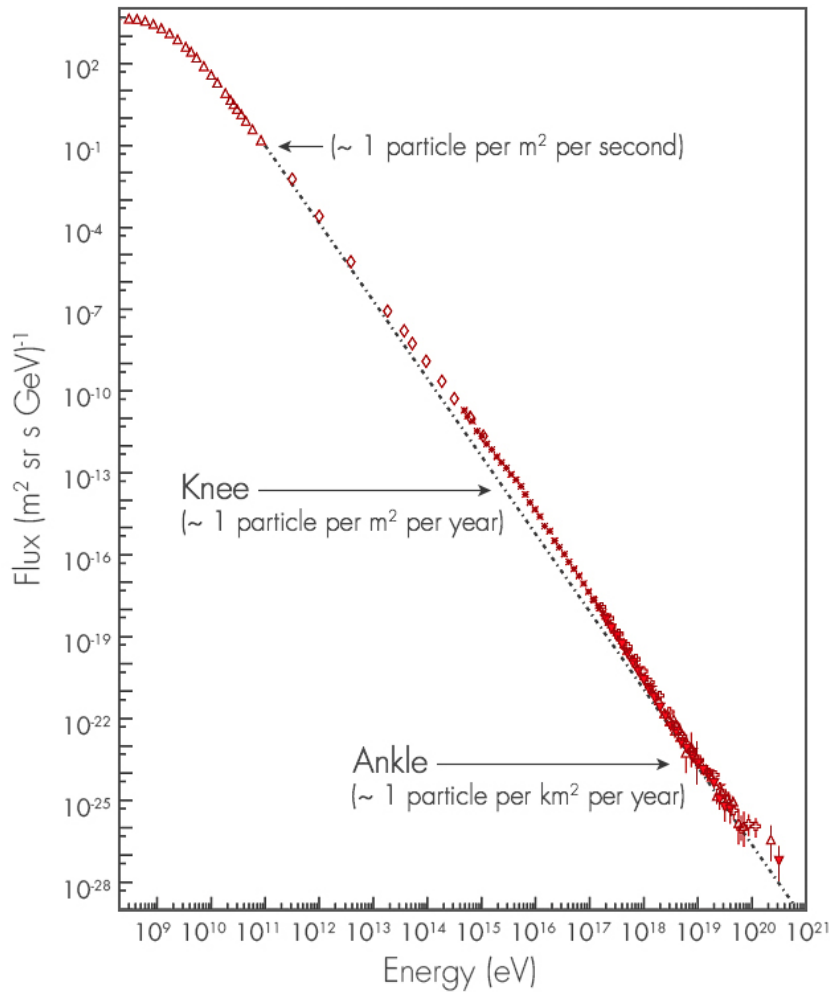


FIGURE 2.4: The flux of incoming primary cosmic rays in function of energy-per-nucleus [36].

The power-law form of the spectrum already holds some significant information concerning the origin and acceleration mechanisms of the cosmic rays. Sources emitting radiation due to their non-zero temperature like stars are not able to generate power-law shaped energy spectra, indicating that cosmic rays are produced through non-thermal processes [28]. Any mechanism hypothesized as a possible source of cosmic rays should be able to reproduce the power-law shape of the energy spectrum, as it is clearly one of its most prominent features. Only for the lowest energies shown in Figure 2.4 the power law (2.1) does not seem to hold. This can however readily be explained by taking into account the solar modulations [28]. Through the emission of solar winds, streams of charged particles carrying a magnetic field, spreading out throughout the solar system the Sun slows down incoming cosmic rays and prevents the least energetic ones from reaching Earth. This indeed creates a deficit from a power-law behavior towards smaller fluxes in the low-energy range of the spectrum as shown in Figure 2.4. It also implies that the sources in fact generate an energy spectrum which is less steep as the one measured on Earth.

### 2.1.4 Galactic Cosmic Rays

Observations done so far have led to the conclusion that except for the most energetic ones the cosmic rays reaching Earth originate from within our own galaxy, the Milky Way. These cosmic rays are known as galactic cosmic rays. Assuming the locally measured kinetic energy density of the cosmic rays, corrected for the effects of the solar winds, applies throughout the entire Universe leads to the conclusion that about 1% of the energy of all baryons would correspond to relativistic particles<sup>1</sup> [28]. As this is rather unlikely the measured kinetic energy density of the cosmic rays seem to indicate at least a significant portion of the cosmic rays are concentrated in the disk of the Milky Way.

Moreover, as shown in Figure 2.5, the abundances of elements observed in the cosmic rays are very similar to those of the Solar System, again suggesting the cosmic rays are bound to star systems like galaxies. The remarkably higher abundances in elements with a nucleus composed of even amounts of protons and neutrons, indicated by an even atomic number  $Z$ , in both composition curves is due to the fact that these nuclei are simply more stable. The discrepancies between the composition of the cosmic rays and that of the Solar System can be explained by taking into account different possible spallation processes. During their propagation within our galaxy the cosmic rays are subject to numerous interactions, causing the nuclei of heavier elements to break up in parts. This way nuclei of the Li-Be-B group ( $Z = 3 - 5$ ) and the Sc-Ti-V-Cr-Mn group ( $Z = 21 - 25$ ) are created out of respectively the C-N-O group ( $Z = 6 - 8$ ) and the Fe-Co-Ni group ( $Z = 26 - 28$ ).

Finally a third piece of evidence hinting at the galactic origin of cosmic rays can be found by looking at the gamma-ray emission in the galactic plane [37]. Cosmic ray protons interacting with protons of interstellar gas should lead to the production of neutral pions, which through their decay would then create gamma ray photons. Current observations in the gamma-ray window have indeed demonstrated the existence of the so-called pion bump, i.e. an excess of gamma rays in the energy interval corresponding to photons generated by pion decay, coming mainly from the galactic plane and so revealing most of the cosmic rays originate from within our galaxy.

The basically stable rate of galactic cosmic rays over at least a period approaching the order of  $10^9$  years, which can be deduced e.g. from the study of meteorites, implies we should look for continuous sources [39]. Throughout the years multiple processes taking place in the Galaxy have been proposed as acceleration mechanisms for galactic cosmic rays, most of them connected to type II supernovae (SN) or their remnants [28]. When very massive stars reach the end of their fusion processes, i.e. when their core is completely fused to iron, they can no longer counter the ever present gravitational pressure, leading to the collapse of the star. As a result the density increases tremendously and through inverse beta decay protons together with free electrons start to form neutrons and by neutrinos. The neutrinos, subject to weak interactions only, can easily flee from the violent incident, while the neutrons start to form a proto-neutron star. Due to the core density now reaching extreme values this forming process is characterized by a powerful shock wave propagating outwards, further heated by the neutrino emission and in the end leaving behind either a neutron star or a black hole. With an energy release of the order of several  $10^{56}$  MeV, of which 99% is emitted through neutrinos, 1% is transferred into kinetic energy of the exploding star and only 0.01% is released in the form of photons, a typical supernova II event are the most energetic phenomena of our galaxy. It can

<sup>1</sup>Relativistic particles are particles with a velocity approaching the speed of light in vacuum, meaning Einstein's laws of special relativity apply.

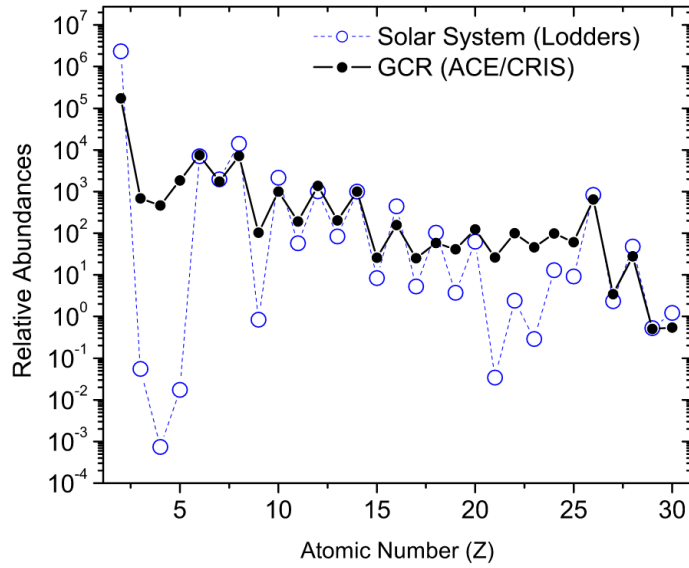


FIGURE 2.5: Abundances of elements observed in the cosmic rays (GCR) and elements in the proto-sun (Solar System abundances), normalized to 1000 for Si [38].

be shown that with an average SN rate in the Milky Way of one every thirty years only about 1% of the kinetic energy released during the SN explosion needs to be converted into the acceleration of charged particles in order to explain all galactic cosmic rays, a scenario that does not seem unlikely.

One possible acceleration mechanism uses pulsars, neutron stars born fast rotating with a strong magnetic field. Study of the Crab nebula, the remnant of a SN observed by Chinese astronomers in 1054 housing the Crab pulsar and shown in Figure 2.6, indicates that they can create strong electromagnetic fields able to accelerate charged particles up to considerable energies. The currently most realistic models describing acceleration by pulsars indicate however this hypothesis comes with some problems, like high energy losses due to synchrotron radiation<sup>2</sup> and presence of a hampering plasma. Probably only young pulsars contribute to the acceleration of cosmic rays, which means most of the charged particles reach their high energies through other mechanisms.

A popular acceleration mechanism is the first-order Fermi acceleration through SN shock waves [28, 40]. This acceleration model describes the effect of the moving shock front following a supernova explosion on charged particles. During their encounter with the shock front the charged particles gain energy proportional to its velocity. A significant amount of particles get trapped in the shock wave and are scattered back and forth, repeatedly gaining energy not unlike a ping-pong ball during a heated game. One of the main assets of this acceleration mechanism is that, next to being very efficient, its outcome is mainly determined by the characteristics of the shock hydrodynamics only. This elegantly leads to the sought-after power law a spectral index independent of the properties of the accelerated particles. The theory of shock acceleration however comes with some assumptions that have never been validated so far by first-principles calculations or clear observations.

As a result of interactions during their propagation through the Galaxy, several radionuclides like  $^{10}\text{Be}$ ,  $^{26}\text{Al}$ ,  $^{36}\text{Cl}$  and  $^{54}\text{Mn}$  are expected to be found among the

<sup>2</sup>Synchrotron radiation is the electromagnetic radiation emitted by charged particles when undergoing radial acceleration.

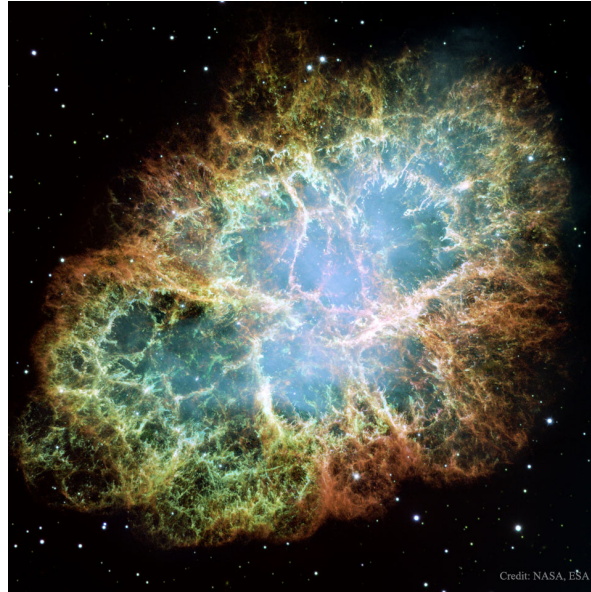


FIGURE 2.6: The Crab nebula, taken by the Hubble Space Telescope [42]. It is the remnant of SN1045, a supernova observed by Chinese astronomers in 1054.

cosmic rays [41]. As these radionuclides are subject to  $\beta$ -decay they are not stable, meaning their abundances can be used to determine the average time cosmic rays propagate through the Milky Way before reaching Earth. A high abundance of these nuclides means that the period between the start of their propagation through the Galaxy, i.e. the moment they start producing the radionuclides, and the moment they reach the Earth is relatively short, while a low abundance means this period is rather large. Measurements using these radioactive clocks indicate the period of propagation through the Galaxy is of the order of several  $10^6$  years. This long timescale can only be explained if the propagation of cosmic rays through the Milky Way is not simply a straight line, but instead resembles a random walk<sup>3</sup> [28]. This could be due to random scattering of the cosmic rays on interstellar matter or diffusion of the particles in turbulent magnetic fields. As high-energy particles only have a small scattering probability and are mainly scattered in forward direction, the main reason is probably the diffusion in turbulent magnetic fields. An important consequence of the random-walk like propagation of the galactic cosmic rays is that they lose all directional information. The cosmic rays observed on Earth do not point towards their sources, forming one of the main reasons why the search for galactic sources and acceleration mechanisms is non-trivial and to date still ongoing.

### 2.1.5 Extragalactic Cosmic Rays

Since the discovery of the knee in the cosmic ray energy spectrum several explanations have been put forward in an attempt to clarify the origin of this feature. One possible explanation could be the leakage of cosmic rays with energies of about  $10^{15} - 10^{16}$  eV or more from the Galaxy [35]. A second explanation suggests that most of the galactic accelerators have reached their maximum energy at this point, with the ankle reflecting the overtaking of an extragalactic population of cosmic rays

<sup>3</sup>A random walk describes a path build up of straight lines, one connected to the other in a random direction.

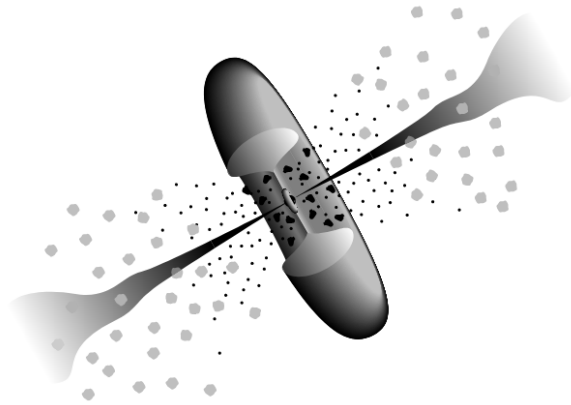


FIGURE 2.7: An illustration of an AGN showing the central black hole surrounded by an accretion disk, emitting two jets perpendicular on the plane of the disk [43].

which dominates at sufficiently high energies. Whatever the exact reason might be, the fact is that the energy limits of the most plausible acceleration mechanisms of galactic cosmic rays discussed in Section 2.1.4 are expected to lie several orders of magnitude below the highest measured cosmic ray energies. It thus seems very plausible the cosmic rays falling in the tail of the energy spectrum find their origin outside of the Milky Way, which are therefore referred to as extragalactic cosmic rays.

A rough estimate suggests that the minimal power dissipated by an accelerator accelerating charged particles up to  $10^{20}$  eV is of the order of  $10^{37}$  W [28]. As the observed energy density of these ultrahigh energy cosmic rays (UHECR) is about  $3 \times 10^{39}$  J/(Mpc<sup>3</sup>yr) the density of their sources should be roughly  $10^{-5}$  Mpc<sup>-3</sup>. Since one of its most common types has a density of approximately  $(1 - 5) \times 10^{-5}$  Mpc<sup>-3</sup> this points to active galactic nuclei (AGNs). AGNs are galaxies with an extreme luminous center region, probably due to it containing a supermassive black hole with a mass of a million to a few billion times that of the Sun in their center [43]. Although it could very well be that such supermassive black holes can be found in every galaxy, only those able to aggregate matter from its surroundings will lead to a remarkable increase in luminosity of its host. In doing so the black hole converts gravitational energy of its surroundings to form two collimated jets, twisted magnetic fields accelerating ionized matter. An illustration of an AGN is shown in Figure 2.7. With their jets as acceleration mechanism the AGNs indeed form a plausible origin of extragalactic cosmic rays.

Another astronomical phenomenon that might be at the origin of extragalactic cosmic rays are the very short and intense explosions observed at cosmological distances throughout the universe, known as gamma-ray bursts [44, 45]. The process powering this highly energetic event might be once again the aggregation of a massive disk by a heavy and compact body, most likely a black hole. An other possibility could be the collapse of a massive star, called a hypernova, collapsar or failed supernova. These bursts are at the moment best described by the so-called relativistic fireball model, indeed allowing the possibility of extreme particle acceleration and hence production of UHECR.

Just like the galactic cosmic rays also the extragalactic cosmic rays can be expected to lose all directional information during their propagation towards Earth.

Simply detecting the cosmic radiation will thus never disclose the origin of its galactic component nor that of its extragalactic component. Fortunately other astrophysical messengers are out there, which just might contain all the information we need.

## 2.2 Astrophysical Neutrinos

### 2.2.1 Predictions

At their production sites or along their path of travel cosmic rays are expected to interact with other hadrons or photons, leading to the creation of pions and kaons [46]. These mesons will then decay, mainly into muons, resulting in the creation of neutrinos:

$$\begin{aligned} \pi^+ (K^+) &\rightarrow \mu^+ + \nu_\mu & \pi^+ (K^-) &\rightarrow \mu + \bar{\nu}_\mu \\ \mu^+ &\rightarrow e^+ + \nu_e + \bar{\nu}_\mu & \mu &\rightarrow e + \bar{\nu}_e + \nu_\mu \end{aligned} \quad (2.2)$$

Therefore besides energetic charged particles also high energy neutrinos of astronomical origin are expected to reach Earth's surface. If indeed produced at the cosmic ray production sites, studying the astrophysical neutrinos would yield unique and valuable information about the extraordinary accelerators at work throughout the Universe. As they can only interact weakly neutrinos, in contrast to cosmic rays, are not affected by matter, radiation or magnetic fields during their travels, still containing information about their initial energy as well as pointing towards their origin when reaching Earth. For this reason astrophysical neutrinos are often called ideal messengers. Similar to the cosmic rays it is natural to divide the astrophysical neutrinos in galactic and extragalactic neutrinos, both containing diffuse neutrinos as well as neutrinos originating from point sources or compact regions of the sky [47].

The galactic neutrinos are expected to mainly come from reactions of the cosmic rays with the interstellar medium of the Milky Way [47], creating a diffuse neutrino flux. Their energy spectrum is expected to greatly resemble the power-law like structure of that of the cosmic rays. Next to interactions with the interstellar medium throughout the entire Galaxy also individual neutrino sources in the galactic plane are expected, revealing individual galactic cosmic ray accelerators. Point sources could be for example supernova remnants accelerating particles in nearby molecular clouds.

The cosmogenic neutrinos form the diffusive component of the extragalactic neutrinos [47]. These are neutrinos produced by ultra-high energy cosmic rays interacting with the cosmic microwave background<sup>4</sup>. In the same way astrophysical neutrinos are expected to come from interactions in the Milky Way other galaxies are expected to act as point sources for extragalactic neutrinos. Galaxies with higher star formation rates will generate higher neutrino fluxes, as this implies more supernova explosions and hence more cosmic rays. Interactions between the photons of intense radiation fields and cosmic ray protons in the inner regions of active galactic nuclei or gamma-ray bursts would form point sources for extragalactic neutrinos as well.

As most of the astrophysical neutrinos are assumed to be produced in the decays of pions, kaons and their corresponding daughter muons we do not expect a contribution of mechanisms creating astrophysical tau neutrinos to the incoming neutrino flux [48]. We do however expect the observation of tau neutrinos with an astronomical origin here at Earth since we know that, as explained in section 1.4, neutrinos

<sup>4</sup>The cosmic microwave background is electromagnetic radiation filling the Universe as a remnant from an early stage following the Big Bang.

undergo flavor oscillations, implying the created electron and muon neutrinos can change into tau neutrinos during propagation. From the decays (2.2) we expect a flavor ratio at the source of  $(f_{\nu_e} : f_{\nu_\mu} : f_{\nu_\tau})_S = (1 : 2 : 0)_S$ . Averaging the neutrino flavor oscillations by propagation over astronomical distances then leads to a flavor ratio at Earth of  $(f_{\nu_e} : f_{\nu_\mu} : f_{\nu_\tau}) = (0.93 : 1.05 : 1.02) \approx (1 : 1 : 1)$ . However adding the possibility of muon energy loss in high matter density or magnetic fields before decay, so that the electron neutrinos will have a lower energy compared to the muon neutrinos, or assuming the decay of neutrons produced in cosmic ray interactions form a non-negligible neutrino source through beta decay, which only creates electron neutrinos, can change the source composition from  $(0 : 1 : 0)_S$  to  $(1 : 0 : 0)_S$  [46]. This corresponds to flavor ratios as observed on Earth ranging from  $(0.6 : 1.3 : 1.1)$  to  $(1.6 : 0.6 : 0.8)$ .

### 2.2.2 Observation

The first ever evidence confirming the existence of astrophysical neutrinos was provided by the Antarctic IceCube Neutrino Observatory in 2013 [49, 46], to date still up and running. Taking into account the expected flux of neutrinos created in atmospheric air showers, usually referred to as the atmospheric neutrinos, the IceCube Neutrino Observatory detected a significant diffuse excess of incoming high-energetic neutrinos, reporting on striking neutrino energies never observed before. More recent IceCube results are shown in Figure 2.8 and Figure 2.9. Although the confirmation of the existence of astrophysical neutrinos is already a remarkable achievement, the current observational data is not yet really satisfying. The spectral index of the measured astrophysical neutrino energy spectrum is to date still marked by high uncertainties, with no significant evidence disclosing their origin. The measured flux cannot confirm or exclude the existence of diffuse galactic or cosmogenic neutrinos, which means both remain undetected. No significant clustering of events in certain directions have been observed so far, meaning at the moment no convincing point sources and thus individual cosmic ray accelerators have been found either.

Figure 2.10 shows the results of a flavor composition analysis based on IceCube data. As indicated in the figure the currently best fit for the flavor ratio can only exclude the scenario with a pure neutron source at  $3.7 \sigma$ . The ratios corresponding to a dominant meson source, with or without substantial muon energy losses, are well within the contours.

Clearly a solid progress in observation and data analysis is required. The announcement of the detection of high-energetic neutrinos by the IceCube collaboration only marks the beginning of a new field of astronomy opening up an additional window through which we can observe our Galaxy and beyond, a window using particles that do not lose any information during their journey towards Earth. Combining neutrino astronomy with other observation techniques, like optical telescopes, gamma-ray detectors and even gravitational wave observatories, should lead us to a better understanding of some of the most extreme events taking place in the Universe. The construction of new impressive neutrino detectors, like the Cubic Kilometre Neutrino Telescope (KM3NeT) in the Mediterranean Sea or the Askaryan Radio Array (ARA) joining the IceCube observatory at the South Pole, together with a considerable upgrade of the IceCube detector are essential in exploiting this new observational window.

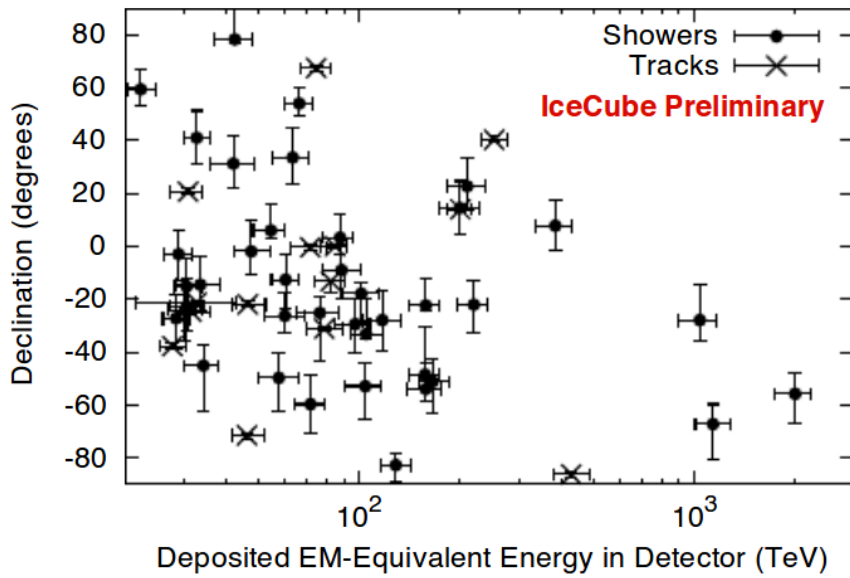


FIGURE 2.8: High-energy events detected in four years of IceCube data as a function of deposited energy. A declination of 90 degrees corresponds to neutrinos coming from the direction of the North Pole, with the Earth only becoming opaque to neutrinos only at the highest energies. Showers are events in which the energy is deposited spherically in the detector, tracks are events in which the energy is deposited in a straight line throughout the detector (see Chapter 3) [46].

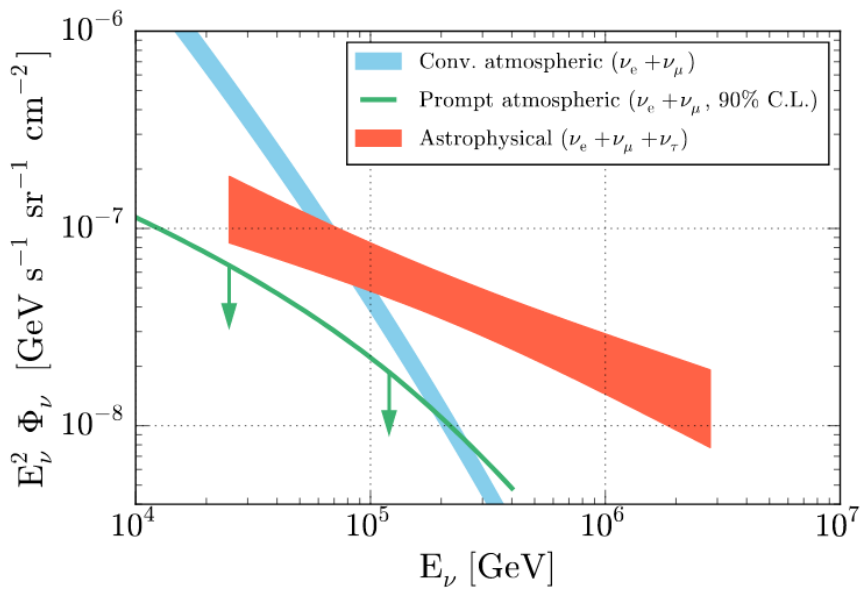


FIGURE 2.9: Best fit for the astrophysical neutrino spectrum following results of the IceCube experiment. The  $1\sigma$  uncertainties are indicated by the linewidths. The blue line represents the conventional atmospheric neutrino flux, the component of the atmospheric neutrino flux produced by the decay of pions and kaons. The green line represents the 90% C.L. upper limit on the prompt atmospheric neutrino flux, the component of the atmospheric neutrino flux produced by the decay of heavier mesons typically containing a charm quark [50].

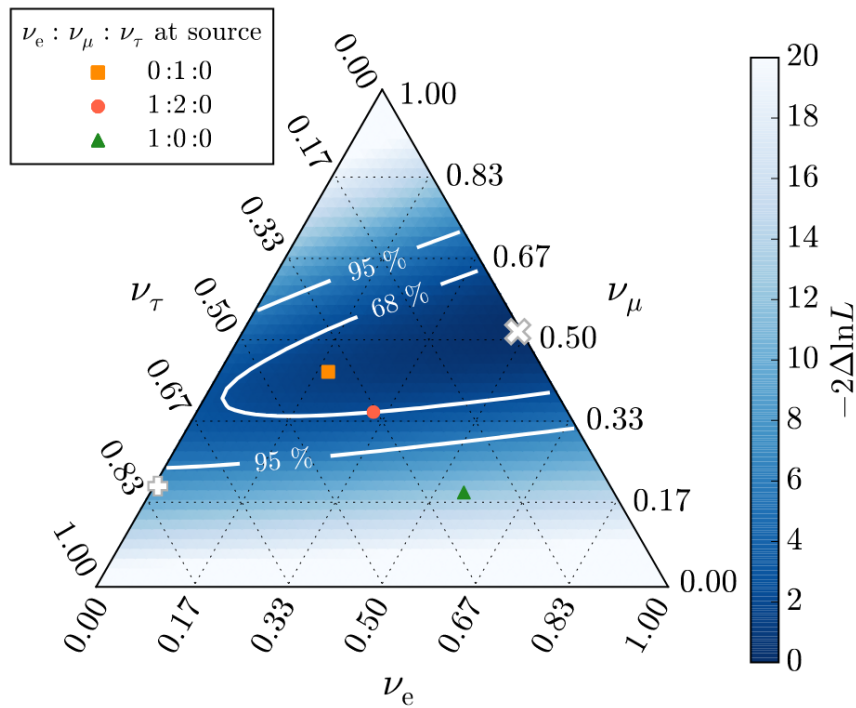


FIGURE 2.10: The profile likelihood scan of the neutrino flavor ratio as measured on Earth following results of the IceCube experiment. The individual contributions are read off the three sides of the triangle by following the lines parallel to the labels. The ratio measured at Earth corresponding to a  $(1 : 2 : 0)$  source composition is marked by the circle. Those corresponding to source compositions of  $(0 : 1 : 0)$  and  $(1 : 0 : 0)$  are marked with respectively a square and triangle. The best fit for the flavor fit analysis is indicated with a  $(x)$ , which excludes the  $(1 : 0 : 0)$  source composition at  $3.7 \sigma$ . A previous IceCube result is indicated with a  $(+)$  [50].



## Chapter 3

# The IceCube Neutrino Observatory

As explained in Chapter 2 the detection and analysis of high-energy astrophysical neutrinos could play an important role in modern astronomy, providing us with information which remains hidden using other observational techniques. Easier said than done as due to their very own nature neutrinos are extremely unlikely to interact with any type of matter or, more particularly, detectors, a statement especially true for the high-energetic ones. As we can not change the incoming neutrino flux, the only option left to increase detection probability is to use gigantic detectors. A higher detector volume means more neutrinos passing through, leading to a higher detection rate. To this end the Antarctic IceCube Neutrino Observatory was built, finished in 2011 and currently still the largest telescope on Earth. Constructed close to the South Pole it is designed to detect high-energy astrophysical neutrinos at a considerable rate, opening up a yet unexplored energy range in neutrino physics and new possibilities in astroparticle physics. This chapter will describe the IceCube experiment and highlight and discuss some of its main features.

### 3.1 General Detector Layout

This section aims to give an overview of the general features of the IceCube Neutrino Observatory [51]. In order to detect high-energetic neutrinos the observatory relies on occasional deep inelastic scattering interactions taking place in its enormous detection volume made up of Antarctic ice. As explained in Section 1.3 both CC and NC deep inelastic scattering interactions of high-energetic neutrinos with nucleons will lead to hadronic cascades, with CC interactions creating an additional charged lepton as well. These energetic cascades and charged leptons can subsequently be observed thanks to the so-called Cherenkov effect. Charged particles traveling through a medium faster than the speed of light in that medium will continuously emit radiation in the form of a cone, as shown in Figure 3.4 for a high-energetic muon propagating through ice, similar to the sound waves created by an airplane traveling faster than the speed of sound in air. In the case at hand the medium is the Antarctic ice, with the Cherenkov radiation being visible, blueish light. The inelastic deep scattering of a high-energetic neutrino with a nucleon in the ice will thus create a charged hadronic cascade possibly accompanied with a charged lepton, which in their turn will start to emit visible Cherenkov light. Other processes contributing to the energy loss of these secondary particles are ionization<sup>1</sup>, bremsstrahlung<sup>2</sup>,

<sup>1</sup>Here used to refer to the process in which a charged particle interacts with an atom, hereby removing an electron from the atom.

<sup>2</sup>Bremsstrahlung is the term used for radiation created during the interaction of a charged particle with the electromagnetic field of another charged particle, here mostly nuclei.

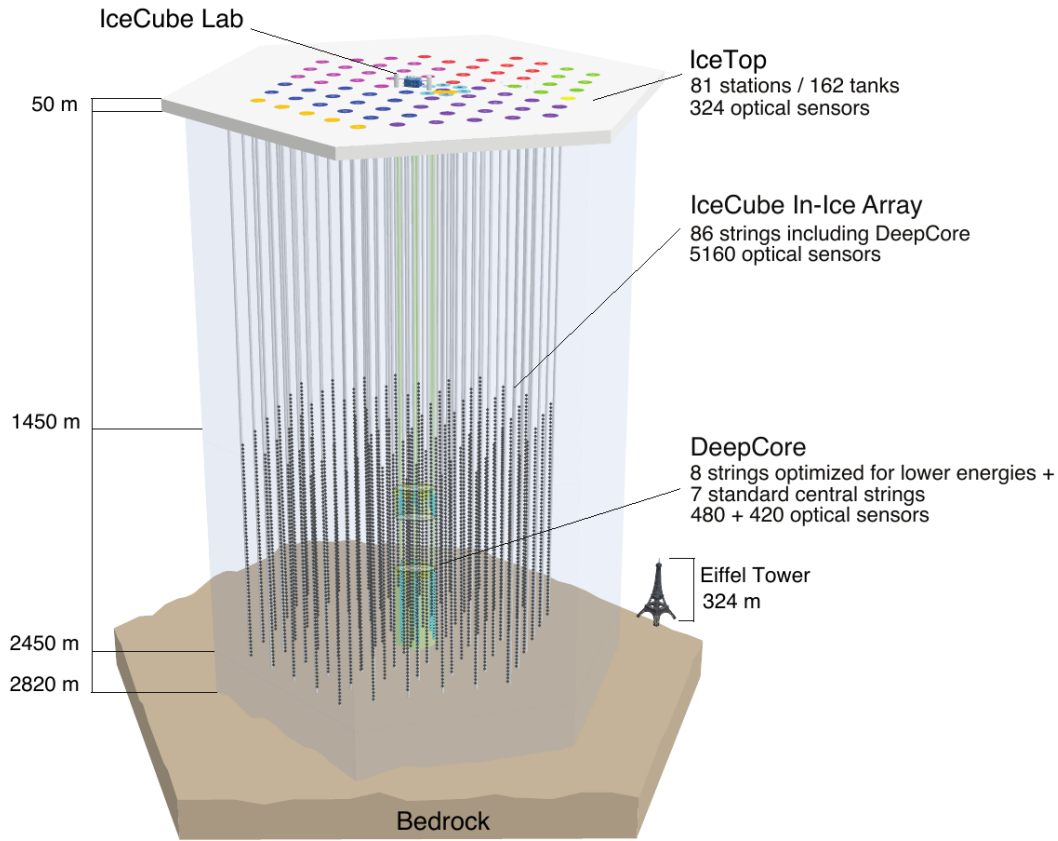


FIGURE 3.1: The IceCube In-Ice Array, DeepCore, IceTop and the IceCube Laboratory together forming the IceCube Neutrino Observatory.

electron-positron pair productions in the field of a nucleus and photo-nuclear interactions<sup>3</sup>, leading to more Cherenkov radiation [20, 52]. Thanks to its good optical properties placing photosensitive detectors inside the Antarctic ice can thus lead to the detection of high-energetic neutrinos, which is exactly the main idea behind the IceCube Neutrino Observatory. Its general layout is shown in Figure 3.1.

### 3.1.1 IceCube In-Ice Array

Located between 1450 m and 2450 m below the surface of the Antarctic ice we find the IceCube In-Ice Array. It consists of 5160 digital optical modules, usually referred to as DOMs, attached in groups of 60 to a total of 86 strings, filling up a volume of one cubic kilometer. The DOM forms the basic detection unit of the IceCube Neutrino Observatory, designed to detect Cherenkov radiation propagating through the ice. It is discussed in more detail in Section 3.2. Out of the 86 strings, 78 form the primary in-ice array. They are spread over a hexagonal surface, forming a triangular grid with 125 m horizontal spacing. For each of the primary in-ice array strings the vertical separation between consecutive DOMs is 17 m. This setup allows for an efficient detection of high-energy neutrinos with energies of the order TeV - PeV, meaning in practice the energy threshold of most data analyses lies around 100 GeV.

<sup>3</sup>A photo-nuclear interaction is an inelastic scattering of a charged particle on a nucleus breaking up the nucleus.

### 3.1.2 DeepCore

The remaining eight strings are part of what is called DeepCore. Starting at a depth of 1750 m it provides a denser instrumented subvolume in the center of the primary in-ice array, suited for data analyses requiring a lower energy threshold of about 10 – 100 GeV. The total DeepCore volume encompasses the eight remaining strings together with seven of the standard primary in-ice array strings. For the eight specialized DeepCore strings the vertical separation between consecutive DOMs is 7 m for the bottom 50 DOMs, deployed at depths of 2100 m to 2450 m, and 10 m for the other 10 DOMs. The separation between the strings located in DeepCore varies from 41 m to 105 m. A dust layer has been discovered between 2000 m and 2100 m below the surface of the ice, increasing the scattering and absorption of light significantly in this region. Therefore DeepCore is not instrumented at these depths. Six of the eight DeepCore strings are fully equipped with special DeepCore DOMs allowing for more efficient light detection, with the other two strings being equipped with both DeepCore and standard DOMs.

### 3.1.3 IceTop

Situated atop the in-ice array are the 162 ice-filled IceTop tanks divided in pairs of two over 81 stations on the surface of the ice, designed to be used for the detection of air showers. The stations approximately follow the grid defined by the in-ice strings. The eight DeepCore strings correspond with eight stations in the center of IceTop placed closer together. The two station tanks are separated by 10 m and each contain two standard IceCube DOMs, their settings differing from each other to increase the dynamic range for air shower detection. Charged shower particles generate light in the ice of the tanks which is subsequently detected by the two DOMs, with a typical cosmic-ray induced air shower reaching several IceTop tanks. This way the IceCube Neutrino Observatory contributes in the study of cosmic ray events with energies surrounding the knee region of the cosmic ray energy spectrum up to values where possibly a shift from Galactic cosmic rays to an extragalactic population occurs.

### 3.1.4 IceCube Laboratory

The central operations building for the observatory is called the IceCube Laboratory and accompanies the IceTop tanks at the surface of the ice. It houses the data acquisition and filtering computers further explained in Section 3.3. The two cable towers on either side of the building are used to collect the surface cables of the array. Power is supplied by The South Pole Station.

## 3.2 Digital Optical Module

As already mentioned the digital optical module or DOM forms the basic detection unit of the IceCube Neutrino Observatory. An illustration of a DOM is shown in Figure 3.2. Its main components are its downward-facing photomultiplier tube (PMT), the single-board data-acquisition computer called the Main Board and the LED Flasher Board. A glass sphere protects its components from the pressure of the ice. A penetrator assembly brings out three wire pairs through a small hole in the glass sphere, connecting the DOM with its neighboring DOMs directly above and below as well as to a computer in the IceCube Laboratory.

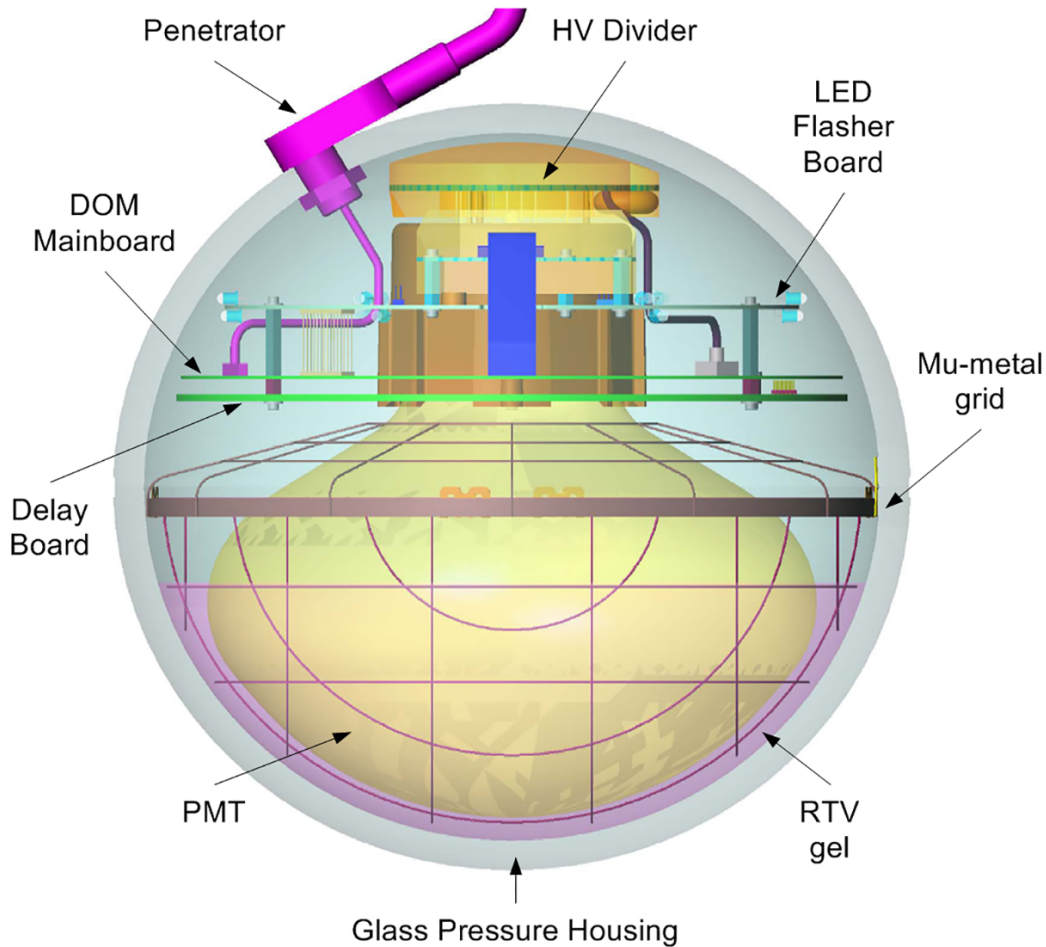


FIGURE 3.2: The digital optical module (DOM), the light sensor and data acquisition unit for IceCube.

### 3.2.1 Photomultiplier Tube

The photomultiplier tube or PMT allows the DOM to detect the Cherenkov light created in the ice. A single photon entering the PMT has a probability, indicated by what is called the quantum efficiency of the PMT, to create a free electron inside its bulb-shaped photocathode, usually referred to as a photoelectron [53]. The photoelectron will migrate through the cathode towards the multiplier portion of the PMT where it will induce a cascade of secondary electrons, leading to the multiplication of the single photoelectron with a factor of  $10^7$  and so generating a measurable electric pulse. The PMTs used in the standard DOMs have a peak quantum efficiency of around 25% near 390 nm, meaning one in four photons with a wavelength of about 390 nm entering the PMT will lead to an electric pulse. For the DeepCore DOMs the peak quantum efficiency has been increased to 34%. The PMT bulb faces downwards, with the photocathode area surrounded by a high-strength silicone gel providing good optical coupling and mechanical support. A mu-metal cage surrounds the PMT bulb to reduce effects of the South Pole magnetic field on the PMT collection efficiency.

### 3.2.2 Main Board

The Main Board could be considered the brain of the DOM, providing many key functions for data acquisition and management. This includes the control of all other devices inside the DOM like the flasher board and various sensors, digitization of the PMT waveforms, temporary storing the data and taking care of communications with the data acquisition system on the surface. If the voltage output of the PMT surpasses a certain threshold the Main Board starts its high-speed waveform capture and digitization process, resulting in what is called a hit record. In order to completely cover its dynamic range the Main Board is provided with the ability to amplify the PMT output with three different amplifier gains, their nominal values being 16, 2 and 0.25. The Main Board CPU bundles the hits and sends them on request to the surface computers. If a nearest or next-to-nearest neighbor DOM also signals a launch  $1\ \mu\text{s}$  before or after recording a hit, the full digitized waveform is compressed and included. Such hits are called Hard Local Coincidence (HLC) hits. In case of an isolated signal the digitization process is aborted and only a time stamp and brief charge summary are sent to the surface. These hits are referred to as Soft Local Coincidence (SLC) hits.

### 3.2.3 Flasher Board

All DOMs are equipped with an LED Flasher Board able to generate light in situ, used for calibration processes like verifying the time response of the DOMs, studying the optical properties of the ice, measuring the positions of the DOMs in the Antarctic ice and checking the accuracy of shower reconstruction algorithms in determining position, direction and energy. It consists of 12 LEDs designed to emit monochromatic light with a wavelength of  $405 \pm 5\ \text{nm}$ , arranged in six pairs evenly spaced around the board forming a regular hexagon. In each pair one LED is tilted so that its light is emitted horizontally into the ice after refraction through the DOM glass. The other one is tilted so that after refraction its light is emitted at an angle of  $48^\circ$ , which closely matches that of the Cherenkov angle in ice. Sixteen so-called color DOMs (cDOMs) are equipped with a multi-wavelength Flasher Board. Eight of the cDOMs are attached to a string in the center of the in-ice IceCube array, the other eight to a string on the edge of the array. The six LED pairs now consists of three pairs made up of a 370 nm and a 450 nm LED and three pairs made up of a 340 nm and a 505 nm LED.

## 3.3 Data Acquisition System

Most registered DOM hits are due to what is called dark noise, i.e. effects occurring inside the DOM that also lead to the creation of a photoelectron inside the cathode of the PMT. Examples of such effects are electronic noise, radioactive decays inside the DOM and scintillation or luminescence in the glass of the PMT and the pressure sphere. As they have nothing to do with Cherenkov light generated in the ice these signals are clearly not of interest. In order to keep the data transfer to the surface manageable and their dead times minimal, the DOMs carry out a first data selection as explained in Section 3.2.2. The full waveform of the HLC hits is compressed and included in the hit record, while only a time stamp and some information about the charge of the hit are sent in case of SLC hits.

On the surface the data acquisition system (DAQ) reads out all DOM hits and performs the next step in the data selection procedure. It examines the HLC events

searching for temporal and in some cases spatial patterns that might indicate causal relationship. Both the HLC and SLC hits found to be related are then combined into single events, which is the main output of the DAQ. The total output data rate of the DAQ is about 1 TB/day. Through the generation of time calibration and monitoring data by the DAQ the health and quality of the data-taking runs are monitored.

Of all DAQ events only about 15%, selected by applying approximately 25 filters, is transferred over satellite to the IceCube data center in the Northern Hemisphere. Each filter typically selects events useful for a particular physics analysis and is run over all events using a computer cluster at the IceCube Laboratory. Only fast directional and energy reconstructions are applied, as the total computing power and available processing time are limited. All processed events are archived locally, including those not selected by the above-mentioned filters.

Once the DAQ events are stored in the Northern Hemisphere data center they can be accessed by all IceCube Collaboration members. More computationally heavy standard data processing is carried out, providing a high level event reconstruction of all stored events. Data processed this way is said to be on Level 2, which is where most analyses start of.

### 3.4 Signal Topologies

As mentioned before the NC or CC deep scattering interaction of neutrinos on nucleons in the ice will induce hadronic cascades, with CC interactions creating an additional charged lepton as well. The neutrino created in a NC interactions will simply leave the in-ice array without leaving a single trace, meaning the only Cherenkov radiation following the reaction comes from the hadronic particle shower. The charged leptons created in CC interaction on the other hand will contribute to the development of Cherenkov radiation inside the detector, with the difference in mass of the electron, muon and tau resulting in mainly three IceCube event topology classes. The timescales of these different types of events are all of the order of  $1 \mu\text{s}$ .

#### 3.4.1 Cascade

All NC interactions together with the CC interaction of an electron neutrino inside the ice lead to cascade events [20]. An example of such an event is shown in Figure 3.3. Due to the creation of many secondary particles and the repeated scattering of the corresponding Cherenkov photons the hadronic particle shower leads to a generic spherical light pattern in the ice, independent of the flavor of the interacting neutrino. In case of a CC interaction of an electron neutrino the created electron rapidly loses its energy through bremsstrahlung, creating photons which on their turn create electron-positron pairs [54]. The same goes for positrons created by electron antineutrinos. The subsequent bremsstrahlung and pair production processes initiate an electromagnetic cascade close to the CC interaction point, leading to a spherical light distribution as well and so amplifying the spherical light pattern of the hadronic cascade. Both a NC interaction as well as a CC interaction of an electron neutrino thus lead to the same signature, with the cascade of the CC electron neutrino interaction being more energetic.

Being fully contained in the detector cascade-like events have a good energy resolution of about 15%. Their spherical form however leads to a rather poor angular resolution of the order of  $10^\circ$  for energies larger than 100 TeV [46].

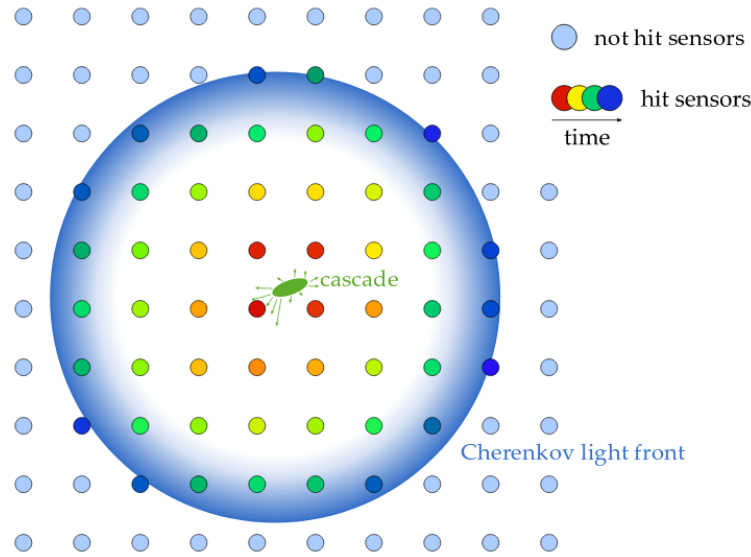


FIGURE 3.3: Example of a cascade-like signal following a NC or CC electron neutrino interaction in the IceCube in-ice array [55]. The colors of the hit sensors indicate the time of light detection.

### 3.4.2 Track

Muons or antimuons, both of which will simply be called muons here, traveling through the in-ice array lead to a track-like signal, an example of which is shown in Figure 3.4. With a mass of about 200 times larger than that of the electron they are far less subjected to bremsstrahlung, meaning their trajectory is a straight line through the ice. At lower energies they mainly lose energy continuously through ionization and Cherenkov radiation. At energies above about 1 TeV energy losses by bremsstrahlung, photo-nuclear interactions and electron-positron pair production start to dominate, leading to stochastic energy loss patterns along the track [56]. Muon neutrinos and antineutrinos interacting in the the detector will lead to the combination of a cascade-like signal following the hadronic particle shower together with a track-like signal created by the outgoing muon.

In contrast to cascade-like signals a track typically has a very good angular resolution, better than  $1^\circ$  for muons with energies above 1 TeV, marked however by a poor energy resolution [46]. At energies above about 100 GeV muons generally travel distances through the ice longer than the length of the detector. This means many IceCube muon events are not contained in the detector, leading to imprecise muon energy reconstructions. A common way of reconstructing the energy of a passing muons is using the proportionality of the mean energy loss rate of a muon to its energy, valid at energies above roughly 1 TeV.

With a rate of roughly three thousand per second atmospheric muon track signals by far dominate the IceCube data. That of muons created by atmospheric muon neutrinos for example is only about one every six minutes. High-energy astrophysical neutrinos are detected only about once every month.

### 3.4.3 Double Bang

The CC interactions of tau neutrinos or antineutrinos in the ice containing and surrounding the in-ice array lead to a variety of signatures, of which the Double Bang can be considered the standard one. As shown in Figure 3.5 it consists of two well

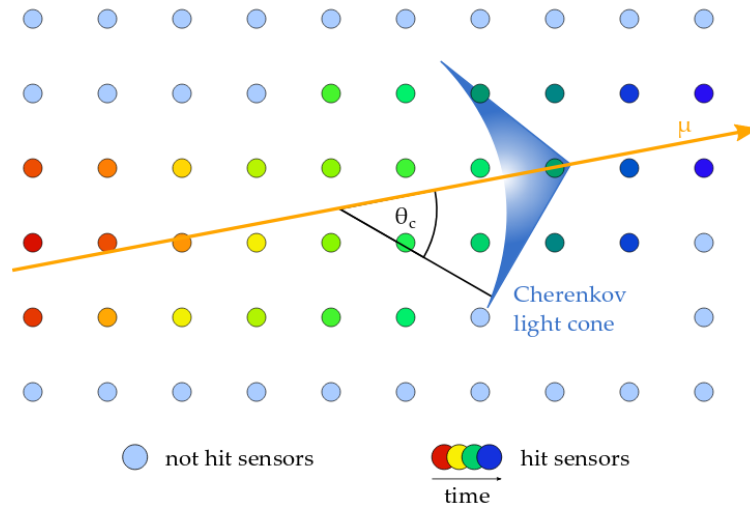


FIGURE 3.4: Example of a track-like signal created by a muon propagating through the IceCube in-ice array [55]. The colors of the hit sensors indicate the time of light detection.

separated cascade-like signals contained in the detector, i.e. the bangs, connected by a track-like signal. The first cascade is caused by the hadronic cascade initiated during the CC deep inelastic scattering of the neutrino. The created tau lepton leaves the point of interaction, leading to a track signal just as a muon propagating through the detector does. Due to its large mass value the tau neutrino has the tendency to rapidly decay, in roughly eight out of ten cases creating hadrons or an electron and so producing a second cascade [57]. With the average distance covered by the tau lepton before decay roughly scaling as  $5 \text{ cm/TeV}$ , only tau energies of above a few hundred TeV will lead to two resolvable cascades [58]. In less energetic events the two cascades will overlap. These are called Double Pulse signals instead, referring to the double-peaked structure appearing in the waveforms of the DOMs located close by such events. Events with energy higher than roughly 20 PeV will lead to tau lepton tracks of the order of the dimensions of the in-ice array, moving one of the two cascades out of the detector. If only part of the track of the tau together with the second cascade are located inside the detector we talk about a Lollipop event. The other case is called an Inverted Lollipop event, whereby the first cascade together with a part of the tau track are contained instead.

Being fully contained in the detector while also having a track-like structure, Double Bang signals typically lead to good energy as well as angular resolutions. The combination of the cascade and track topology however makes it hard to distinguish Double Bang signals from other types of events. Small tau tracks lead to Double Bangs resembling high-energy single cascade events, while long tau tracks make them look like track events. They also correspond to a limited range of high energies, implying that Double Bang signals are relatively rare.

For completion it should be mentioned that next to the topologies related to the Double Bang signature CC tau neutrino interactions can also lead to two other types of events [57]. A tau lepton entering the detector and subsequently decaying to a muon will produce a track-like signal which suddenly becomes brighter, as the muon is less massive and so generates more light. This topology is referred to as the Sugardaddy. If a low-energetic tau neutrino leads to a tau lepton that almost immediately decays into a muon, we talk about a Tautsie Pop event. It is very similar to the Inverted Lollipop, with as main difference that in case of a Tautsie Pop two

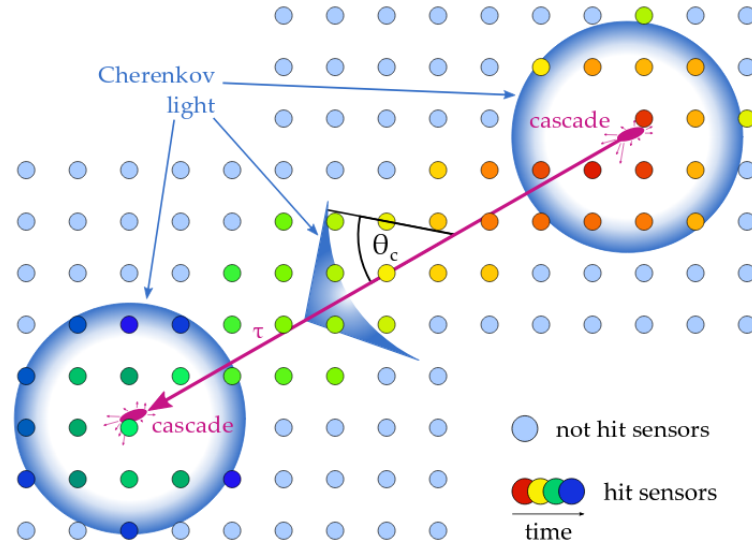


FIGURE 3.5: Example of a Double Bang signal following a tau neutrino interaction in the IceCube in-ice array [55]. The colors of the hit sensors indicate the time of light detection.

neutrinos leave the cascade, carrying away a significant amount of energy. This leads to a larger ratio between the measured cascade energy and the measured track energy.

### 3.5 Simulation and Software

As is the case in many other modern particle physics experiments, the concept of data simulation plays a vital role in both verifying our understanding of the detector and the ongoing physics as well as performing dedicated data analyses. Based on all sorts of calibration campaigns detailed models of the detector and the Antarctic ice are constructed. Combining these with the physical models predicting the relevant particle fluxes passing through the in-ice array and their corresponding interactions in the ice, special designed so-called Monte Carlo simulation software is developed. They aim to provide the members of the IceCube Collaboration with man-made data, which if the used models indeed accurately describe reality should resemble closely real IceCube data.

Comparing the simulated data with real data is thus a very practical way of verifying our understanding of the detector and the ongoing physics. Both should be very similar, with significant deficits possibly indicating e.g. misunderstandings in the working of the detector, errors in the applied ice models, wrong assumptions made during the calculations of the relevant particle fluxes or even a fundamental lack in knowledge of the relevant physical phenomena. It is also extensively used during data analyses. Most studies focusing on a certain type of events will try to construct efficient data reduction algorithms, trying to cut out other types of events, referred to as background, from the IceCube data while keeping the loss in signal of interest minimal. Simulated data can then be used to find effective data cuts accepting or rejecting signals based on their properties. Since they were man-made it is exactly known which kind of particles and processes were involved in the creation of the simulated signals, in clear contrast to the IceCube data. By applying the cut algorithm to simulation data it can thus readily be estimated how much background

would be removed and how much signal of interest would be lost when used on IceCube data.

With a lot of analyses focusing on high-energy events, marked by a substantial lower event rate compared to low-energy events, simulation data comes with a little twist. Simulating the true expected particle fluxes would result in simulation datasets with little high-energy events, meaning their properties would be subject to considerable statistical fluctuations. Simply simulating more events would be a very inefficient and computationally heavy solution. To this end the concept of weighting has been introduced, a technique often used to deal with such kind of problems. Instead of simulating events based on their measured or predicted energy spectrum the simulation software produces data following a spectrum leading to more high-energy events, however assigning every event a certain weight depending on both the physical and the simulated spectrum. In essence a weight of an event reflects the expected number of such kind of events over a predefined time period, which when taken into account corrects for the wrong energy spectrum used during simulation. High-energy events typically have weights smaller than one, indicating in reality we expect them to occur less frequently than simulated. Weights larger than one indicate that the corresponding events actually represents multiple similar ones, typical for those living in the high-rate part of the energy spectrum. For example the total number of expected events within a certain energy range during the predefined time period is given by the sum of the weights of these events, only resulting in the number of simulated events in that energy range if all the corresponding event weights equal one. By using the concept of weighting the simulation data sets are much more sensitive for details in the high-energy tails of the spectra, reducing the statistical fluctuations in their simulated rates and properties.

Next to programs taking care of simulation lots of other software is being developed and used within the IceCube Collaboration. This includes for example software made to visualize IceCube events, called Steamshovel, as well as many algorithms designed to be used in event reconstruction and computation of event properties. Examples of the latter are Millipede, in the first place developed to measure the energy loss of a muon along its track, and Portia, used to compute the number of photoelectrons created during a given event. The software is available for all IceCube Collaboration members.

### 3.6 Experimental Capabilities

As already stated the main reason for the construction of the IceCube Neutrino Observatory is the need for exceptionally large neutrino detectors in the study of astrophysical neutrinos, which could play an important role in modern astronomy. Carrying information no other particle does they could be of great help in the search for the acceleration mechanisms behind the cosmic rays and the study of the Universe in general. It should however not be surprising that a gigantic detector like that of the IceCube Neutrino Observatory has some other interesting capabilities as well, including the following.

A lot of astronomical observations made so far, including studies of single galaxies, galaxy clusters and properties of the Universe as a whole, hint at the existence of something called dark matter, repeatedly making up for a substantial deficit in mass. As up till now it has never been observed directly, it is believed the dark matter particles do not carry any form of charge. Due to their small mass values cosmological arguments exclude the possibility of dark matter solely being made

up from the three known types of neutrinos, meaning perhaps other still unknown elementary particles are out there for us to discover. With it being a very hot topic the IceCube Neutrino Observatory participates in the search for dark matter candidates, for example by looking for a decay signature of WIMPs, or weakly interacting massive particles, in the form of a neutrino excess coming for example from the Sun [59].

The IceCube Neutrino Observatory can also be used to further study neutrino flavor oscillations. So far it has been able to provide the first significant detection of atmospheric neutrino flavor oscillations together with values for the oscillations parameters which are in good agreement with other experiments [60]. Studying the oscillation behavior of the neutrinos could lead to the discovery of the existence of a fourth type of neutrino. To explain anomalies in accelerator, reactor and radioactive source oscillation experiments a so-called sterile neutrino has been proposed. This fourth type of neutrino would not even be able to interact weakly, only showing itself through its coupling with the three conventional types of neutrinos. By looking for deficits in predicted neutrino fluxes which could be interpreted as neutrinos having oscillated into the fourth type of neutrino, the IceCube detector once again contributes to the search for new elementary particles [61].

Besides dark matter candidates and sterile neutrinos theoreticians have come up with a variety of other possibly existing elementary particles. Various extensions of the Standard Model predict the existence of magnetic monopoles, elementary particles which are in essence isolated magnetic poles. With all forms of magnets observed so far having both a north and a south pole, the observation of a magnetic monopole would be groundbreaking. The IceCube Neutrino Observatory can be used to search for stable magnetic monopoles created during an early stage of the Universe, the existence of which is motivated by a variety of theories [62]. An other example of predicted particles which could be detected by IceCube are fractionally charged leptons. They could for example be created during the development of the energetic air showers in the atmosphere and subsequently reach the in-ice array [63, 64].

As IceCube is sensitive to neutrinos coming from galactic supernova explosions it is also part of the Supernova Early Warning System or SNEWS, an international group of experimenters from several neutrino-sensitive experiments with as primary goal alerting the astronomical community in case of a galactic supernova event [65]. As the supernova neutrinos do not interact during their propagation towards Earth they will arrive after a period of the order of tens of seconds following the explosion. This in contrast to the electromagnetic signals coming from the same event, only arriving hours or days later. Neutrino-sensitive experiments can thus provide an early alert allowing conventional observatories to prepare for detailed observations of a supernova.



## Chapter 4

# Tau Neutrino Search

The main goal of this project is to improve the search for astrophysical tau neutrinos with the IceCube Neutrino Observatory performed by Matthias Vraeghe at the University of Ghent, which mainly focused of Double Bang events [66]. To that end I have included a more advanced statistical approach in the data reduction scheme and compared its expected performance with that of the original analysis.

At the time of writing no IceCube analysis so far has been able to disclose any tau neutrino signals. There is however clear motivation for studying tau neutrino and in particular Double Bang events in IceCube. In contrast to electron and muon neutrinos no significant amount of tau neutrinos are produced in atmospheric interactions [57]. As at the energy and distance scales relevant for IceCube atmospheric neutrinos flavor oscillations of electron and muon neutrinos into tau neutrinos is very limited as well, this means that we do not expect any atmospheric tau neutrino events in IceCube. In other words studying tau neutrino events in IceCube gives us high confidence we are looking at astrophysical neutrinos only. To top it off the Double Bang tau neutrino signature has, as explained in Chapter 3, both good energy as well as angular resolution, which is not the case for electron or muon neutrino events. Combined with the certainty of their astrophysical origin this makes Double Bang tau neutrino events outstanding tools in neutrino astronomy. Finally even just measuring the total IceCube tau neutrino rate could lead to interesting limits on the astrophysical neutrino flavor ratio as measured on Earth, telling us more about the origin and propagation of cosmic rays (see Section 2.2.1).

This chapter aims to briefly describe the original search as well as the advanced statistical approach I have included. The expected outcome of the modified analysis is presented as well as a comparison with that of the original one based on simulation.

## 4.1 Double Bang Search by Matthias Vraeghe

In this section the search for astrophysical tau neutrinos with the IceCube Neutrino Observatory by Matthias Vraeghe is briefly described. The study aims to isolate the valuable Double Bang tau neutrino signatures in four years of IceCube data by using a dedicated data reduction scheme based on the study of simulation data. As is usually the case the reduction scheme consists of a number of separate cut algorithms designed to be carried out consecutively, each time improving the signal-to-background ratio and all labeled with a different level number. The most computationally expensive cut algorithms typically correspond to high level numbers, as is the case in this analysis, since at these levels the data sample should already have been reduced significantly. As already mentioned the data coming from the IceCube detector is automatically processed to what we call Level 2, which is where most of the analyses start off. The analysis of Matthias contains five additional levels,

which will be described in following subsections. As illustrated by Fig 4.1 the background is initially dominated by atmospheric muons generated in air showers, yet the analysis clearly needs to deal with the other types of background as well. The atmospheric muon background is weighted to the GaisserH3a flux model. [67]. The conventional atmospheric background, the component of the atmospheric neutrino flux produced by the decay of pions and kaons, is weighted to the HKKMS model [68]. The prompt atmospheric background, the component of the atmospheric neutrino flux produced by the decay of heavier mesons typically containing a charm quark, is weighted to the ERS model [69]. Both are corrected for the knee in the cosmic ray energy spectrum using the GaisserH3a model. A more detailed discussion can be found in the thesis of Matthias Vraeghe.

### 4.1.1 Definition of Double Bang Event

In the analysis a simulated tau neutrino event is only marked as a Double Bang event if it fulfills the following conditions.

- The tau neutrino undergoes a CC interaction in the ice, creating a tau lepton which through decay leads to the development of a cascade.
- The distance of the tau lepton covered is at least 50 m.
- The point of the CC interaction and that of the decay of the tau lepton lie at most 50 m outside of the detector, meaning both should be located inside the volume obtained by extending the in-ice array by 50 m in all directions.

### 4.1.2 Level 3 and 4

As we expect the Double Bang tau neutrino signals to occur only for high energy tau neutrinos, a first and efficient filter applied to the data is a high-energy filter. In practice this means all events with a total charge less than  $10^{3.5}$  photoelectrons as calculated by the Portia project are removed from the data sample. The total charge was determined excluding the DeepCore subarray in order to assure uniformity of the detector. Other cuts included are lower limits on the number of DOM's triggering and their corresponding strings as well as an upper limit on the maximum fraction of the total charge detected by a single DOM.

### 4.1.3 Level 5

Based on six variables developed to distinguish the Double Bang signals from atmospheric muon events a boosted decision tree (BDT) is trained, a method applying the concept of machine learning designed to distinguish signal from background using decision trees. In the end the boosted decision tree is able to label every event with a BDT score ranging from -1 up to 1. All events with a BDT score less than a given value are removed from the data sample.

### 4.1.4 Level 6

This level is based on the output of two reconstruction algorithms and mainly aims at reducing the background of single cascade events, originating from NC neutrino interactions and CC electron neutrino interactions. The reconstruction algorithms combined try to reconstruct an event assuming it has a Double Bang signature. This means that in the end two cascades separated by a tau track will have been fit to the

event regardless of its type. Events for which the reconstruction was not successful, the resulting total  $\chi^2$ , a statistical variable, is too large or at least one of the two reconstructed cascade energies is smaller than or equal to zero are removed from the sample. Three new parameters are introduced on which additional cuts are performed. The Causality of an event is defined as

$$\text{Causality} = t_2 - t_1 - \frac{1}{c} \cdot |\vec{r}_2 - \vec{r}_1|, \quad (4.1)$$

with  $(t_1, \vec{r}_1)$  and  $(t_2, \vec{r}_2)$  the time and position of respectively the first and second reconstructed cascade. We can expect the Causality to be close to zero for events marked as Double Bang signals in the detector, as the tau lepton created during the first cascade propagates at almost the speed of light in vacuum through the ice. The parameter thus indeed tells us something about the causality between the two reconstructed cascades. The Energy Asymmetry is given by

$$\text{Energy Asymmetry} = \frac{E_1 - E_2}{E_1 + E_2}, \quad (4.2)$$

with  $E_1$  and  $E_2$  respectively the first and second reconstructed cascade energy. If  $E_1 \gg E_2$  the Energy Asymmetry lies close to 1, while for  $E_1 \ll E_2$  it approaches the value  $-1$ . As on average the CC tau neutrino interaction produces a tau with 75% of the initial neutrino energy we thus expect the Energy Asymmetry distribution of true events marked as Double Bang signals to favor values close to  $-1$  [57]. The third parameter is the distance between the two reconstructed cascades, called the Reconstructed Length, simply given by

$$\text{Reconstructed Length} = |\vec{r}_2 - \vec{r}_1|. \quad (4.3)$$

Based on the definition of Double Bang events given in Section 4.1.1 we can expect the Reconstructed Length distribution of events marked as Double Bang signals to be dominated by values of the order of 50 m, with maximum values not much larger than 1000 m. The level cuts require the Causality to lie between  $-250$  and  $250$ , the Energy Asymmetry to lie between  $-0.70$  and  $0.60$  and the Reconstructed Length to be larger than 25 m.

#### 4.1.5 Level 7

The final level was designed to deal with the remaining atmospheric muon background. Using the Millipede project a segmented energy loss profile reconstruction is carried out, describing the energy loss along the line of the tau track reconstructed in Level 6. For events marked as Double Bang signals we expect that the main energy losses lie closely to the positions of the previously reconstructed two cascades. As at the considered energy ranges their main loss in energy is through bremsstrahlung, electron-positron pair production and photo-nuclear interactions the atmospheric muons lose their energy stochastically during propagation through the ice, implying significant energy losses will be found all over the line of the reconstructed tau track. Based on the energy loss profile two variables are constructed introducing two more separate cuts in the analysis.

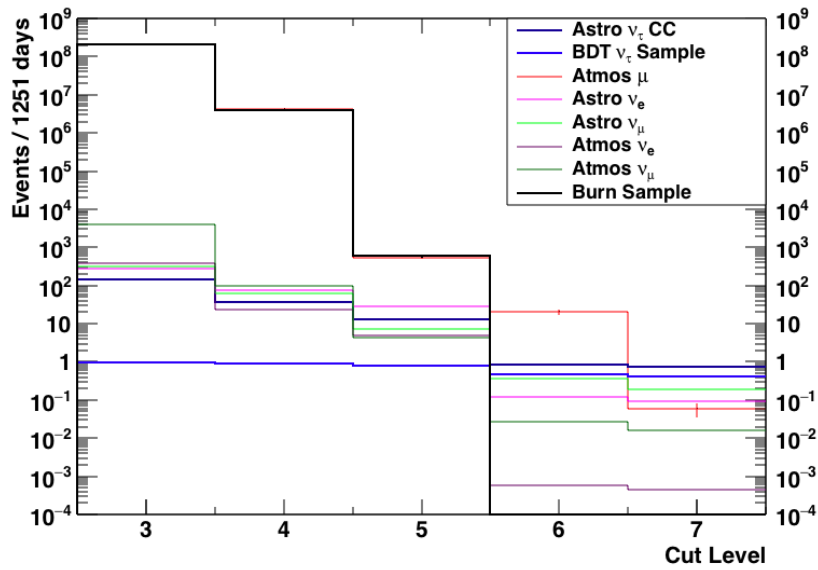


FIGURE 4.1: The number of expected results per year based on simulation as a function of the cut levels of the astrophysical tau neutrino search by Matthias Vraeghe [70]. A small burn sample was used to verify the simulation results. Atmos refers to an atmospheric origin, i.e. generated in air showers. Astro refers to an astrophysical origin.

#### 4.1.6 Results

The number of expected remaining events based on simulation in function of the different cut levels is shown in Figure 4.1. Only 0.76 astrophysical tau neutrino events in 1251 days are expected, which is about two times the expected number of remaining background events. The background reduction is impressive, reducing the dominant background source close to ten orders of magnitude. Unfortunately zero events were found after applying the level cuts on four years of IceCube data. More detailed results, including an astrophysical tau neutrino flux upper limit and a limit on the neutrino flavor ratio as measured on Earth, can be found in the thesis of Matthias Vraeghe.

## 4.2 An Advanced Statistical Approach

As already mentioned I have included a more advanced statistical approach in the data reduction scheme described in previous section. The main goal of this different approach was to improve the performance of Level 6, meaning it should be able to increase the final signal-to-background ratio of the analysis without yielding significantly less expected remaining signals of interest. To this end a more advanced method has been studied, combining the Level 6 parameters (4.1), (4.2) and (4.3) instead of using separate straightforward cuts based on their values. The following subsection will describe this method as well as present some relevant intermediate results.

Type	Dataset	Energy range dataset
Astro Tau Neutrino	Dataset produced by Nancy Wandkowsky	$10^2 \text{ GeV} - 10^8 \text{ GeV}$
Double Bang		
Corsika	11057, 11937	$10^5 \text{ GeV} - 10^{11} \text{ GeV}$
Astro Electron Neutrino	Dataset produced by Nancy Wandkowsky	$10^2 \text{ GeV} - 10^8 \text{ GeV}$
Astro Muon Neutrino	Dataset produced by Nancy Wandkowsky	$10^2 \text{ GeV} - 10^8 \text{ GeV}$
Atmos Electron Neutrino	12034	$10^2 \text{ GeV} - 10^7 \text{ GeV}$
Atmos Muon Neutrino	11883	$10^2 \text{ GeV} - 10^7 \text{ GeV}$

TABLE 4.1: The types of signals considered in the advanced statistical approach together with their corresponding simulation data sets used. All simulation data sets listed were produced using the SpiceLea ice model. The Double Bang signals are a subset of the astro tau neutrino signals, meeting the requirements of a Double Bang signature. Corsika signals are the signals created by downgoing atmospheric muons, the type name referring to the program used for simulating these events. Astrophysical is shortened to astro, atmospheric to atmos.

### 4.2.1 Likelihood Distributions

Based on simulation data estimations of the probability distributions of the three parameters given the type of signal have been constructed, from here on referred to as the likelihood distributions. For example, the Double Bang likelihood distribution of the Causality gives the probability distribution of the Causality given the event is marked as a Double Bang signal. Each likelihood distribution has been constructed by computing the three different parameters for events of suitable simulation datasets processed to Level 5 of Matthias' analysis, out of which then normalized histograms are constructed. Events of which at least one of the two reconstructed cascade energies is smaller than or equal to zero are left out during the construction of the distributions. As the simulation sets are generated following non-physical energy spectra to optimize the simulations, this includes the proper weighting of the events to the models mentioned in Section 4.1. The events have been weighted to four years of IceCube data, however due to normalization of the histograms this should not be a consequential factor. All the different types of signals for which likelihood distributions have been made together with the corresponding datasets used are listed in Table 4.1. The three likelihood distributions for the Double Bang signal are shown in Figure 4.2. As can be seen the distributions match the expectations of the behavior of the three parameters as discussed in Section 4.1.4. The other constructed likelihood distributions can be found in Appendix A.

The Double Bang distributions indeed differ from those of the background signals, with perhaps some notable features that will shortly be discussed here without losing ourselves in the details of the reconstruction algorithm. The difference in the

Energy Asymmetry likelihood distributions for the Double Bang and the Astro Tau Neutrinos is probably due to the reconstruction algorithm mentioned in Section 4.1.4 apparently assigning a large fraction of the tau neutrino signal to the first decay in case of small tau lepton tracks, which are not classified as Double Bang events and result in a more cascade-like signal.

As the Corsika events are atmospheric muon bundles stochastically losing their energy throughout the detector we indeed expect the three corresponding distributions to generally be more spread out over the entire appropriate ranges.

The electron neutrino signals result in an Energy Asymmetry distribution favoring values of  $+1$ . This is probably due to the reconstruction algorithm in most cases identifying the main part of the single electron neutrino cascades as the first Double Bang cascade, being left with only a small and less energetic substructure of the signal to assign to the second Double Bang cascade. It does however also sometimes seem to assign the main part of the signals to the second bang. The sudden rise at a value of  $-1$  in the Astro Electron Neutrino Energy Asymmetry distribution looks like an artificial feature introduced by the reconstruction algorithm. This is probably occurring mainly in case of high energy events as the feature is less prominent in the corresponding distribution for the atmospheric electron neutrinos, which have typically lower energy values than astrophysical electron neutrinos. The distribution for the astrophysical electron neutrinos also show a notable bump close to zero, possibly due to the reconstruction algorithm dividing up the most energetic single electron neutrino cascades in two more similar Double Bang cascades. As a result of its movement towards the sea the grains inside the ice are orientated in the same direction, causing the velocity of light in the ice to be higher in one specific direction [71]. This results in these high energetic single cascades to take on a bean-like structure, perhaps leading the reconstruction algorithm to reconstruct it as a somewhat symmetrical Double Bang event. An other feature of the ice possibly causing this bump is the infamous dust layer at about 2 km deep in the ice. A high-energetic single electron neutrino cascade cut in two by the layer could once again lead to a fairly symmetrical Double Bang reconstruction.

The muon neutrinos mainly dump energy in the detector through the CC-induced cascade, leading to the same trend in their Energy Asymmetry distribution as the electron neutrinos. Only a small fraction of the detected energy is located in the track left by the muon. It probably forms an anchor point for the second bang, resulting in an even larger shift towards an Energy Asymmetry value of one.

The shift towards smaller values of the electron and muon neutrino Reconstructed Length distributions can be attributed to the fact that the main energy deposit of the corresponding signals is concentrated in their single cascades. It seems likely that, guided by the cascade, the reconstruction algorithm places the two bangs in general closer together when fitting a Double Bang signal to electron or muon neutrino events.

## 4.2.2 TS distributions

The next step in the more advanced statistical approach is the construction of so-called test statistic (TS) distributions. A test statistic is a variable constructed to test a hypothesis, in this case whether a given event is a Double Bang signal or not. After constructing the TS distributions for all given types of signals, they can be used to try to classify or reject a given event based on its TS value within a certain confidence level. As it is common practice to base the TS value on likelihood values,

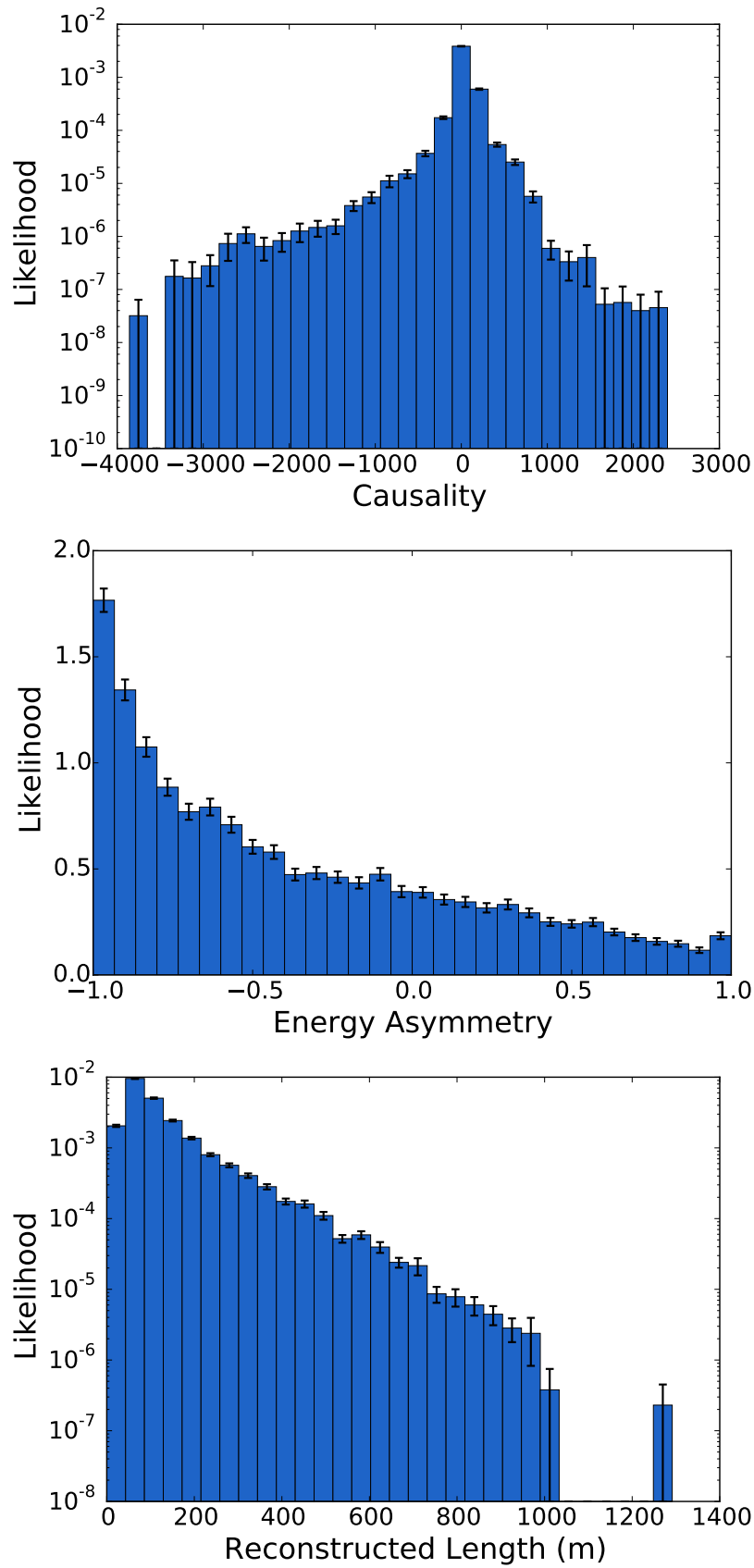


FIGURE 4.2: The likelihood distributions of the three parameters for the Double Bang signal. The error bars show the statistical errors based on Poisson statistics.

the TS parameters discussed here are constructed out of the likelihood distributions discussed in the previous section.

First of all for every type of signal the three separate likelihood distributions are combined into one by means of multiplication. This results in a total likelihood distribution for every type of signal given by

$$\mathcal{L}_S(x, y, z) = \mathcal{L}_{S,\text{caus}}(x) \cdot \mathcal{L}_{S,\text{asym}}(y) \cdot \mathcal{L}_{S,\text{reco}}(z), \quad (4.4)$$

with  $\mathcal{L}_{S,\text{caus}}$ ,  $\mathcal{L}_{S,\text{asym}}$  and  $\mathcal{L}_{S,\text{reco}}$  respectively the likelihood distributions for the Causality, Energy Asymmetry and Reconstructed Length corresponding to the type of signal  $S$ . This total likelihood distribution can readily be interpreted as the combined probability distribution of the three parameters given the type of signal. With the different types of signals given in Table 4.1 a total of six of these likelihood distributions can be created. Hereby the Astro Tau Neutrino signal type has been omitted as we will prefer using the Double Bang total likelihood anyway, since we can expect the latter to distinguish Double Bang signals from background more accurately. It is important to realize that all of these likelihoods can be evaluated for a given event, independent of its type, as long as its Causality, Energy Asymmetry and Reconstructed Length are known.

Next we can start combining these total likelihoods to form a variety of TS parameters. The general recipe can be summarized by

$$\text{TS} = \frac{\prod_S \log(\mathcal{L}_S)}{\prod_{S'} \log(\mathcal{L}_{S'})}, \quad (4.5)$$

i.e. building up the TS parameter as a the ratio of two products of total log-likelihood distributions. More specifically this work focused on TS parameters of the form

$$\text{TS} = \frac{\log(\mathcal{L}_{\text{DB}})^n}{\prod_{i=1}^n \log(\mathcal{L}_{S_i})} \quad (4.6)$$

with  $S_i \neq S_j$  for  $i \neq j$ , restricting the maximum value of  $n$  to 5, and DB referring to the Double Bang signal type. This reduces the otherwise infinite number of possibilities to a manageable number of TS parameters. Using Eq. (4.6) and (4.4) we can now compute a variety of TS parameters for the same simulation data events mentioned before and so construct estimations of corresponding TS distributions, one for the Double Bang signal type and five for the background signal types. Examples of these can be found in Appendix B. As can be seen changing the TS parameter, although still following the restriction (4.6), can bring about significant changes in the TS distributions. Events with total likelihood values of zero have undefined corresponding total log-likelihood values. These are left out during the construction of distributions of TS parameters requiring these specific log-likelihood values to be defined.

In order to find the TS parameter most suited for the analysis we do the following. As the number of expected remaining Double Bang events after performing the cuts on the Causality, Energy Asymmetry and Reconstructed Length as described in Section 4.1.4 is about 0.5 in four years of IceCube data, we search for the TS parameter leading to the cut which yields the best signal-to-background ratio requiring at least as many Double Bang signals survive. Hereby we restrict ourselves to cuts of the form

$$\text{TS} < \text{cut value} .$$

As the TS distributions are normalized this means that in practice the most efficient

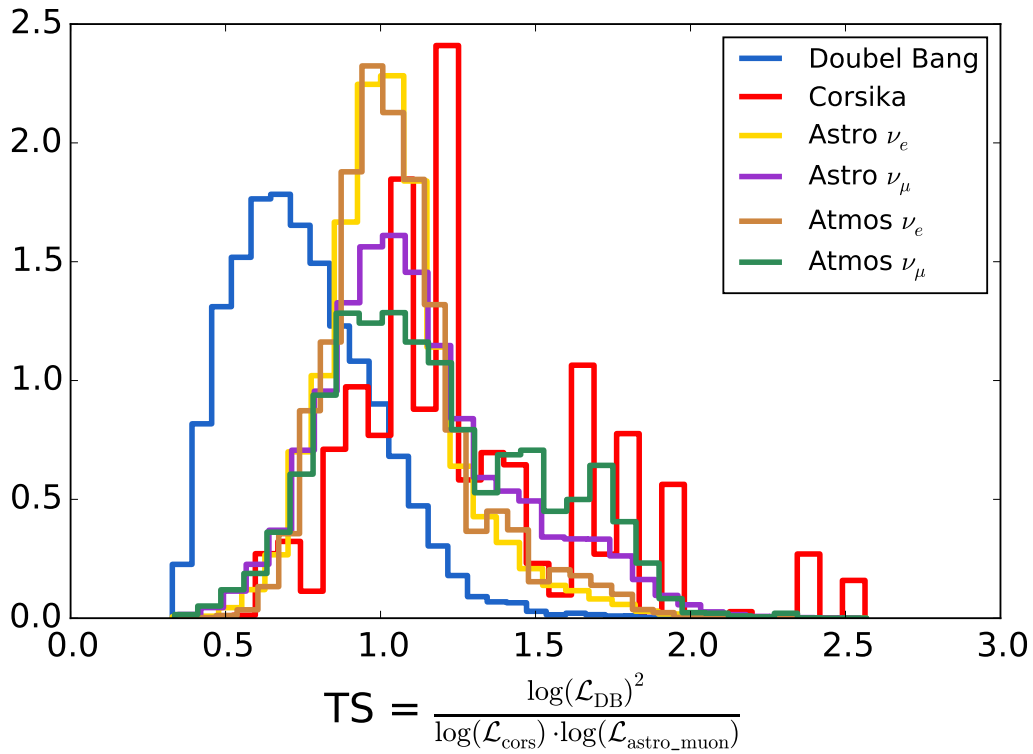


FIGURE 4.3: The normalized TS distributions of the optimal TS parameter for the Double Bang signal type and the five background signal types.

way of testing the potency of a TS parameter is by integrating the corresponding TS distributions up to different upper limits, giving us estimations of the fraction of surviving events for every signal type given the upper limit would be used as cut value. Combined with the number of events that survived the processing up to Level 5 of every signal type this yields the expected number of events for every signal type that will survive this specific cut. The signal-to-background ratio can then be found by comparing the number of expected surviving Double Bang events with that of the background events. Using the integration method and requiring that at least about 0.5 remaining Double Bang events are expected in four years of IceCube data it was found that the TS parameter shown in Figure 4.3 resulted in the best signal-to-background ratio. It is expected to increase the signal-to-background ratio from  $6.18 \times 10^{-3}$  up to 0.111 using a cut value of 0.682, hereby reducing the number of remaining Double Bang events to 0.502. It was also found to yield the best signal-to-background ratios requiring at least 0.25 and 1.00 events are expected to survive.

By the definition of the optimal TS parameter given in Figure 4.3 it is only to be expected to find its Double Bang distribution separated from the others, tending to smaller TS values. We recall that the total likelihood distribution  $\mathcal{L}_S$  can be interpreted as the probability of an event having a certain Causality, Energy Asymmetry and Reconstructed Length value assuming it is an event of type  $S$ . This means we can expect for events labeled as Double Bang signals that in general its  $\mathcal{L}_{DB}$  value is larger than its  $\mathcal{L}_{cors}$  or  $\mathcal{L}_{astro\_muon}$  value, or equivalently that its  $\log(\mathcal{L}_{DB})$  is larger

than its  $\log(\mathcal{L}_{\text{cors}})$  or  $\log(\mathcal{L}_{\text{astro\_muon}})$  value:

$$\log(\mathcal{L}_{\text{DB}}) > \log(\mathcal{L}_{\text{cors}}), \log(\mathcal{L}_{\text{astro\_muon}}).$$

As the total likelihood values represent probabilities we know they lie in the interval  $[0, 1]$ , which means the condition stated above implies

$$\log(\mathcal{L}_{\text{DB}})^2 < \log(\mathcal{L}_{\text{cors}}) \cdot \log(\mathcal{L}_{\text{astro\_muon}}).$$

We thus indeed expect most TS values corresponding to events marked as Double Bang signals to be smaller than one. An analogous reasoning leads us to predict true Corsika and Astro Muon Neutrino events to be shifted to TS values larger than one. As the Astro Muon Neutrino and Atmos Muon Neutrino signals are similar it should not be surprising also the distribution corresponding to the atmospheric muon neutrinos shows a prominent tale towards TS values larger than one. And finally, as they are fish nor fowl, the electron neutrino related signals yielding distributions peaked at  $\text{TS} = 1.0$  also agrees with our expectations. We can thus understand the general features of the TS distributions shown in Figure 4.3. Creating a TS variable capable of separating the Double Bang distribution from the rest is the main reason why the restriction (4.6) was imposed.

We now have a modified Level 6 cut for the Double Bang analysis by Matthias Vraeghe. First we demand both of the reconstructed cascade energies of the event to be larger than zero. Next we compute its TS value given by

$$\text{TS} = \frac{\log(\mathcal{L}_{\text{DB}})^2}{\log(\mathcal{L}_{\text{cors}}) \cdot \log(\mathcal{L}_{\text{astro\_muon}})}, \quad (4.7)$$

removing the event if  $\mathcal{L}_{\text{DB}} = 0$ ,  $\mathcal{L}_{\text{cors}} = 0$  or  $\mathcal{L}_{\text{astro\_muon}} = 0$ . Finally we require the TS value to be smaller than a given cut value, of which several are discussed in the next section.

## 4.3 Results

### 4.3.1 Modified Level 6

This section will discuss the expected performance of the modified Level 6 cuts compared to the original Level 6 cuts based on simulation. To this end the same datasets as listed in Table 4.1 are used. Cut values of 0.682, 0.561 and 0.995 are applied, which were predicted to respectively yield about 0.50, 0.25 and 1.00 Double Bang events in four year of IceCube data by the integration method mentioned above. Based on these results also a cut  $\text{TS} < 0.600$  has been performed. The numerical results can be found in Table 4.2.

**TS < 0.682** Figure 4.4 shows the expected remaining events after processing four years of IceCube data to the modified Level 6 using the cut  $\text{TS} < 0.682$ , as well as the expected remaining events after processing the data to Level 5 and the original Level 6. As can be seen the number of expected remaining Double Bang signals of both the modified as well as the original Level 6 are approximately equal, which is exactly the reason why the cut value of 0.682 was chosen, meaning about 60% of the Double Bang events were lost. Looking at all Astro Tau Neutrino signals we see that a considerable amount is lost, about 90%, which is however a smaller loss compared to the original Level 6. The reduction of Corsika events is significantly

	Level 5	original Level 6	modified Level 6			
			TS < 0.682	TS < 0.561	TS < 0.995	TS < 0.600
DB	1.21	0.461	0.502	0.257	1.00	0.325
Astro $\nu_\tau$	13.2	0.864	1.40	0.446	6.67	0.661
Corsika	156	13.8	3.49	0.105	30.7	0.208
Astro $\nu_e$	28.5	0.118	0.621	0.112	10.2	0.209
Astro $\nu_\mu$	8.99	0.352	0.356	9.67e-2	2.98	0.149
Atmos $\nu_e$	1.63	6.02e-3	1.72e-2	1.71e-3	0.525	4.10e-3
Atmos $\nu_\mu$	1.06	1.92e-2	4.28e-2	1.29e-2	0.316	1.84e-2
sig/bg DB	6.18e-3	3.22e-2	0.111	0.783	2.23e-2	0.552
sig/bg Astro $\nu_\tau$	6.70e-2	6.03e-2	0.309	1.36	0.149	1.13

TABLE 4.2: The expected results after processing to the modified Level 6 using different cut values, compared with the expected results after processing to Level 5 and the original Level 6. The signal-to-background ratio (sig/bg) of both the Double Bang events as well as the Astro Tau Neutrino events are shown.

better, reducing the number of expected remaining events further down from 13.8 to 3.49. Going through the remaining four background signal types we see that the original Level 6 performs just as well or even better than the modified Level 6. Due to the serious decrease in Corsika signals the signal-to-noise ratio of both the Double Bang events as well as the Astro Tau Neutrino events are notably larger compared to the original Level 6.

**TS < 0.561** The results using TS < 0.561 are shown in Figure 4.5. The cut is clearly more strict, bringing the expected Double Bang and Astro Tau Neutrino rates of the original Level 6 further down with respectively a factor of 1.8 and 1.9. The reduction of the Corsika events is however striking, reducing the expected rate after processing to the original Level 6 by two orders of magnitude. Both the Astro Tau Neutrino and the Double Bang event rates now surpass all individual background signal rates, with the first one even exceeding the total expected background event rate. This is clearly illustrated by the signal-to-background ratios. The modified Level 6 now reduces the other four remaining background event rates to lower values compared to the original Level 6, yet keeping in mind the loss in Astro Tau Neutrino and Double Bang signal the actual gain here does not seem significant.

**TS < 0.995** Figure 4.6 shows the results obtained when using a cut value of 0.995. The original Level 6 clearly rejects more Double Bang and Astro Tau Neutrino events as well as background events. Although at first glance processing the data from Level 5 to the modified Level 6 does not seem to change the relative abundances of the different types of events a lot, at least not when the rates of both levels are plotted on a logarithmic scale, the modified Level 6 actually reduces the individual backgrounds with a notably larger factor than the Double Bang and the Astro Tau Neutrino events. This is again clearly illustrated by the signal-to-background ratios, as going from Level 5 to the modified Level 6 the Double Bang and the Astro Tau Neutrino signal-to-background ratios are respectively increased by a factor of 3.6 and 2.2. Compared to those corresponding to the original Level 6 the Double Bang

signal-to-background ratio decreases with a factor of 1.4, while that of the Astro Tau Neutrino signal increases with a factor of 2.5. At higher cut values the modified Level 6 seems to focus less on the Double Bang signatures of tau neutrinos only, especially when compared to the original Level 6. Using the modified Level 6 with  $TS < 0.995$  results in what could be called an economical cut, ending up with about 3.5 times more data compared to the original Level 6 yet improving the signal-to-background ratio obtained at Level 5 significantly.

**TS < 0.600** In an attempt of finding a compromise between limiting Double Bang and Astro Tau Neutrino signal losses and removing Corsika events a cut value of 0.600 has been tested, the result of which is shown in Figure 4.7. Both the Astro Tau Neutrino and the Double Bang event rates again surpass all individual background signal rates as is the case using a cut value of 0.561, now bringing the two corresponding rates of the original Level 6 further down with respectively a factor of 1.4 and 1.3. The reduction of the Corsika event rate is once again striking. Compared to the results obtained when using a cut value of 0.561 we see that we end up with about two times more expected Corsika event rates, with an expected Double Bang and Astro Tau Neutrino event rate of respectively only 1.3 and 1.5 times larger. The increase of both types of tau neutrino event rates is thus smaller than that of the Corsika event rate. Looking at the number of expected Astro Electron Neutrino and Astro Muon Neutrino events, together with the Corsika events forming the main background components at the modified Level 6, we see the same trend. We should thus not be surprised that both the signal-to-background ratios are now smaller compared to those of the  $TS < 0.561$  cut. Using a cut value of 0.600 instead of 0.682 does however reduce the Corsika event rate significantly more than the Double Bang and Astro Tau Neutrino event rates, increasing the corresponding signal-to-background ratios with a factor of 3.7 and 5.0. The loss in Double Bang and in particular Astro Tau Neutrino signals is however substantial.

We can conclude that it is not straightforward to determine the optimal cut value. The two lowest values discussed here increase the signal-to-background ratio of the original Level 6 to much higher values, however also losing notably more Double Bang and Astro Tau Neutrino events. The increase in the signal-to-background ratios is mainly due to the considerable reduction of Corsika events. The change in the other types of background event rates compared to the original Level 6 is far less favorable and in itself does not really justify the loss in signals of interest. The two highest cut values on the other hand cut out significantly less Double Bang and Astro Tau Neutrino events, yet at the cost of an increase in the individual background event rates. Only thanks to the efficient removal of Corsika events the signal-to-background ratios are in general still higher than those of the original Level 6.

The general conclusion of the comparison between the performance of the original Level 6 and the modified Level 6 is therefore the following. We recall that the determination of the best TS parameter is based on its resulting Double Bang signal-to-background ratio given some constraints. Based on the way the modified Level 6 was designed it is thus only to be expected that it mainly results in a reduce of total background which, as they form by far the main background component on Level 5, translates to significantly better cuts on the Corsika events. In contrary, the original Level 6 was designed to deal with Astro Electron Neutrino events in particular. The modified Level 6 only just equals the original cut at the lowest cut value tested, hereby also losing significantly more Double Bang and Astro Tau Neutrino events. As Level 7 was especially designed to filter out Corsika events we can thus expect

combining it with the original Level 6 to give the best results, as both levels then focus on two different type of backgrounds. The combination of Level 7 with the modified Level 6 will probably be a far less efficient scheme.

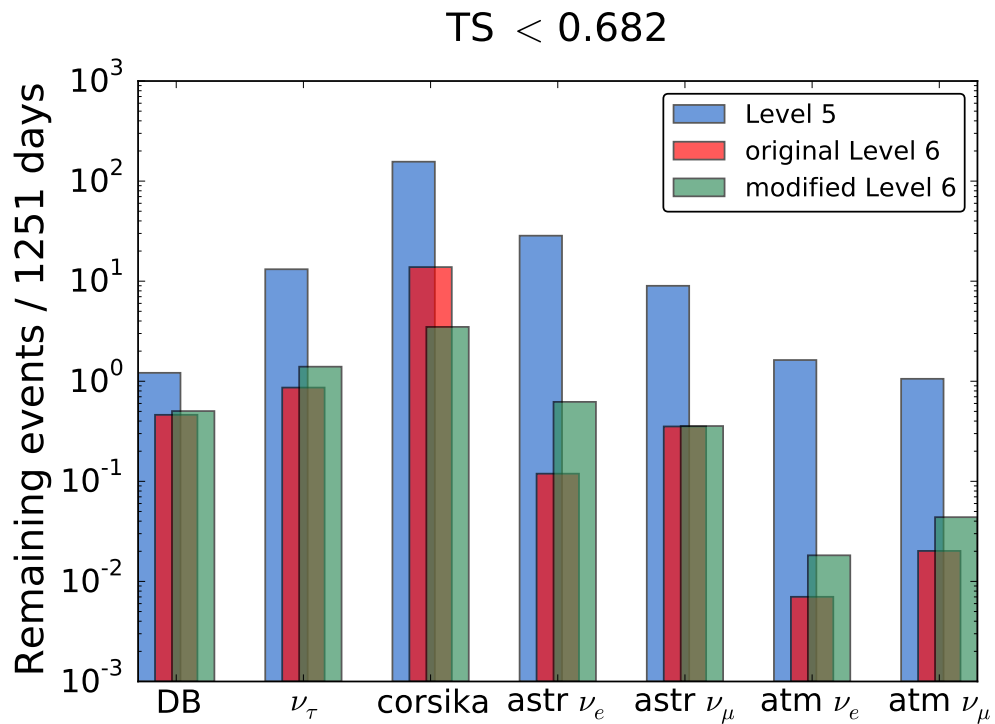


FIGURE 4.4: The expected results after processing to the modified Level 6 using the cut  $TS < 0.682$ , compared with the expected results after processing to Level 5 and the original Level 6.

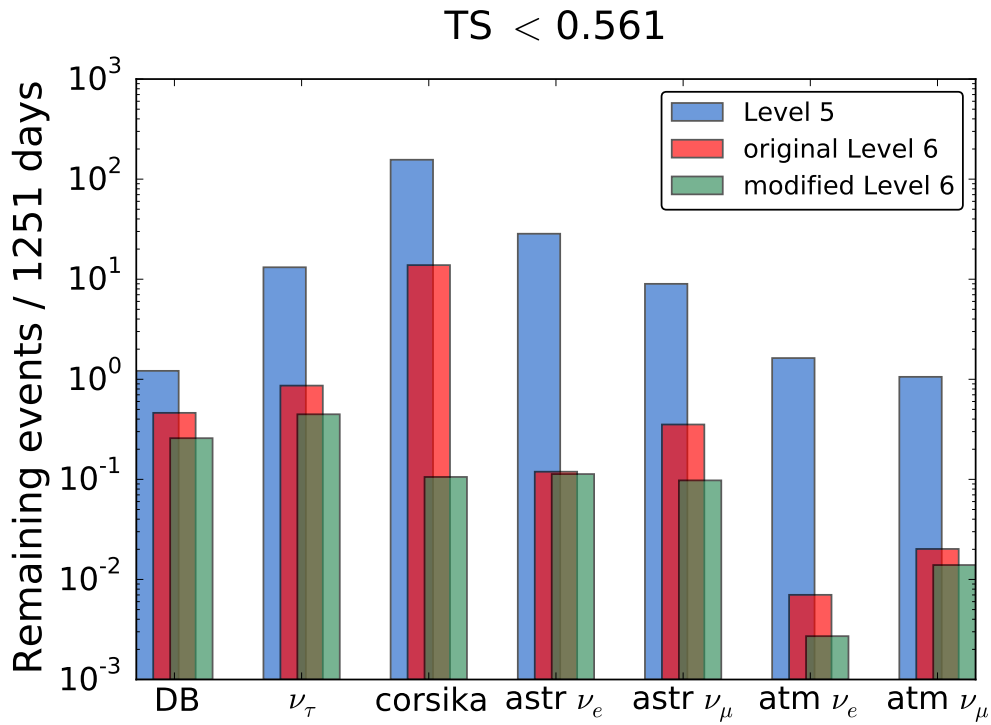


FIGURE 4.5: The expected results after processing to the modified Level 6 using the cut  $TS < 0.561$ , compared with the expected results after processing Level 5 and the original Level 6.

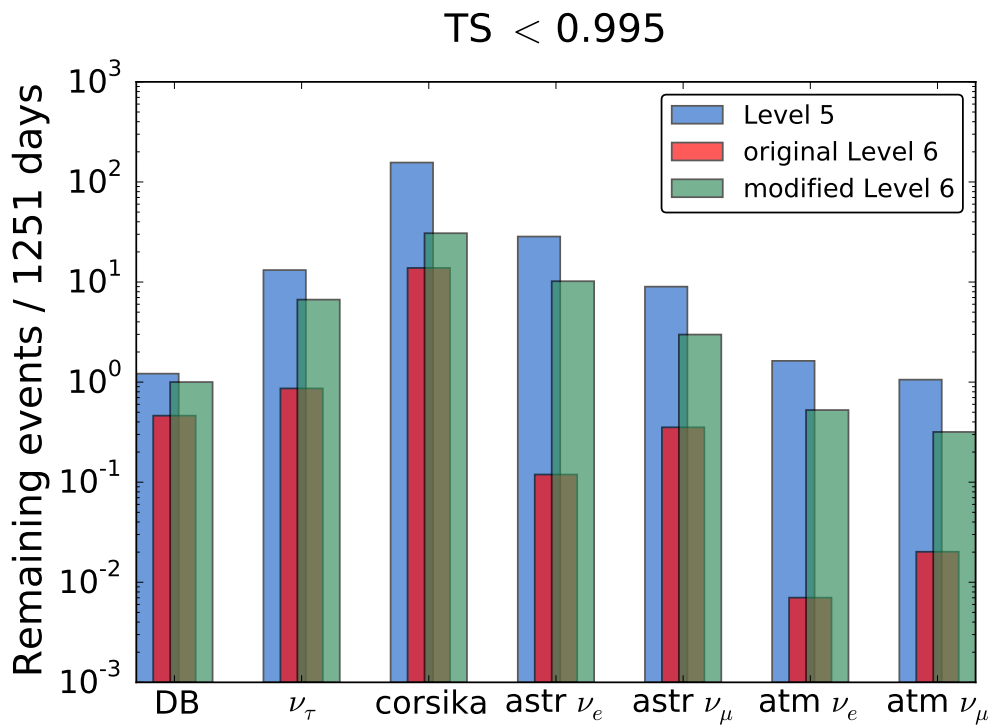


FIGURE 4.6: The expected results after processing to the modified Level 6 using the cut  $TS < 0.995$ , compared with the expected results after processing to Level 5 and the original Level 6.

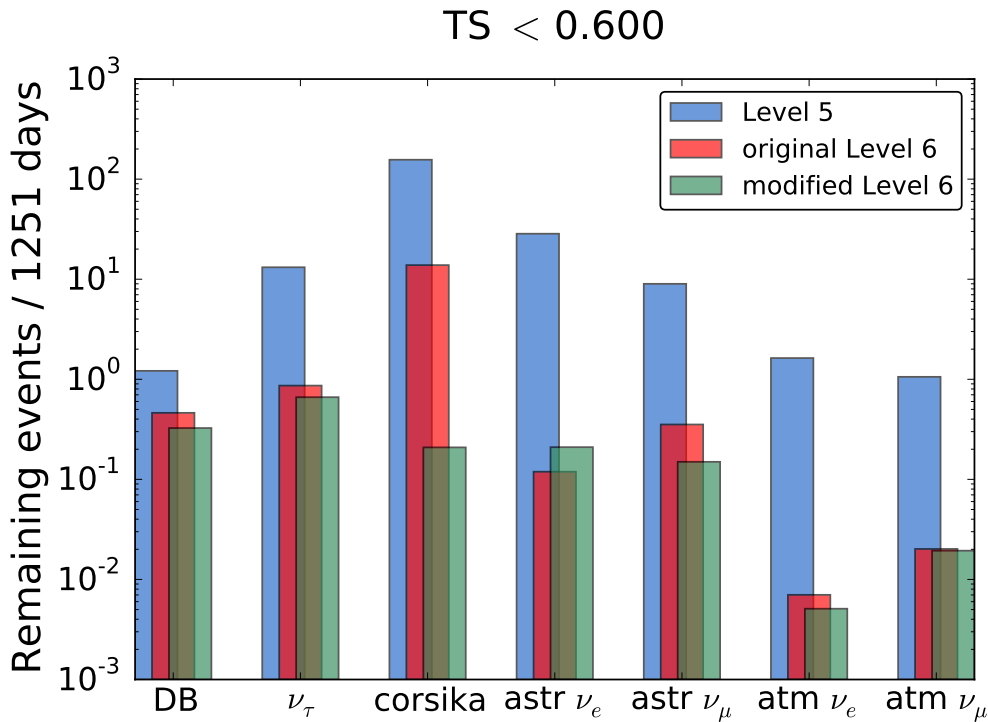


FIGURE 4.7: The expected results after processing to the modified Level 6 using the cut  $TS < 0.600$ , compared with the expected results after processing to Level 5 and the original Level 6.

### 4.3.2 Level 7 via Modified Level 6

This section will discuss the expected remaining events after processing the data to Level 7 while replacing the original Level 6 with the modified Level 6. The same cut values as in the previous section have been considered. The numerical results can be found in Table 4.3. The expected remaining rates of the Astro Tau Neutrino events and the different types of background events based on the simulation datasets used in this thesis have been compared with the values given by Matthias and were found to be consistent.

**$TS < 0.682$**  The results obtained using a cut value of 0.682 are shown in Figure 4.8. While expecting considerably more Astro Tau Neutrino events, it is clear using the modified Level 6 instead of the original Level 6 results in less removal of background events. The gain in the Astro Tau Neutrino event rate does not compensate the increase of the Astro Electron Neutrino rate, which forms the main background component using the modified data reduction scheme. The expected signal-to-background ratio of the Double Bang signal using the modified Level 6 is about half that using the original Level 6, while the signal-to-background ratio of the Astro Tau Neutrino signal has decreased with a factor of 1.5.

**$TS < 0.561$**  Figure 4.9 shows the results requiring  $TS < 0.561$ . Although expecting less Double Bang and Astro Tau Neutrino events, the scheme implementing the modified Level 6 still ends up with more Corsika events compared to the original analysis. The other types of background event rates are reduced further down,

	original analysis	modified analysis			
		TS < 0.682	TS < 0.561	TS < 0.995	TS < 0.600
DB	0.403	0.416	0.213	0.803	0.267
Astro $\nu_\tau$	0.759	1.08	0.347	4.49	0.510
Corsika	2.55e-2	8.14e-2	3.70e-2	5.34	3.70e-2
Astro $\nu_e$	9.55e-2	0.386	6.26e-2	6.21	0.122
Astro $\nu_\mu$	0.189	0.207	5.44e-2	1.61	8.31e-2
Atmos $\nu_e$	4.69e-3	1.06e-2	9.82e-4	0.288	2.12e-3
Atmos $\nu_\mu$	1.43e-2	2.89e-2	9.90e-3	0.210	1.40e-2
sig/bg DB	1.22	0.583	1.29	5.88e-2	1.03
sig/bg Astro $\nu_\tau$	2.31	1.51	2.10	0.329	1.97

TABLE 4.3: The expected results after processing to Level 7 via the modified Level 6 using different cut values, compared with the expected final results of the original analysis. The signal-to-background ratio (sig/bg) of both the Double Bang events as well as the Astro Tau Neutrino events are shown.

however not justifying the additional losses in signals of interest. The signal-to-background ratios of the modified and the original analysis are very similar, yet the modified one yielding only about half the number of both the Double Bang and Astro Tau Neutrino events.

**TS < 0.995** As clearly depicted by Figure 4.10 using the modified Level 6 with a cut value of 0.995 results in a far less efficient background reduction. With about 209.4 times more Corsika events and 65.0 times more Astro Neutrino Events and only an increase in Double Bang signals and Astro Tau Neutrino with respectively a factor of 2.0 and 5.9, the data reduction scheme fails in reducing the total background signal rate below those of the signals of interest. The final Double Bang and Astro Tau Neutrino signal-to-background ratios are smaller than one, with those of the original analysis 20.7 and 7.0 times larger.

**TS < 0.600** The rates obtained after processing to Level 7 using the modified Level 6 with the condition TS < 0.600 is shown in Figure 4.11. Compared to the original analysis it again cuts out less Corsika events. It does however remove more Astro Muon events, which form the main background component in the final results of the original analysis. The Double Bang and Astro Tau Neutrino rates are both further reduced with a factor of 1.5, again not compensated by the reduction of background events. This leads to a decrease of the Double Bang and Astro Tau Neutrino signal-to-background ratios, each with a factor of 1.2.

Based on the results shown in the previous section it might be surprising that using the modified Level 6, regardless of the cut value used, results in higher Corsika event rates at Level 7. Together with acknowledging the impressive efficiency of Matthias' Level 7 cut, this can be understood by considering the physics behind the TS distribution. As explained earlier in this chapter we expect Corsika-like events to score TS values higher than one by construction of the TS parameter. This means that after cutting out the events with a TS value higher than a given cut value smaller

than one we are left with what we could call atypical Corsika events. These atypical Corsika events correspond to lower TS values, meaning that according to Figure 4.3 they look more like Double Bang or Electron Neutrino events than typical Corsika events. It is therefore to be expected that the cut of Level 7, designed to filter out typical Corsika signals, reduces the Corsika event rate of data on the modified Level 6 with a substantially lower factor. The main fraction of events Level 7 would have removed have already left the dataset by processing to the modified Level 6. The original Level 6 however focuses more on removing single cascade events, which means it also leads to the removal of some of these atypical Corsika events.

As foreshadowed in the previous section we see that the combination of the modified Level 6 with Level 7 indeed results in a far less efficient data reduction scheme compared to the original one. The two levels are in essence designed to remove the same background data. The original Level 6 on the other hand focuses on reducing the rate of single cascade events, which leads to the removal of significantly more Astro Neutrino events as well as some of the atypical Corsika events. The original analysis outperforms the modified one, leading to notably better Double Bang and Astro Tau Neutrino signal-to-noise ratios and thus confirming the general conclusion of Section 4.3.1.

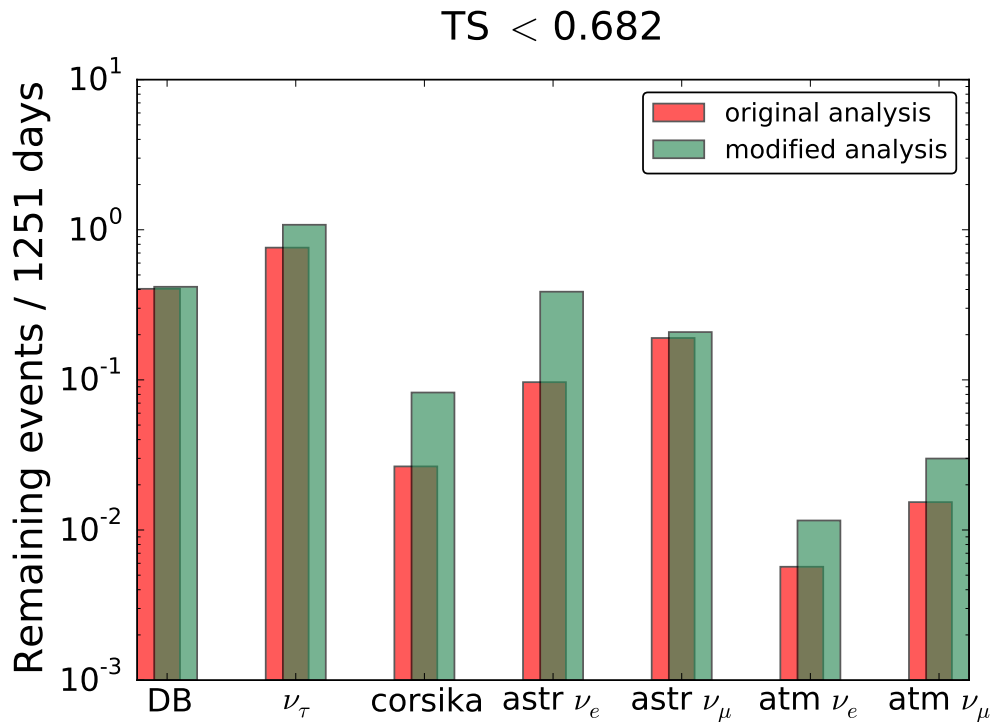


FIGURE 4.8: The expected results after processing to Level 7 via the modified Level 6 using the cut TS < 0.682, compared with the expected final results of the original analysis.

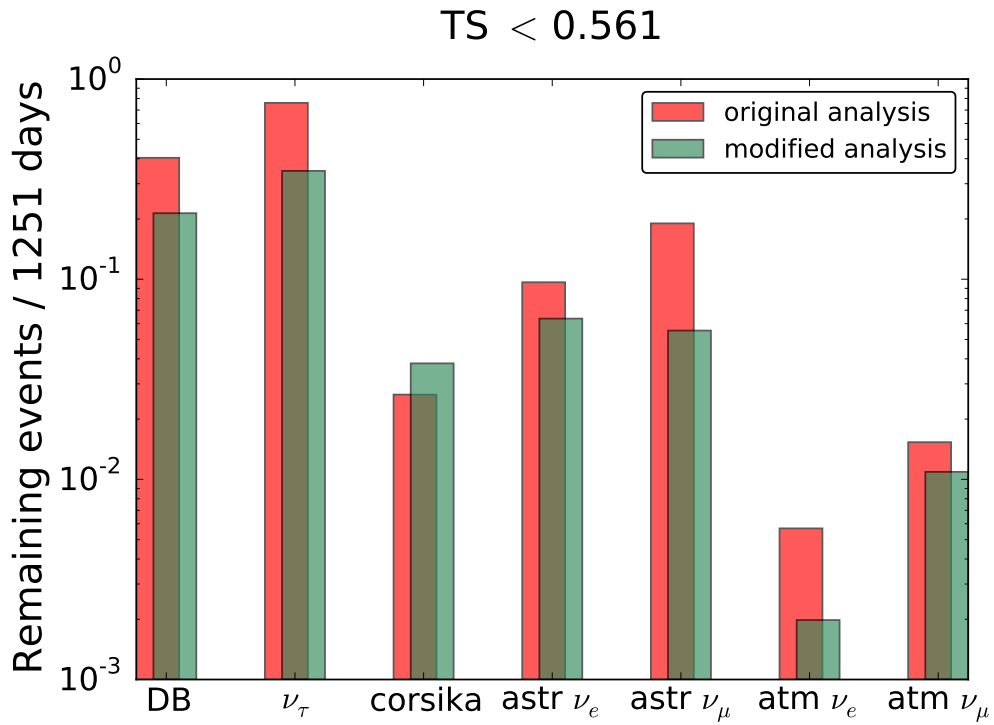


FIGURE 4.9: The expected results after processing to Level 7 via the modified Level 6 using the cut TS < 0.561, compared with the expected final results of the original analysis.

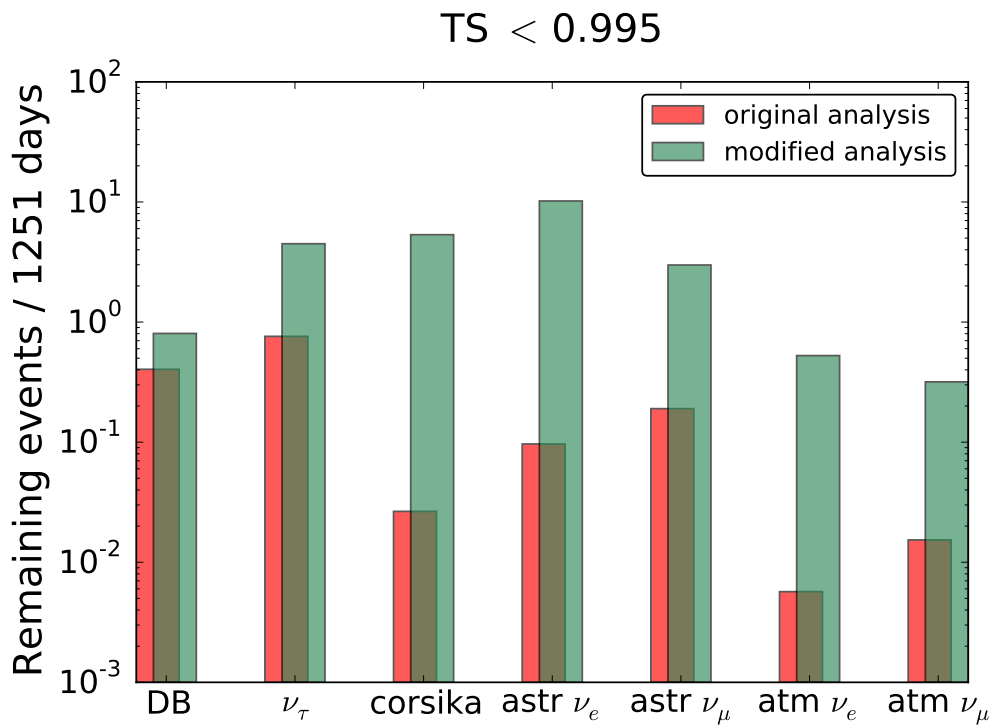


FIGURE 4.10: The expected results after processing to Level 7 via the modified Level 6 using the cut TS < 0.995, compared with the expected final results of the original analysis.

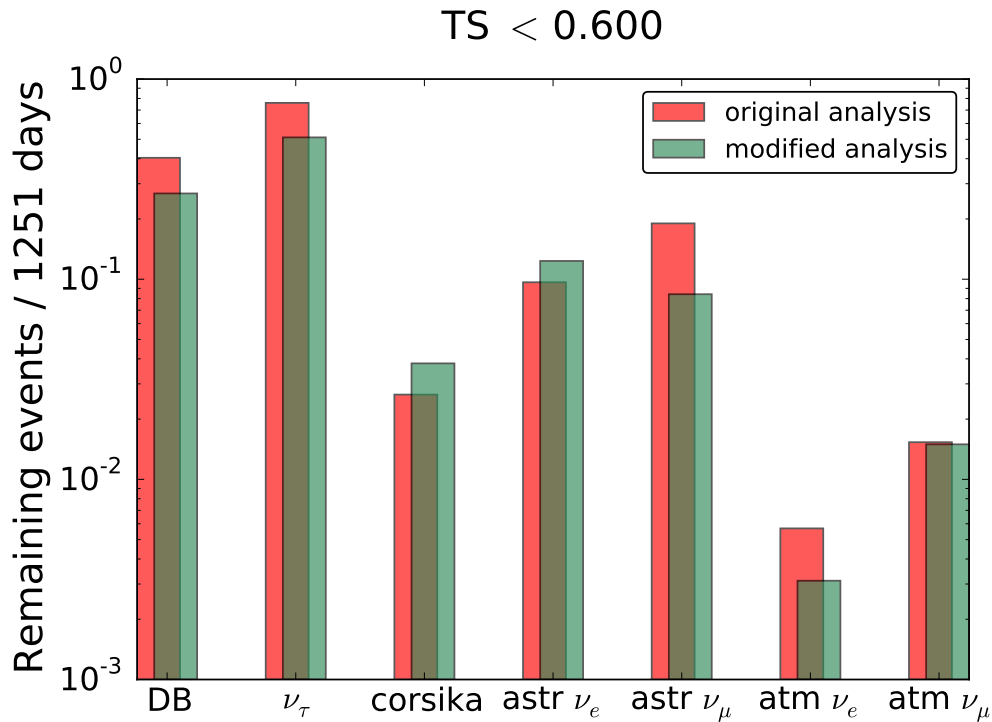


FIGURE 4.11: The expected results after processing to Level 7 via the modified Level 6 using the cut TS < 0.600, compared with the expected final results of the original analysis.

### 4.3.3 Level 7+

As can be seen in Table 4.3, after using the original data reduction scheme most of the remaining background is dominated by astrophysical muon neutrinos. The modified reduction scheme can, with for example a cut value of 0.600, lower the Astro Muon Neutrino rate significantly, however losing signals of interest as well as increasing the rate of Astro Electron Neutrino and Corsika events. With this in mind a final attempt at improving the original data reduction scheme has been made by combining both the original and the modified Level 6. In practice the modified data reduction scheme has been applied, which processes the data up to Level 7 by passing through the modified Level 6, followed by reducing the data further by using the cuts of the original Level 6. I will refer to data processed this way as being on Level 7+. This reflects my interpretation of the inclusion of the modified Level 6 cuts to the analysis as a possible refinement of the analysis instead of the addition of an entirely new level, hereby hoping to reduce the Astro Muon Neutrino event rate without losing much of the Double Bang and Astro Tau Neutrino events. Next to the same values discussed in the two previous sections also the cut value of 0.839 is considered, the reason of which will become clear further down. The numerical results can be found in Table 4.4. It can be seen that all the final event rates of the original analysis have been further reduced by processing to Level 7+, regardless of the TS cut value used, as should be. Four of the Corsika neutrino rates being identical is an artificial feature introduced by the simulation, as it corresponds to the weight of the only remaining Corsika event in the simulation data set.

	original analysis	Level 7+				
		TS < 0.682	TS < 0.561	TS < 0.995	TS < 0.600	TS < 0.839
DB	0.403	0.177	8.62e-2	0.375	0.109	0.300
Astro $\nu_\tau$	0.759	0.322	0.109	0.739	0.153	0.588
Corsika	2.55e-2	8.95e-3	8.95e-3	1.57e-2	8.95e-3	8.95e-3
Astro $\nu_e$	9.55e-2	1.61e-2	2.07e-3	8.95e-2	6.55e-3	7.18e-2
Astro $\nu_\mu$	0.189	2.40e-2	7.97e-3	0.130	1.20e-2	7.41e-2
Atmos $\nu_e$	4.69e-3	3.57e-4	9.21e-5	4.00e-3	1.40e-4	3.53e-3
Atmos $\nu_\mu$	1.43e-2	2.61e-3	8.19e-4	1.11e-2	1.30e-3	7.11e-3
sig/bg DB	$1.22 \pm 0.06$	$3.41 \pm 0.62$	$4.33 \pm 1.98$	$1.50 \pm 0.08$	$3.75 \pm 1.20$	$1.81 \pm 0.12$
sig/bg Astro $\nu_\tau$	$2.31 \pm 0.11$	$6.19 \pm 1.12$	$5.46 \pm 2.49$	$2.95 \pm 0.16$	$5.29 \pm 1.69$	$3.55 \pm 0.23$

TABLE 4.4: The expected results after processing to Level 7+ using different cut values, compared with the expected final results of the original analysis. The signal-to-background ratio (sig/bg) of both the Double Bang events as well as the Astro Tau Neutrino events are shown.

**TS < 0.682** The results of using a cut value of 0.682 are shown in Figure 4.12. Compared to the original results the expected numbers of Double Bang and Astro Tau Neutrino events in four years of IceCube data have been reduced with respectively a factor of 2.3 and 2.4, meaning we expect to require about 12 years of IceCube data in order to find one astrophysical tau neutrino if using this data reduction scheme and TS cut value. The total background is however reduced to a significantly smaller fraction of the total data, yielding a Double Bang and Astro Tau Neutrino signal-to-background ratio of 2.8 and 2.7 times larger as those of the original analysis. We do note however that, due to the substantial loss in events, the statistical errors on these values are large compared to the original analysis. The Astro Muon Neutrino event rate is indeed notably lower, being decreased by a factor of 7.9. The loss in astrophysical tau neutrino events is compensated by the loss in background signals, yet its rate is just too low to be used in practice. Compared to the results obtained at Level 7 when using only the modified Level 6 the Astro Electron Neutrino rate has been decreased with a factor of 24.0, while the Double Bang and Astro Tau Neutrino rates are reduced with a factor of 2.4 and 3.4.

**TS < 0.561** Figure 4.13 shows the results when applying a cut value of 0.561. The Double Bang and Astro Tau Neutrino rates are now respectively 4.7 and 7.0 times smaller than those of the original analysis, implying we only expect to see an astrophysical tau neutrino signal in about 40 years of IceCube data. As this is of the order of the estimated lifespan of the IceCube Neutrino detector it is clear that using this cut value is not an option. Although the number of expected remaining astrophysical muon neutrinos is reduced with a factor of 23.7 and, somewhat surprisingly, the Astro Electron Neutrino rate even with a factor of 46.1, the loss in astrophysical tau neutrino signals is simply far too much. The cut value of 0.682 gives both higher rates in signals of interest as well as a better Astro Tau Neutrino signal-to-background ratio. The corresponding statistical errors make it hard to determine the gain in signal-to-noise ratios.

**TS < 0.995** The Level 7+ rates obtained using a cut value of 0.995 are shown in Figure 4.14. The Double Bang and Astro Tau Neutrinos are only about 1.07 and 1.02 times smaller compared to the original results, while the Astro Muon Neutrino events are reduced with a factor of 1.45. The loss in background signals compensates for the loss in signals of interest, increasing the Double Bang and Astro Tau Neutrino signal-to-background ratios respectively from 1.22 to 1.50 and from 2.31 to 2.95. As the expected Corsika event rate given here is based on only two remaining simulated events, the statistical error is substantial. Based on Poisson statistics we find a statistical standard deviation of  $1.12 \times 10^{-2}$ , meaning the magnitude of the further reduction in Corsika events is unclear. It has however only a small impact on the uncertainty on the signal-to-background ratios. With no significant loss in both the Double Bang and Astro Tau Neutrino events, processing the data up to Level 7+ using a TS cut value of 0.995 seems to improve the Double Bang Search by Matthias Vraeghe. Compared to processing to Level 7 using only the modified Level 6, the Astro Electron Neutrino rate has been reduced with a factor of 47.8.

**TS < 0.600** Using the condition  $TS < 0.600$  results in the event rates shown in Figure 4.15. We again see a considerable loss in Double Bang and Astro Tau Neutrino signals, reducing the rates to respectively 0.109 and 0.153 expected remaining events in four years of IceCube data. This means we expect to see one astrophysical tau neutrino in 26 years of IceCube data, making clear using this cut value too results in an unsatisfying data reduction scheme. The reduction of the Astro Muon Neutrino event rate by a factor of 15.8 and that of the Astro Electron Neutrino by a factor of 14.6 nor the Double Bang and Astro Tau Neutrino signal-to-background ratios being increased with a factor of 3.1 and 2.3 can save the data reduction scheme with a TS cut value of 0.600 from being discarded.

**TS < 0.839** Up till now only by using the cut value of 0.995 we have found an improvement of the original results of the analysis. All other values tested simply throw away too much signals of interest. Therefore an additional cut value of 0.839 has been tested, lying right in between 0.682 and 0.995, in the hope of increasing the signal-to-background ratios further while still retaining sufficient high Double Bang and especially Astro Tau Neutrino event rates. The results of this new cut value are shown in Figure 4.16. Again a substantial part of the Double Bang and Astro Tau Neutrino signals are lost, however still corresponding to practicable event rates. Using this TS cut value during the processing of the data to Level 7+ we expect to find about one astrophysical tau neutrino event in 7 years of IceCube data. The background rates have been driven back to significantly lower rates, increasing the original final Double Bang and Astro Tau Neutrino signal-to-background ratios from respectively 1.22 to 1.81 and from 2.31 to 3.55. We should again keep in mind that the expected Corsika rate given here carries a large statistical error of the same value as the actual predicted rate. The Astro Muon Neutrino and Astro Electron Neutrino event rates, i.e. the two largest background event rates after performing the original data reduction scheme, are approximately a factor of 2.6 and 1.3 lower compared to the original final results.

We can conclude the following. Processing the data to what I called Level 7+ by combining the original Level 6 and the modified Level 6 can result in an improvement of the original results of Matthias Vraeghe, mainly by further reducing the Astro Muon Neutrino event rate. Therefore it is required to apply a relatively lax cut on the TS

value proposed in Section 4.2.2, as using too low TS cut values results in impractical Astro Tau Neutrino event rates. It is advised to use TS cut values restricted in a range of about 0.840 to 1.000, with higher values retaining more Double Bang and Astro Tau Neutrino events yet yielding smaller signal-to-background ratios. The values for the Double Bang and Astro Tau Neutrino signal-to-background ratios are predicted to go respectively from roughly 1.50 to 1.80 and 2.90 to 3.60. The inclusion of the modified Level 6 cut to the data reduction scheme can thus indeed be considered as a refinement of the analysis. It leads to a notable reduction of expected remaining Astro Muon Neutrino events, which forms the main background component at Level 7. Its higher sensitivity towards Corsika events seems to show itself again, as in Figure 4.14 and Figure 4.16 also the reduction of the Corsika event rate stands out. We should however keep in mind its large statistical error, indicating it could as well be just a coincidence.

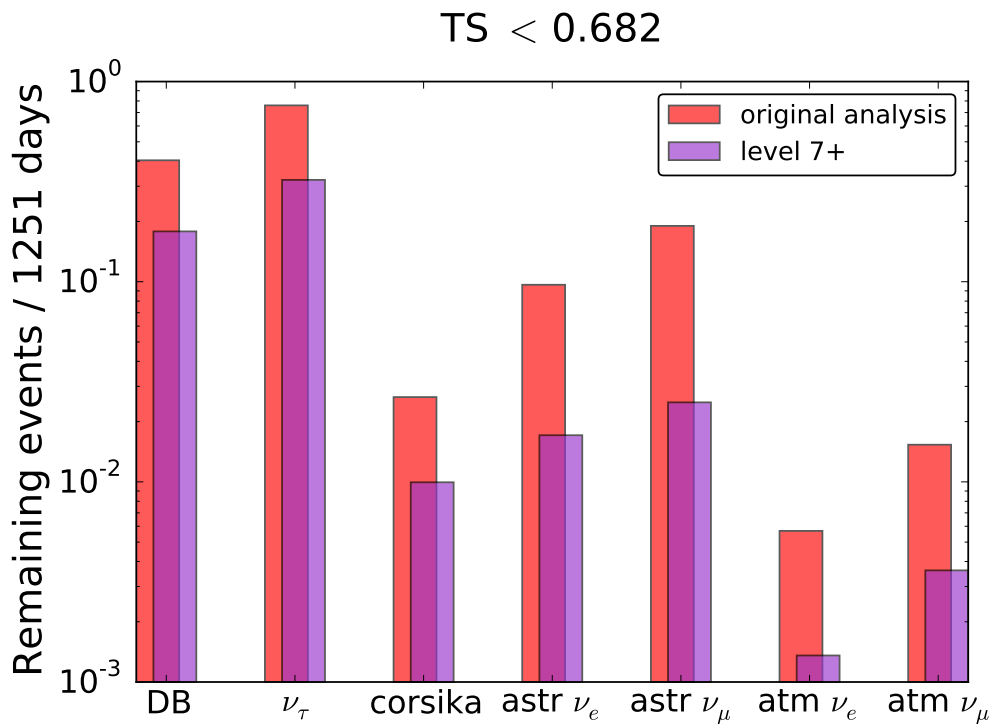


FIGURE 4.12: The expected results after processing to Level 7+ using the cut  $TS < 0.682$ , compared with the expected final results of the original analysis.

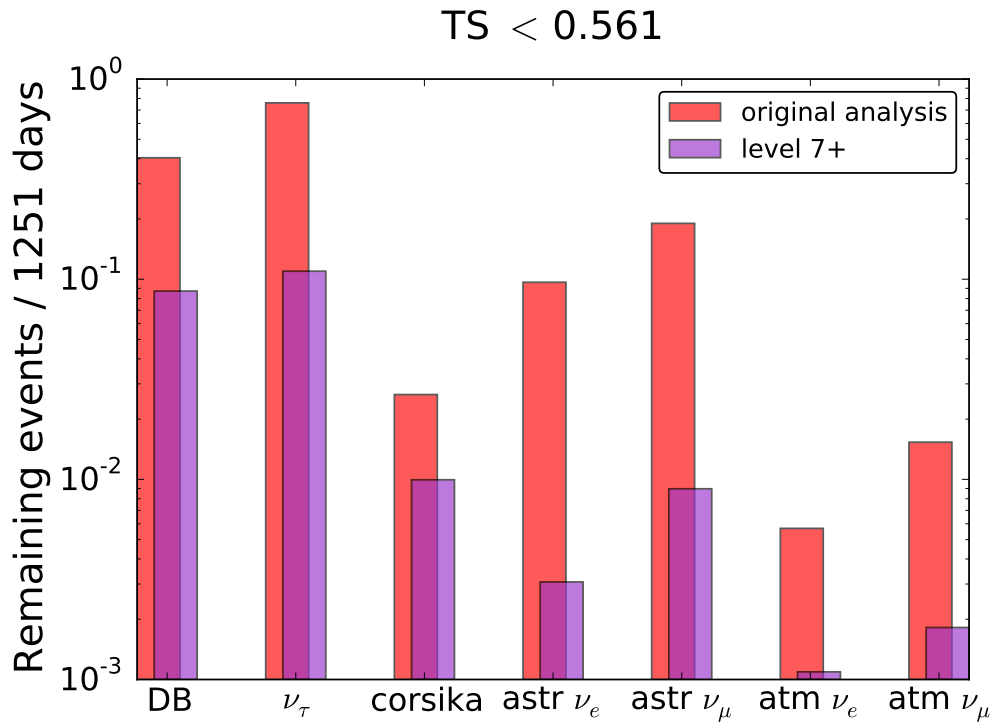


FIGURE 4.13: The expected results after processing to Level 7+ using the cut TS < 0.561, compared with the expected final results of the original analysis.

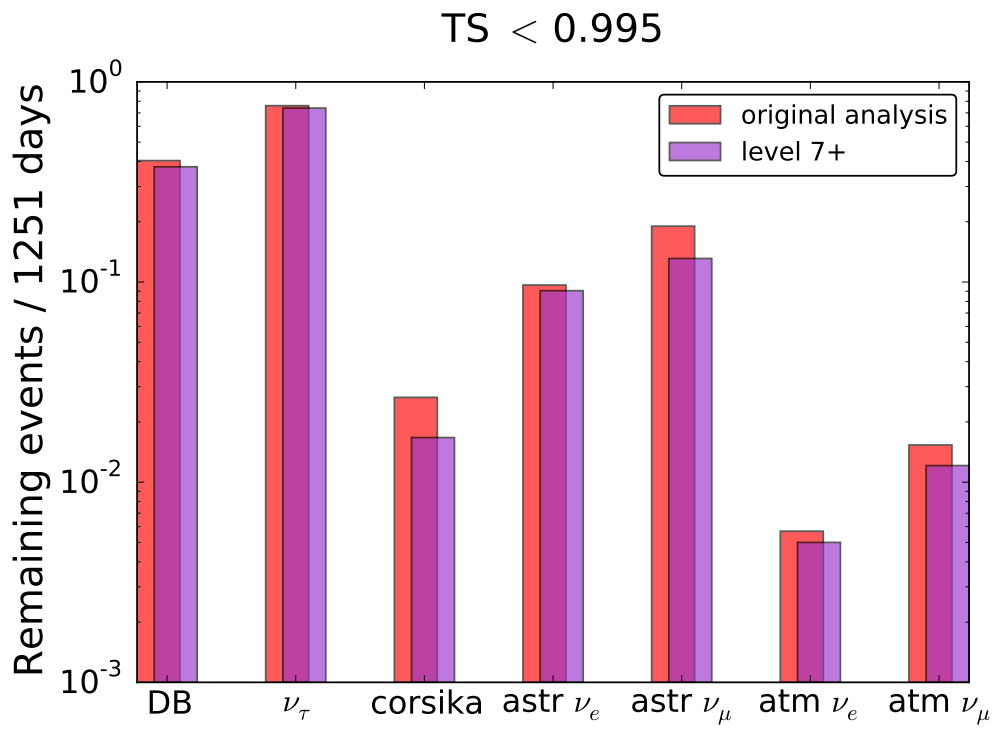


FIGURE 4.14: The expected results after processing to Level 7+ using the cut TS < 0.995, compared with the expected final results of the original analysis.

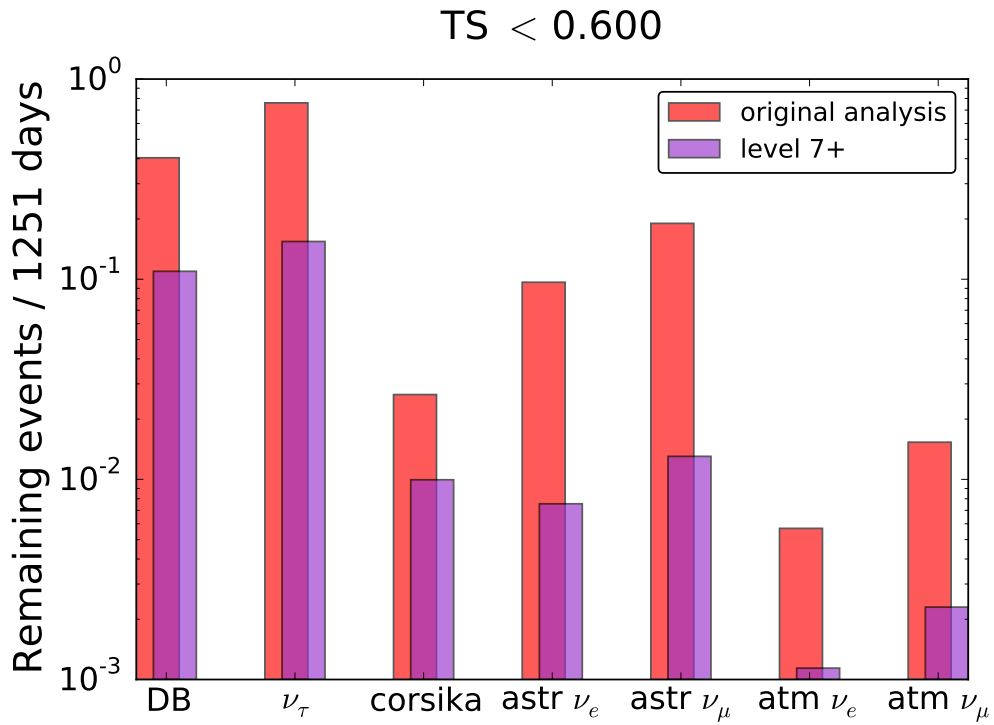


FIGURE 4.15: The expected results after processing to Level 7+ using the cut TS < 0.600, compared with the expected final results of the original analysis.

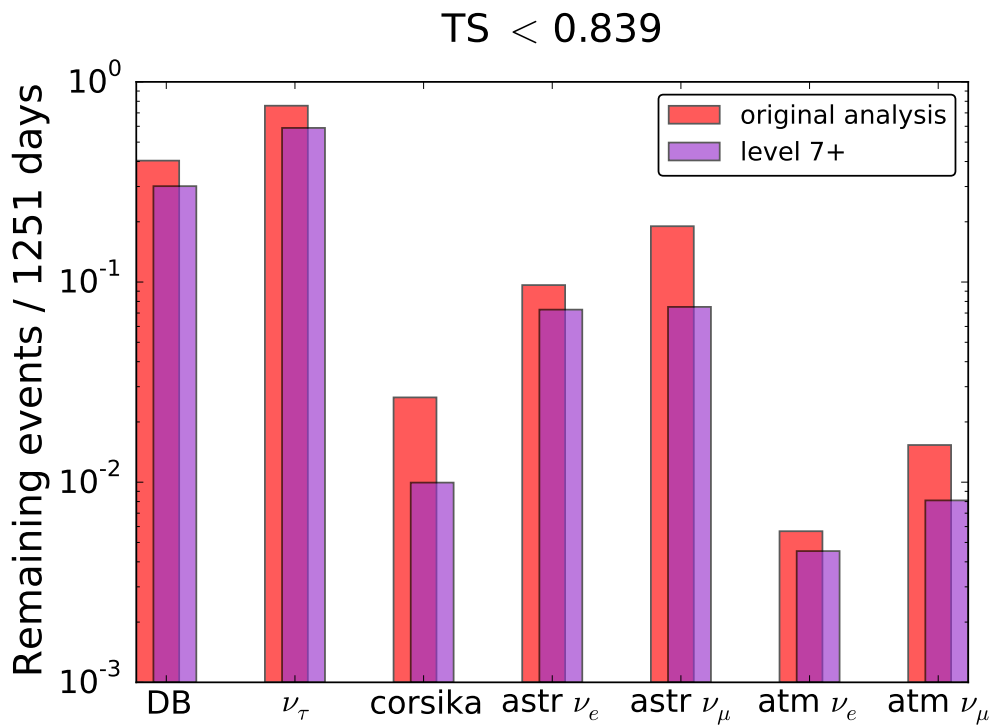


FIGURE 4.16: The expected results after processing to Level 7+ using the cut TS < 0.839, compared with the expected final results of the original analysis.

## Chapter 5

# Conclusions and Outlook

This work studied the possibility of adding a more advanced statistical approach to the Double Bang search by Matthias Vraeghe. Matthias introduced three new parameters at Level 6 of his analysis, the Causality, the Energy Asymmetry and the Reconstructed Length. Events for which the value of at least one of the three parameters falls outside predefined intervals are discarded when processed to Level 6. Instead of dealing with them separately, the more advanced statistical approach combines the three parameters into a single test statistic (TS) based on different log-likelihood distributions. Events with a TS value larger than a predefined cut value are removed from the dataset at what we called the modified Level 6. The TS parameter has been chosen so that, if we require at least about 0.5 Double Bang events of four years of IceCube data survive, out of all the considered possibilities it yields the data cut increasing the signal-to-background ratio the most.

Comparing the original Level 6 with the modified Level 6 using different TS cut values we see that in general the latter increases the signal-to-background ratio significantly more, mainly by discarding Corsika events more efficiently. The change in the other types of background event rates is far less favorable, with a poor performance in especially the reduction of the Astro Electron Neutrino event rate. With the Corsika events dominating the background at this point in the analysis and the TS parameter chosen based on its capability of increasing the signal-to-background ratio it should not be surprising that the advanced approach focuses on reducing the Corsika event rate. This in contrast to the original cuts, which were designed to mainly deal with the Astro Electron Neutrino events and thus lead to a more efficient reduction of the corresponding event rate.

Comparing the final results of the analysis using the original Level 6 with those obtained when applying the modified Level 6 instead, we see that the latter are clearly inferior to the first. The final level, Level 7, focuses on the removal of Corsika events, which is complementary to the original Level 6 focusing on Astro Electron Neutrino events. The combination of Level 6 with the modified Level 7 is less efficient, with both designed to remove the same type of background events.

We found that combining both approaches however can lead to improvement of the analysis. Using a relatively lax TS cut value falling in the range of about 0.840 to 1.000 improves the final Double Bang and Astro Tau Neutrino signal-to-background ratios of the original analysis, mainly by decreasing the Astro Muon Neutrino event rate, without reducing the Double Bang and Astro Tau Neutrino signal rate much further. Although based on the same three variables the more advanced approach seems to focus less on the Astro Electron Neutrino type events while however becoming more sensitive to other types of background events. Adding the modified Level 6 to the analysis thus lowers all types of background some further. This mainly leads to a notable reduction in Astro Muon Neutrino events, as they form the main background component in the final results of Matthias' analysis.

As after applying all the cuts of the original analysis on 1251 days of IceCube data no events remained, adding the modified Level 6 will of course also not disclose any events either. If in the future the analysis will be used to study more days of IceCube data it seems a good idea to include the cut of the modified Level 6 using a soft TS cut value as described above. The results of both the original analysis as well as the analysis including the modified Level 6 reflect the difficulty of distinguishing Double Bang signals from background events, yielding expected rates about one every ten years. They do however result in somewhat more practicable Astro Tau Neutrino event rates, expecting about one event every five years.

Processing the simulation data to Level 5 results in substantial loss in Corsika events. With only one more dataset covering the same energy interval while using the same ice model and the complexities processing new simulation datasets to Level 5 brings about, the loss could not be countered. This results in rather poor statistics for the Corsika-related likelihood distributions, TS distributions and event rates. Especially the final Corsika event rates quoted carry a substantial statistical error of the order of the rate value itself. As the rates are so low the impact on the corresponding signal-to-background ratios is limited, however using more accurate likelihood distributions could lead to a cut able to better distinguish signal from background.

The datasets used to predict the number of remaining events quoted in this work were also used to construct the different likelihood distributions on which the cut of the modified Level 6 is based, introducing a form of bias. We can however expect it to be small as the TS parameter on which the actual cut is performed is build out of several likelihood distributions, all corresponding to a different type of signal. This means its correlation to every individual dataset is only at most partial. A more clean approach would be using different datasets for construction of the likelihood distributions and the prediction of the number of remaining events. Dividing the datasets in a part used for the likelihood distribution constructions and a part used for the determination of event rates would also remove the bias, of course leading to larger statistical errors.

As the range of the Causality and Reconstructed Length depends on the event type, some of the likelihood distributions had to be extrapolated towards lower or higher values of their corresponding parameter. This was done in a way that evaluating a likelihood distributions outside its initial range results in the value of the closest bin. The method of extrapolation could thus be refined. Seen most of the time the likelihood distributions are evaluated within their initial ranges it is however not expected to yield any significant changes in the results. As their TS value is undefined, events yielding relevant total likelihood values of zero were simply discarded. To assign these events non-zero values again extrapolation could be used. It is however not expected to notably change the results seen only a small number of events had to be discarded this way.

In order to create a modified Level 6 which can replace the original Level 6, searching for an optimal TS parameter based on the removal of Astro Electron Neutrinos instead of the increase of the total signal-to-background ratio seems like a better idea. Still restricting ourselves to those of the form given by equation (4.6), this would probably lead to a TS parameter with the Astro Electron Neutrino total log-likelihood distribution in its denominator. It could possibly yield a data cut reducing the Astro Electron Neutrino rate more efficiently, in the end increasing the Double Bang and Astro Tau Neutrino rate of the analysis instead of only reducing the background further.

The advanced approach could possibly be used to increase the final signal-to-background ratio as presented in this work even further. Searching for the TS parameter which is able to remove most of the Astro Muon Neutrino events given at least a certain number of Double Bang or Astro Tau Neutrino events survive could possibly lead to a better or an additional cut reducing the Astro Muon Neutrino event rate even further. Constructing the same likelihood distributions based on data processed to Level 7 and again searching for the optimal TS parameter based on the increase of signal-to-background ratios could also lead to a significant increase of these ratios. This method would however probably have to deal with bad statistics due to the small number of remaining events.

Instead of using only a single TS parameter a combination of different ones could be used. Every TS parameter could for instance yield a separate cut focusing on different types of background events or several could be combined to train a boosted decision tree. It is also possible to abandon the restriction (4.6) Including the electron neutrino related likelihoods in the numerator of the TS parameter given by (4.7) for example could increase the discrepancy between Double Bang events and track-like events, i.e. Corsika and muon neutrino events, as electron neutrinos generally create more spherical signals. The parameter would then however probably be less effective at distinguishing Double Bangs from the electron neutrino events.



## Appendix A

# Likelihood Distributions

### A.1 Astro Tau Neutrino

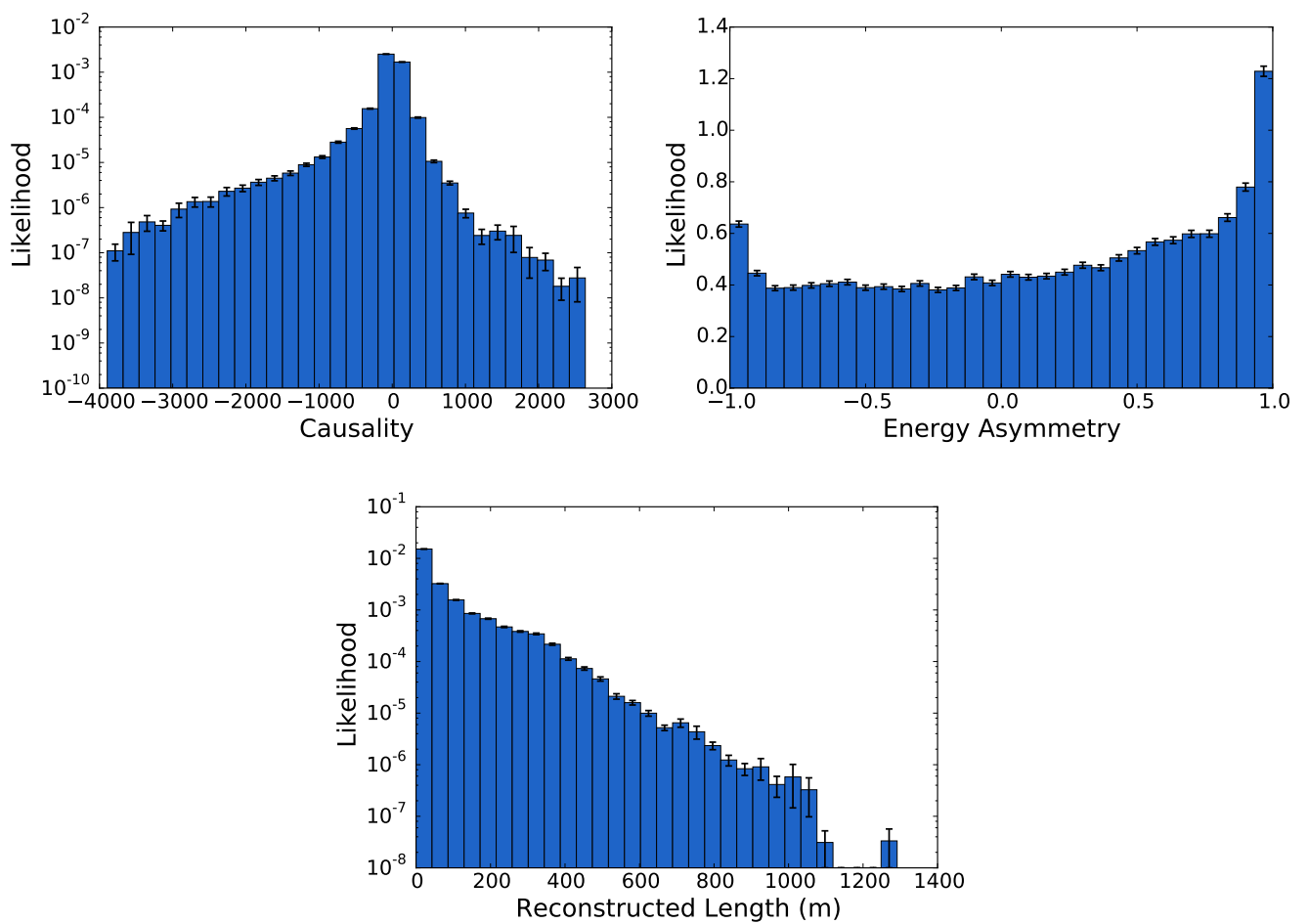


FIGURE A.1: The likelihood distributions of the three parameters for the Astro Tau Neutrino signal. The error bars show the statistical errors based on Poisson statistics.

## A.2 Corsika

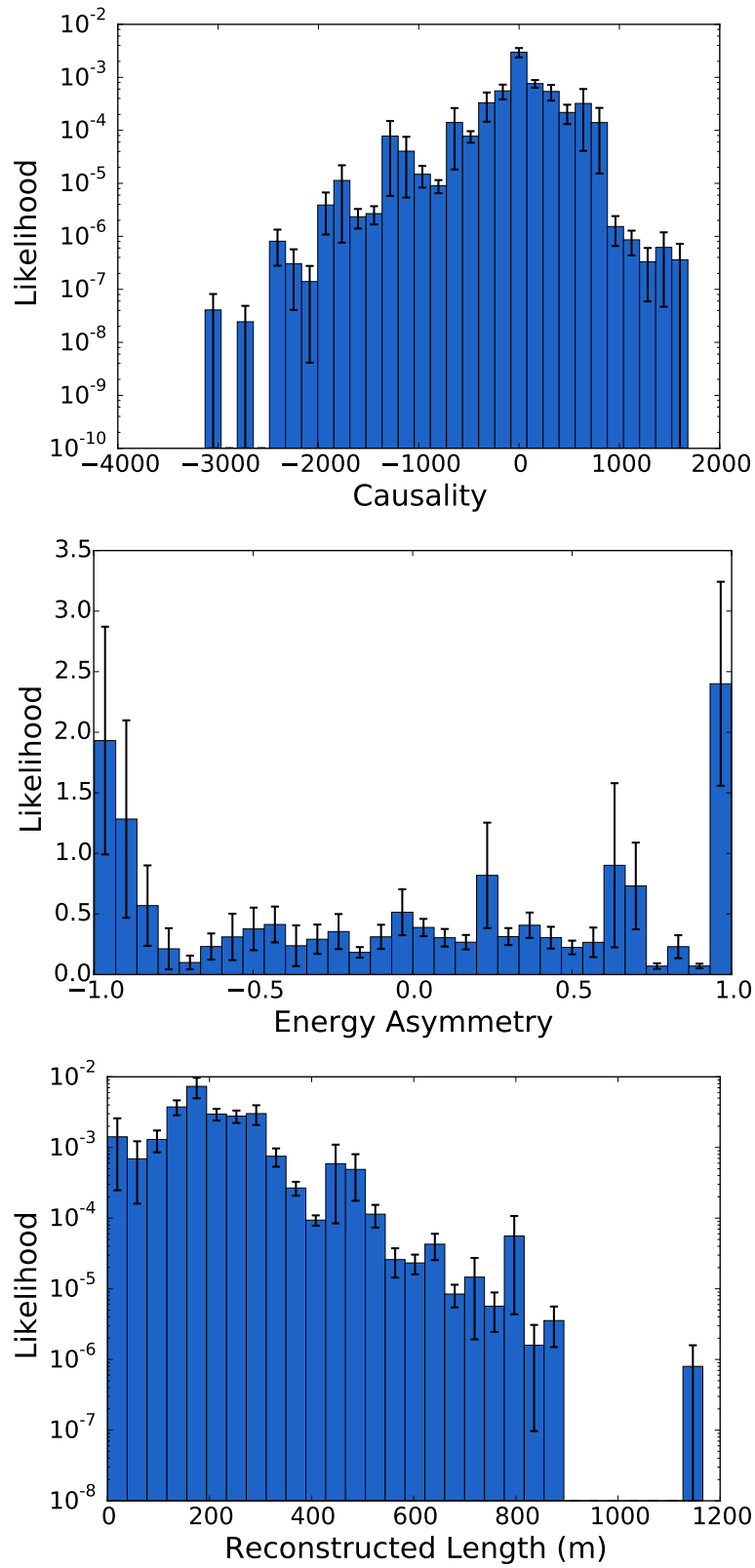


FIGURE A.2: The likelihood distributions of the three parameters for the Corsika signal. The error bars show the statistical errors based on Poisson statistics.

### A.3 Astro Electron Neutrino

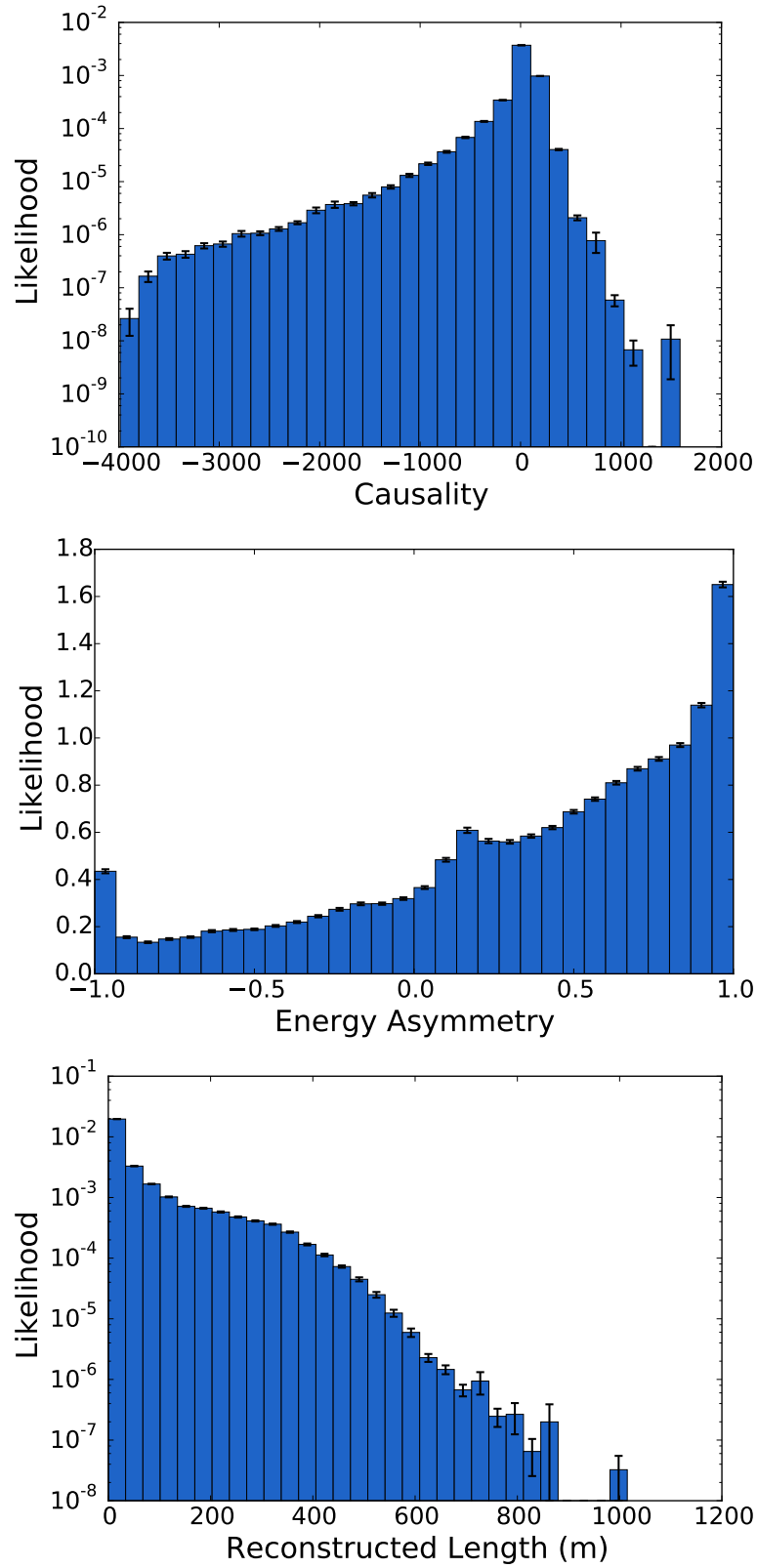


FIGURE A.3: The likelihood distributions of the three parameters for the Astro Electron Neutrino signal. The error bars show the statistical errors based on Poisson statistics.

## A.4 Astro Muon Neutrino

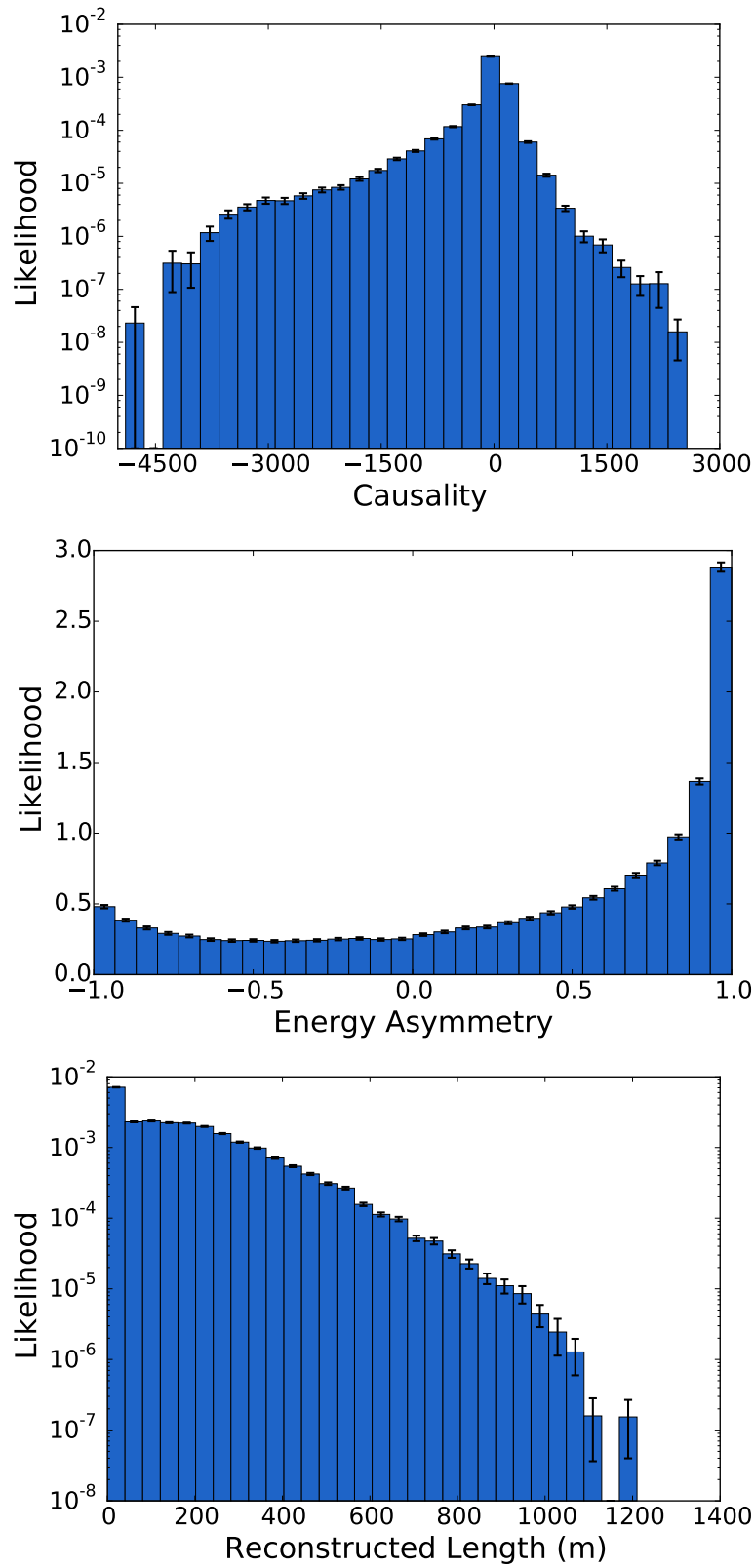


FIGURE A.4: The likelihood distributions of the three parameters for the Astro Muon Neutrino signal. The error bars show the statistical errors based on Poisson statistics.

## A.5 Atmos Electron Neutrino

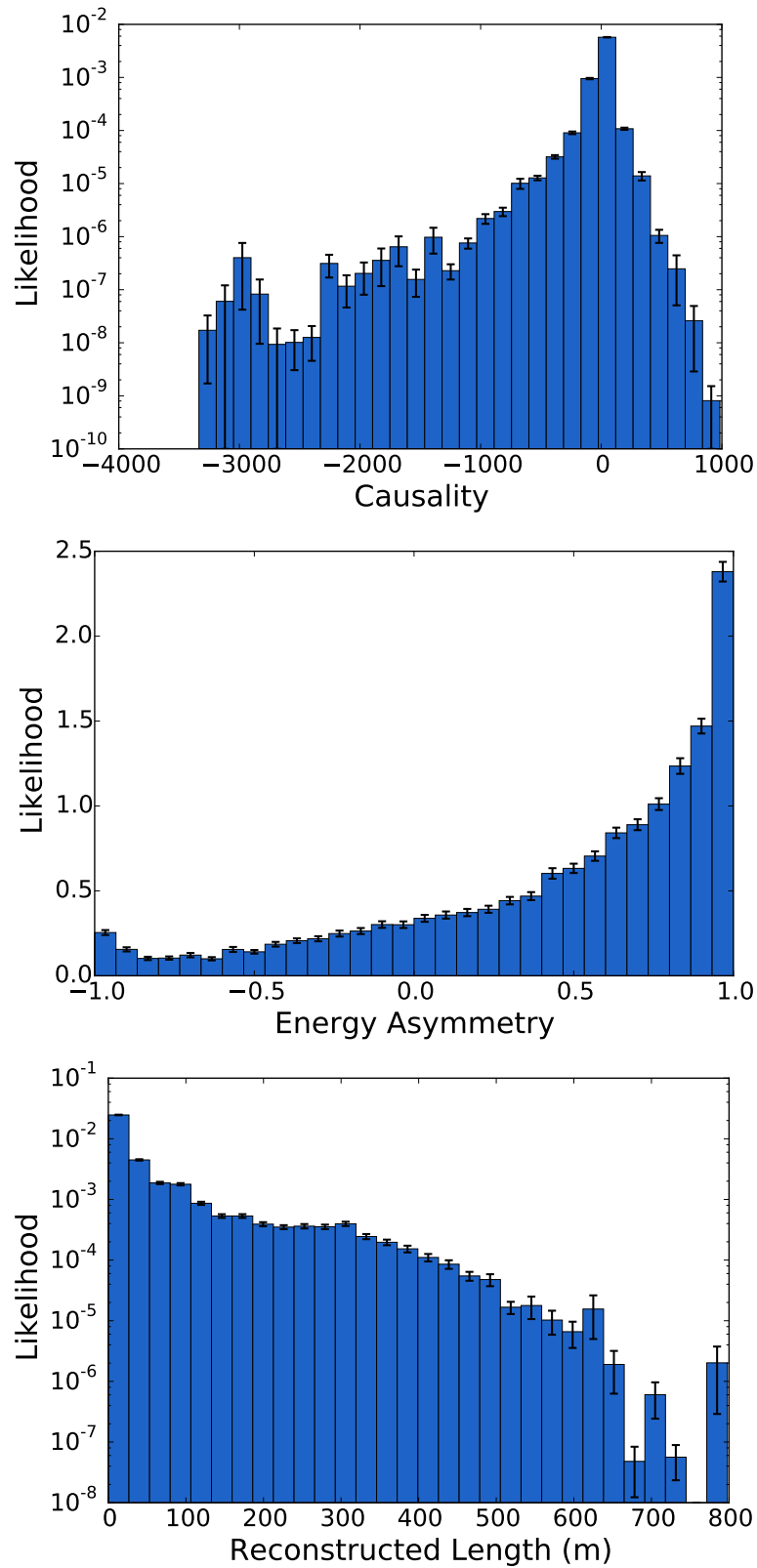


FIGURE A.5: The likelihood distributions of the three parameters for the Atmos Electron Neutrino signal. The error bars show the statistical errors based on Poisson statistics.

## A.6 Atmos Muon Neutrino

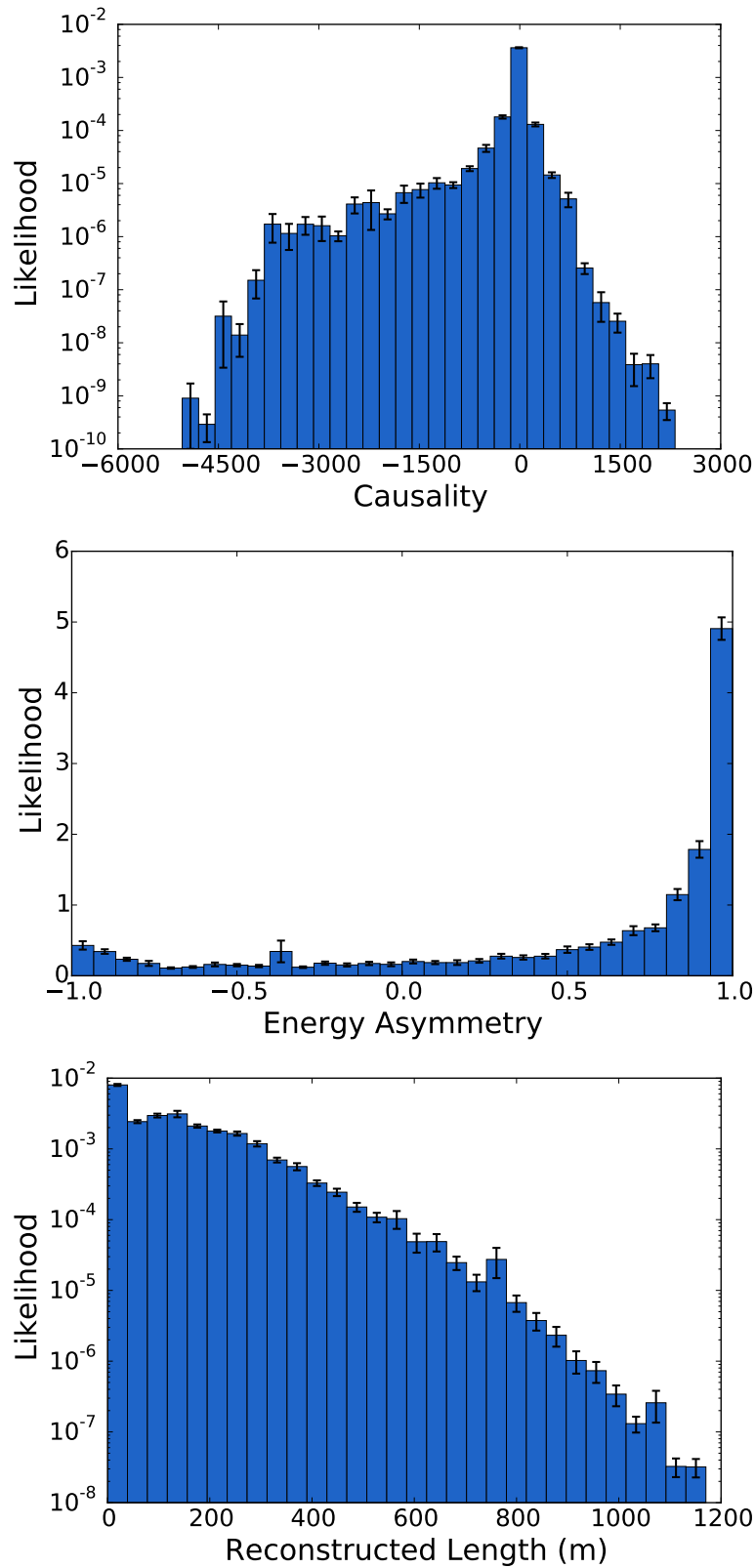


FIGURE A.6: The likelihood distributions of the three parameters for the Atmos Muon Neutrino signal. The error bars show the statistical errors based on Poisson statistics.

## Appendix B

# TS Distributions

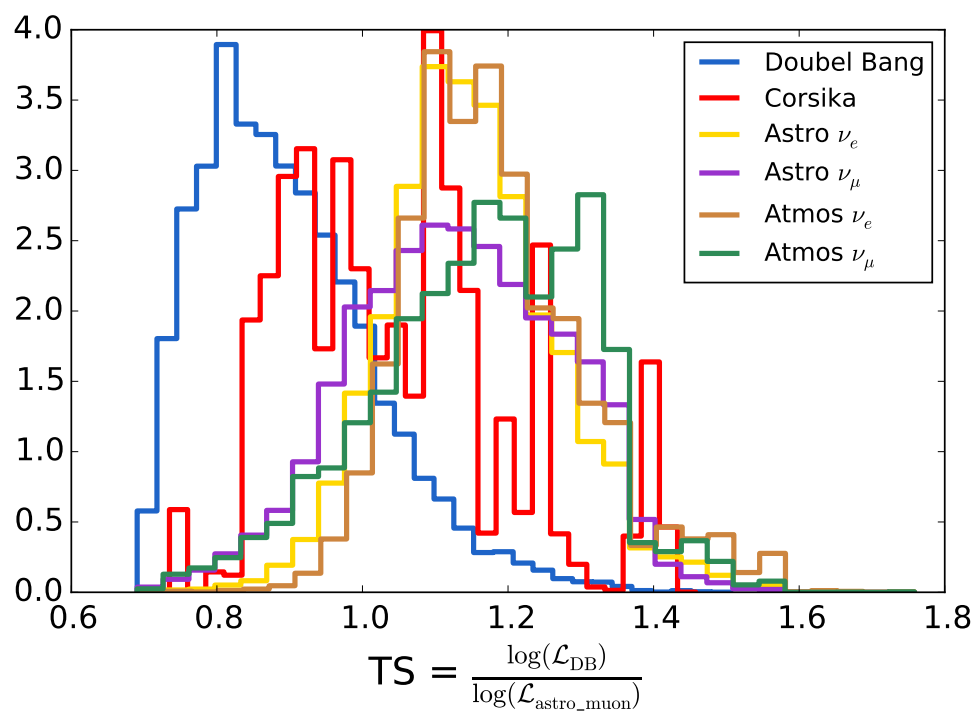


FIGURE B.1: The normalized TS distributions for the Double Bang signal type and the five background signal types for an example TS parameter.

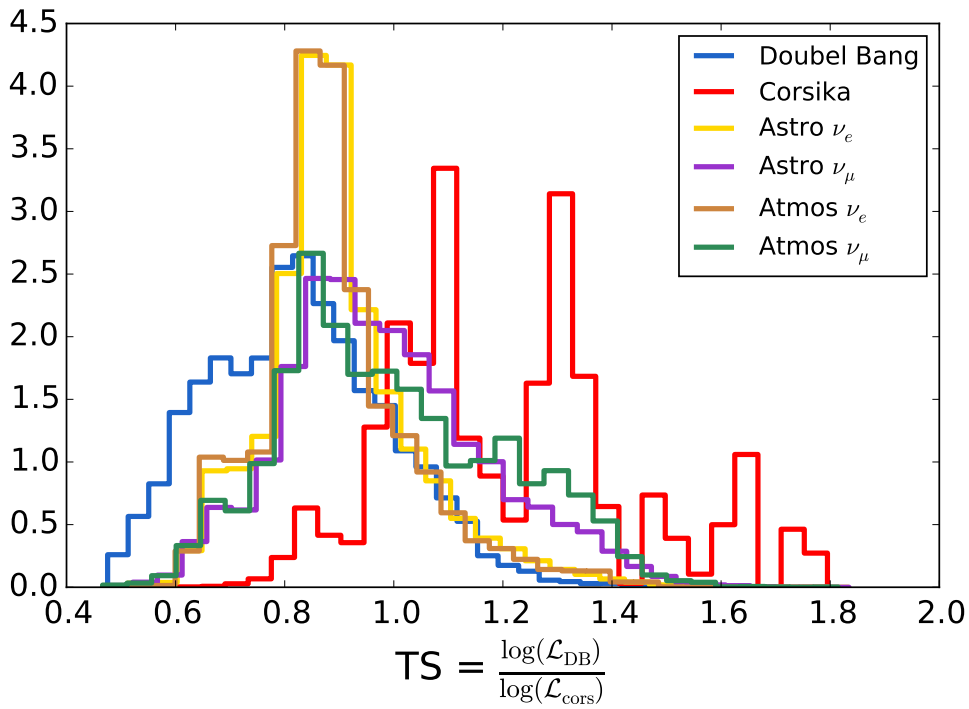


FIGURE B.2: The normalized TS distributions for the Double Bang signal type and the five background signal types for an example TS parameter.

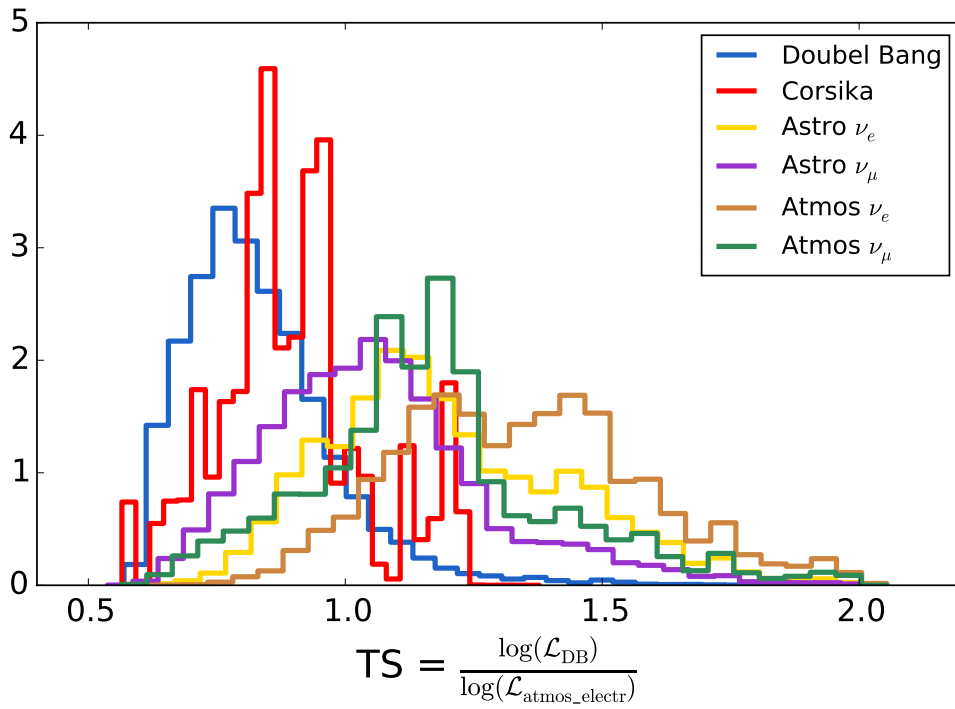


FIGURE B.3: The normalized TS distributions for the Double Bang signal type and the five background signal types for an example TS parameter.

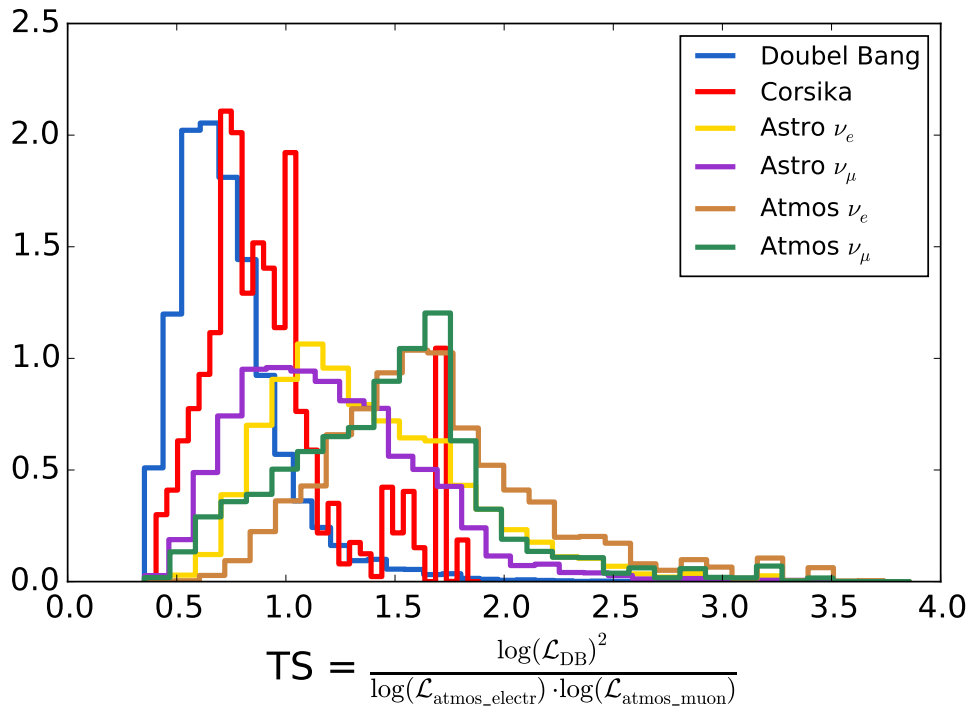


FIGURE B.4: The normalized TS distributions for the Double Bang signal type and the five background signal types for an example TS parameter.

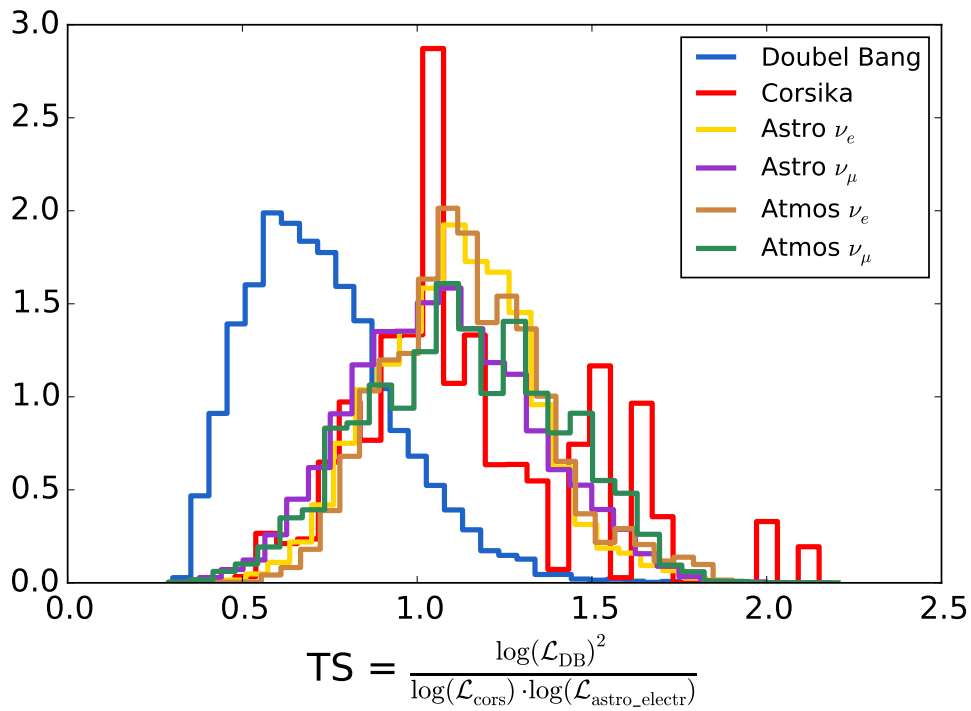


FIGURE B.5: The normalized TS distributions for the Double Bang signal type and the five background signal types for an example TS parameter.

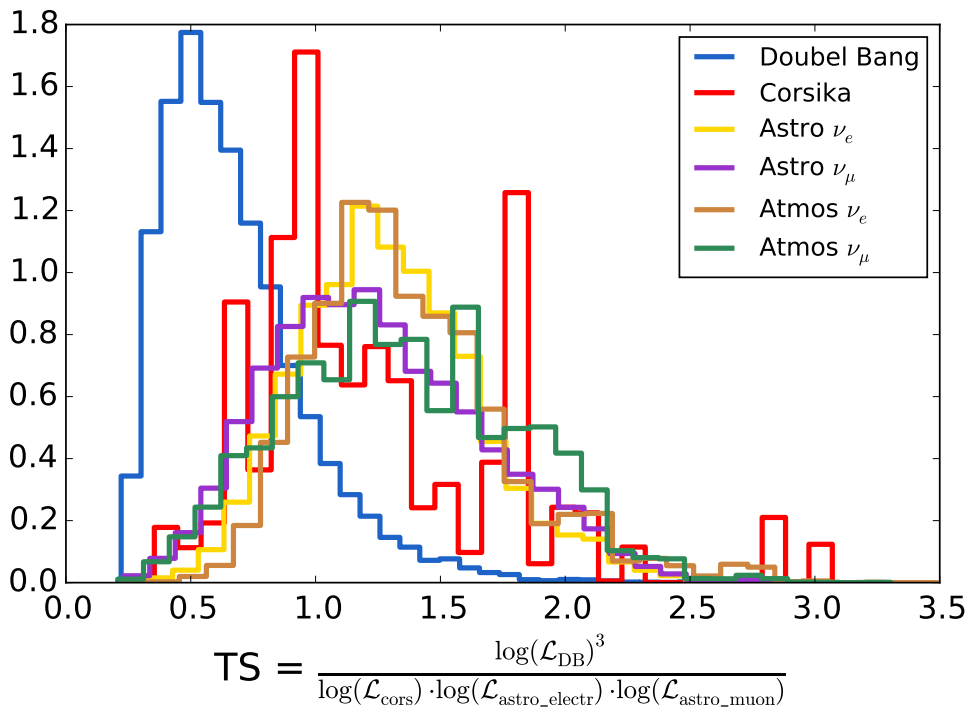


FIGURE B.6: The normalized TS distributions for the Double Bang signal type and the five background signal types for an example TS parameter.

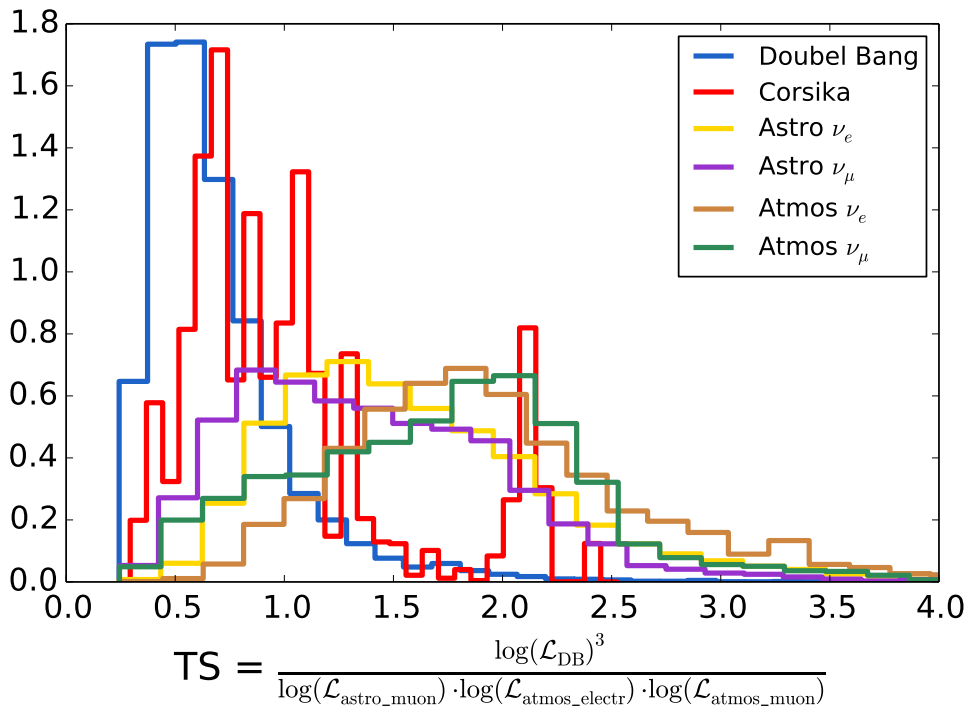


FIGURE B.7: The normalized TS distributions for the Double Bang signal type and the five background signal types for an example TS parameter. The outliers towards high TS values are not shown in the plot.

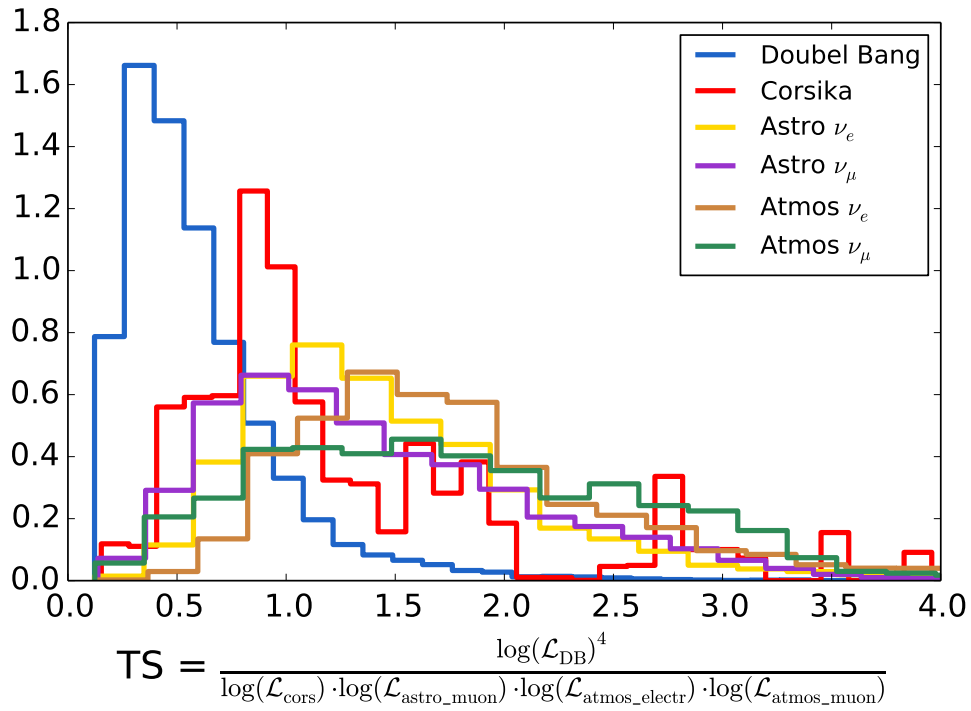


FIGURE B.8: The normalized TS distributions for the Double Bang signal type and the five background signal types for an example TS parameter. The outliers towards high TS values are not shown in the plot.

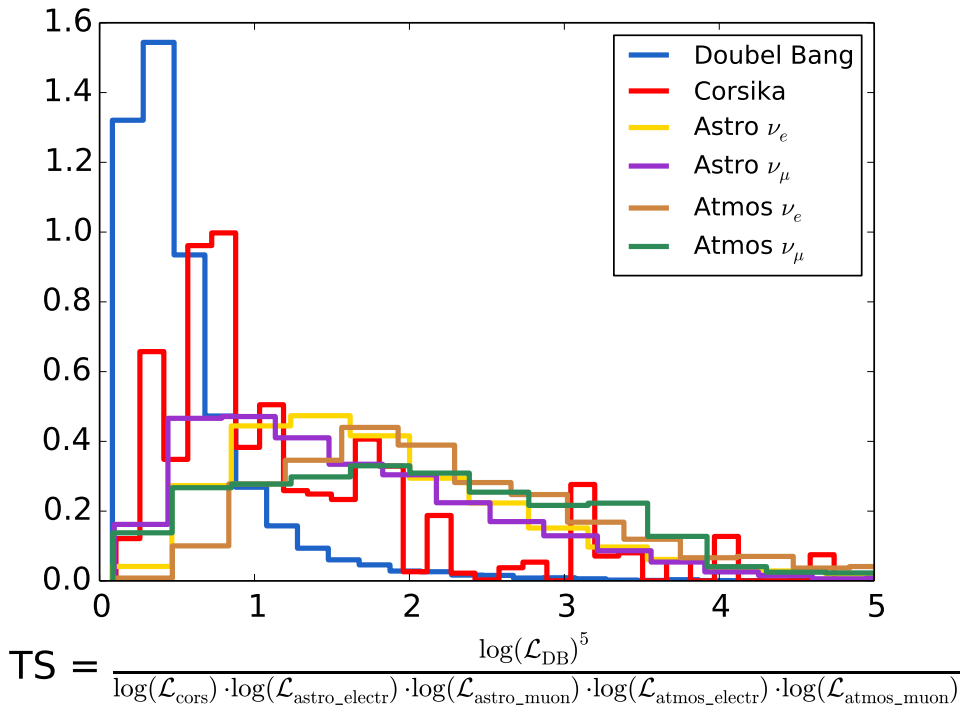


FIGURE B.9: The normalized TS distributions for the Double Bang signal type and the five background signal types for an example TS parameter. The outliers towards high TS values are not shown in the plot.



## Appendix C

# Communication to the General Public

In order to communicate and promote our research at the IceCube Neutrino Observatory to the general public Stef Verpoest and I gave a Dutch introductory talk about particle and astroparticle physics, the observatory itself and our Master's thesis projects. The event was organized by the VVN (Vereniging voor Natuurkunde) and a recording of the talk can be found on YouTube (<https://www.youtube.com/watch?v=aosbqWHZ2Pk>).



# Bibliography

- [1] F. Halzen and A. D. Martin, *Quarks and Leptons: An Introductory Course in Modern Particle Physics*. Wiley, 1984.
- [2] B. Povh, K. Rith, C. Scholz, F. Zetsche, and W. Rodejohann, *Particles and Nuclei*. Springer, 2015.
- [3] The ATLAS Collaboration, “Observation of a new particle in the search for the Standard Model Higgs boson with the ATLAS detector at the LHC,” *Phys. Lett. B*, vol. 716, pp. 1–29, 2012.
- [4] The CMS Collaboration, “Observation of a new boson at a mass of 125 GeV with the CMS experiment at the LHC,” *Phys. Lett. B*, vol. 716, pp. 30–61, 2012.
- [5] C. Patrignani *et al.* (Particle Data Group), *Chin. Phys. C*, vol. 40, 100001 (2016) and 2017 update.
- [6] P. Langacker, *The Standard Model and Beyond*. CRC Press, 2010.
- [7] F. Mandl and G. Shaw, *Quantum Field Theory*. Wiley, 2010.
- [8] M. Thomson, *Modern Particle Physics*. Cambridge University Press, 2013.
- [9] K. Winter, *Neutrino Physics*. Cambridge University Press, 2000.
- [10] G. Rajasekaran, “The Story of the Neutrino,” *ArXiv Physics e-prints*, 2016.
- [11] Published on [t2k-experiment.org](http://t2k-experiment.org).
- [12] G. Rajasekaran, “Fermi and the Theory of Weak Interactions,” *ArXiv Physics e-prints*, 2014.
- [13] “The Reines-Cowan Experiments: Detecting the Poltergeist,” *Los Alamos Science*, no. 25, 1997.
- [14] S. H. Neddermeyer and C. D. Anderson, “Note on the Nature of Cosmic-Ray Particles,” *Phys. Rev.*, vol. 51, pp. 263–271, 1937.
- [15] J. Street and E. Stevenson, “New Evidence for the Existence of a Particle of Mass Intermediate Between the Proton and Electron,” *Phys. Rev.*, vol. 52, pp. 1003–1004, 1937.
- [16] I. V. Aničin, “The Neutrino: Its Past, Present and Future,” *ArXiv Physics e-prints*, 2005.
- [17] G. Danby, J.-M. Gaillard, L. Goulianos, L. Lederman, N. Mistry, M. Schwartz, and J. Steinberger, “Observation of High-Energy Neutrino Reactions and the Existence of Two Kinds of Neutrinos,” *Phys. Rev. Lett.*, vol. 9, pp. 36–44, 1962.
- [18] M. Perl *et al.*, “Evidence for Anomalous Lepton Production in  $e^+ - e^-$  Annihilation,” *Phys. Rev. Lett.*, vol. 35, pp. 1489–1492, 1975.

- [19] DONUT Collaboration (K. Kodama *et al.*), "Observation of Tau Neutrino Interactions," *Phys. Lett. B*, vol. 504, pp. 218–224, 2000.
- [20] M. Ahlers and F. Halzen, "Opening a New Window onto the Universe with IceCube," *ArXiv Physics e-prints*, p. 34, 2018. To appear in *Progress in Particle and Nuclear Physics*.
- [21] J. N. Bahcall, "Solar Models: An Historical Overview," *Nuclear Physics B (Proc. Suppl.)*, vol. 118, pp. 77–86, 2003.
- [22] R. Davis, "A Review of the Homestake Solar Neutrino Experiment," *Prog. Part. Nucl. Phys.*, vol. 32, pp. 13–32, 1994.
- [23] W. Gajewski, "Update of Results from the SuperKamiokande Detector," *Physics of Atomic Nuclei*, vol. 63, pp. 934–942, 1999.
- [24] J. Abdurashitov *et al.*, "Results from SAGE II," *Nuclear Physics B (Proc. Suppl.)*, vol. 38, pp. 60–67, 1995.
- [25] M. Cribier, "Results of the whole GALLEX experiment," *Nuclear Physics B (Proc. Suppl.)*, vol. 70, pp. 284–291, 1999.
- [26] J. N. Bahcall, "Solving the Mystery of the Missing Neutrinos," *ArXiv Physics e-prints*, 2004.
- [27] SNO Collaboration (Q. Ahmad *et al.*), "Direct evidence for neutrino flavor transformation from neutral current interactions in the Sudbury Neutrino Observatory," *Phys. Rev. Lett.*, vol. 89, p. 6, 2002.
- [28] M. Kachelrieß, "Lecture Notes on High Energy Cosmic Rays," *ArXiv Physics e-prints*, 2008.
- [29] A. D. Angelis. Published on Wikipedia, Oktober 2011.
- [30] L. Bonolis, "Walther Bothe and Bruno Rossi: The birth and development of coincidence methods in cosmic-ray physics," *American Journal of Physics*, vol. 79, pp. 1133–, 2011.
- [31] P. K. Grieder, *Extensive Air Showers*. Springer, 2010.
- [32] Published on <https://www.hawc-observatory.org>.
- [33] R. A. Millikan and G. H. Cameron, "The Origin of the Cosmic Rays," *Phys. Rev.*, vol. 32, pp. 533–557, 1928.
- [34] A. H. Compton, "Variation of the cosmic rays with latitude," *Phys. Rev.*, vol. 41, pp. 111–113, 1932.
- [35] J. Blümer, R. Engel, and J. Hörandel, "Cosmic Rays from the Knee to the Highest Energies," *Prog. Part. Nucl. Phys.*, vol. 63, pp. 293–338, 2009.
- [36] Published on <https://www.quantamagazine.org>. Original data via S. Swordy, U. Chicago.
- [37] The Fermi-LAT Collaboration, "Fermi-LAT Observations of the Diffuse Gamma-Ray Emission: Implications for Cosmic Rays and the Interstellar Medium," *The Astrophysical Journal*, vol. 750, p. 35, 2012.

- [38] M. H. Israel *et al.*, "Isotopic Composition of Cosmic Rays: Results from the Cosmic Ray Isotope Spectrometer on the ACE Spacecraft," *Nucl. Phys. A*, vol. 758, pp. 201–208, 2005.
- [39] S. F. SINGER, "Meteorites and Cosmic Rays," *Nature*, vol. 170, pp. 728–729, 1952.
- [40] D. Caprioli, "Cosmic-ray Acceleration and Propagation," *PoS*, vol. 236, p. 24, 2016.
- [41] N.E. Yanasak *et al.*, "Cosmic-ray Time Scales Using Radioactive Clocks," *Advances in Space Research*, vol. 27, pp. 727–736, 2001.
- [42] NASA, ESA, J. Hester, A. Loll (ASU). Published on Astronomy Picture of the Day, August 2015.
- [43] H. Krawczynski and E. Treister, "Active Galactic Nuclei - the Physics of Individual Sources and the Cosmic History of Formation and Evolution," *Front.Phys.(Beijing)*, vol. 8, pp. 609–629, 2013.
- [44] T. Piran, "Gamma-ray Bursts: A Puzzle Being Resolved," *Phys.Rept.*, vol. 333, pp. 529–553, 1999.
- [45] A. Dar, "Are Extragalactic Gamma-ray Bursts the Source of the Highest Energy Cosmic Rays?," *Submitted to: Astrophys. J. Lett.*, p. 11, 1999.
- [46] D. Tosi, "Astrophysical Neutrinos: IceCube Highlights," *Nuclear and Particle Physics Proceedings*, vol. 291-293, pp. 167–174, 2017.
- [47] T. K. Gaisser, "Neutrino Astronomy 2017," *ArXiv Physics e-prints*, 2018.
- [48] IceCube Collaboration (M.G. Aartsen *et al.*), "Flavor Ratio of Astrophysical Neutrinos above 35 TeV in IceCube," *Phys. Rev. Lett.*, vol. 114, p. 8, 2015.
- [49] IceCube Collaboration (M.G. Aartsen *et al.*), "Evidence for High-Energy Extraterrestrial Neutrinos at the IceCube Detector," *Science*, vol. 342, p. 38, 2013.
- [50] IceCube Collaboration (M.G. Aartsen *et al.*), "A Combined Maximum-likelihood Analysis of the High-energy Astrophysical Neutrino Flux Measured with IceCube," *Astrophys.J.*, vol. 809, p. 15, 2015.
- [51] IceCube Collaboration (M.G. Aartsen *et al.*), "The IceCube Neutrino Observatory: Instrumentation and Online Systems," *JINST*, vol. 12, p. 83, 2017.
- [52] J.-H. Koehne, K. Frantzen, M. Schmitz, T. Fuchs, and W. Rhode, "PROPOSAL: A Tool for Propagation of Charged Leptons," *Computer Physics Communications*, vol. 184, pp. 2070–2090, 2013.
- [53] G. F. Knoll, *Radiation Detection and Measurement*. Wiley, 2010.
- [54] L. Rädcl and C. Wiebusch, "Calculation of the Cherenkov-light Yield from Electromagnetic Cascades in Ice with Geant4," *Astropart. Phys.*, vol. 44, pp. 102–113, 2013.
- [55] S. Euler, *Observation of Oscillations of Atmospheric Neutrinos with the IceCube Neutrino Observatory*. PhD thesis, RWTH Aachen University, 2014.

- [56] I. C. M. A. *et al.*), "Energy Reconstruction Methods in the IceCube Neutrino Telescope," *JINST*, vol. 9, p. 20, 2014.
- [57] D. F. Cowen (for the IceCube Collaboration), "Tau Neutrinos in IceCube," *Journal of Physics: Conference Series*, vol. 60, pp. 227–230, 2007.
- [58] I. C. M. A. *et al.*), "Search for Astrophysical Tau Neutrinos in Three Years of IceCube Data," *Phys. Rev.*, vol. D93, p. 11, 2016.
- [59] I. C. R. A. *et al.*), "Limits on a Muon Flux from Kaluza-Klein Dark Matter Annihilations in the Sun from the IceCube 22-string Detector," *Phys. Rev.*, vol. D81, p. 6, 2010.
- [60] I. C. M. A. *et al.*), "Measurement of Atmospheric Neutrino Oscillations with IceCube," *Phys. Rev. Lett.*, vol. 111, p. 6, 2013.
- [61] I. C. M. A. *et al.*), "Searches for Sterile Neutrinos with the IceCube Detector," *Phys. Rev. Lett.*, vol. 117, p. 9, 2016.
- [62] I. C. M. A. *et al.*), "Searches for Relativistic Magnetic Monopoles in IceCube," *Eur. Phys. J.*, vol. C76, p. 18, 2016.
- [63] W. Van Driessche, "SPACE." IceCube internal resource: <https://wiki.icecube.wisc.edu/index.php/SPACE>. An overview of the IceCube SPACE analysis (Stable Particles with Anomalous Charge).
- [64] S. Verpoest, "Search for Particles with Fractional Charges in IceCube based on Anomalous Energy Loss," Master's thesis, Ghent University, 2018.
- [65] P. Antonioli *et al.*, "SNEWS: The Supernova Early Warning System," *New J. Phys.*, vol. 6, p. 25, 2004.
- [66] M. Vraeghe, "A Search for Astrophysical Tau Neutrinos with the IceCube Neutrino Observatory." To be published.
- [67] T. K. Gaisser, "Spectrum of Cosmic-ray Nucleons, Kaon Production, and the Atmospheric Muon Charge Ratio," *Astropart.Phys.*, vol. 35, p. 6, 2011.
- [68] M. Honda, T. Kajita, K. Kasahara, S. Midorikawa, and T. Sanuki, "Calculation of Atmospheric Neutrino Flux Using the Interaction Model Calibrated with Atmospheric Muon Data," *Phys. Rev.*, vol. D75, 2007.
- [69] R. Enberg, M. H. Reno, and I. Sarcevic, "Prompt Neutrino Fluxes from Atmospheric Charm," *Phys. Rev.*, vol. D78, p. 13, 2008.
- [70] Matthias Vraeghe, "IC86 NuTau Double Bang Analysis." IceCube internal resource: [https://wiki.icecube.wisc.edu/index.php/IC86\\_NuTau\\_Double\\_Bang\\_Analysis](https://wiki.icecube.wisc.edu/index.php/IC86_NuTau_Double_Bang_Analysis). An overview of the search for astrophysical tau neutrinos with the IceCube Neutrino Observatory by Matthias Vraeghe.
- [71] S. Klein, "Recent Highlights from IceCube," *Braz.J.Phys.*, vol. 44, pp. 540–549, 2013.